INVESTIGATIONS INTO THE OPTIMAL ENERGY EXTRACTION FROM PM-BLDC MACHINE BASED FLYWHEEL ENERGY STORAGE SYSTEM

By

S R GURUMURTHY

Enrolment No : ENGG01200904044

A thesis submitted to the

Board of Studies in Engineering Sciences

In partial fulfillment of requirements

for the Degree of

DOCTOR OF PHILOSOPHY

of

HOMI BHABHA NATIONAL INSTITUTE

February, 2017

Homi Bhabha National Institute

Recommendations of the Viva Voce committee

As members of the Viva Voce Committee, we certify that we have read the dissertation prepared by **S R Gurumurthy** entitled **"Investigations into the Optimal Energy Extraction from PM-BLDC Machine based Flywheel Energy Storage System"** and recommend that it may be accepted as fulfilling the thesis requirement for the award of Degree of Doctor of Philosophy.

Sr.No	Name	Designation	Signature & Date
1	Prof. Archana Sharma	Chairman, DC−VII	
2	Prof. Vivek Agarwal	Guide	
3	Prof. L Umanand	External Examiner	
4	Prof. V H Patankar	Member	
5	Prof. Gopika Vinod	Member	
6	Prof. B Dikshit	Member	
7	Prof. Archana Sharma	Convener & Guide	

Final approval and acceptance of this thesis is contingent upon the candidate's submission of the final copies of the thesis to HBNI.

We hereby certify that we have read this thesis prepared under our direction and recommend that it may be accepted as fulfilling the thesis requirement.

Date:

Place: **Guide** **Guide**

Statement by Author

S R Gurumurthy

Declaration

I, hereby declare that the investigations presented in this thesis has been carried out by me. The work is original and has not been submitted earlier as a whole or in part for a degree / diploma at this or any other Institution / University.

S R Gurumurthy

List of Publications arising from the thesis

Publications

1. S. R. Gurumurthy, A. Sharma and Kallol Roy, "Armature current spiking problem in a BLDC motor and solution: A case study," International Journal of Electrical, Electronics and Computer Systems (IJEECS), vol. 11, no. 01, November 2012.

2. S. R. Gurumurthy, V. Agarwal and A. Sharma, "Optimal energy harvesting from a high-speed brushless DC generator-based flywheel energy storage system," IET Electr. Power Appl, vol. 7, no. 9, pp. 693–700, November 2013.

3. S. R. Gurumurthy, V. Agarwal, and A. Sharma, "High Efficiency Bi-directional Converter for Flywheel Energy Storage Application," IEEE Trans. Ind. Electron., vol. 63, no. 9, pp. 5477-5487, September 2016.

4. S. R. Gurumurthy, V. Agarwal, and A. Sharma, "A Novel Dual Winding BLDC Generator-Buck Converter combination for enhancement of the harvested energy from a flywheel," IEEE Trans. Ind. Electron., vol. 63, no. 12, pp. 7563-7573, December 2016.

Conference Presentation/Proceedings

1. S. R. Gurumurthy, V. Agarwal, A. Sharma and S. Sarkar, "Apportioning and mitigation of losses in a brushless generator based flywheel energy storage system," IEEE 4^{th} International Symposium on Power Electronics for Distributed Generation Systems (PEDG), Rogers, Arkansas, USA, July 8-11, 2013.

2. S. R. Gurumurthy, A. Sharma, S. Sarkar and S. Satheshkumar, "Effect of leakage inductance on the performance of BLDC machine in generation and motoring mode," 3^{rd} International conference on Power, Signals, Control Computation (EPSCICON 2014), Trissur, Kerala, January 9-11, 2014.

3. S. R. Gurumurthy, V. Agarwal, and A. Sharma, "Design Considerations for a PM-BLDC Machine for Flywheel Energy Storage Applications," IEEE 6^{th} International Symposium on Power Electronics for Distributed Generation Systems (PEDG), Aachen, Germany, June 22-25, 2015.

Publications: Communicated/Under review/Accepted

1. S. R. Gurumurthy, V. Agarwal, and A. Sharma, "Novel Circuit Topologies with Multi-Winding Generator for Enhanced Energy Extraction from a Flywheel Storage System," Submitted to IEEE Trans. Ind. Electron., in December 2016, Manuscript ID: 16-TIE-3749, Under review.

Other publications (Patent)

1. V. Agarwal and S. R. Gurumurthy, "Apparatus and Method for Enhancement of Energy Harvested from a Flywheel Energy Storage System," Applied for Indian Patent 05, May 2015, 1811/RQ/MUM/2015.

Dedicated to
my mother
and
to the memory of
my father

Acknowledgment

I express my gratitude to Prof. Vivek Agarwal, Indian Institute of Technology, Bombay and Prof. Archana Sharma, Homi Bhabha National Institute, Mumbai for accepting me as a student. I thank them for guiding me throughout the project and providing me an opportunity to work on an exciting research topic which is also of contemporary industrial interest. My heartfelt thanks to Prof. Vivek Agarwal for giving me an insight into the control and analysis of power electronics circuits during the discussions and documentation of this research work.

I am grateful to Shri. S. Sarkar, Director, ChTG, BARC, Mumbai for giving me an opportunity to undertake this study at Homi Bhabha National Institute, Mumbai and also for his guidance as technology advisor. Dr. Kallol Roy has encouraged me to undertake this research work to start with and contributed a lot for improving the quality by reviewing the research work. My heartfelt thanks to him. I thank Shri. A. Nandakumar, Sr. Project Manager (MP&D), BARC Mysore for his continuous support and technical inputs in this project. I am grateful to Bhabha Atomic Research Centre and Indian Institute of Technology, Bombay for providing all the facilities to carryout this reasearch work.

Discussions with Nataraj, Chethan Kulkarni and Girigoudar has helped me lot in conceptualizing the ideas. My heart felt thanks to them. I thank Sathesh kumar who was ever ready to for helping me in fabrication and testing of the hardware, documentation of the work throughout this research work. I would like to thank Geethesh, Somashekhara, Venkatarami Reddy, Shruthi and Sangappa for their whole hearted help and support in fabrication and testing of the prototype FES system. I thank ever helping Vignesh and Kumar Raja for their help in the simulation of various novel topologies and schemes for energy harvesting system. Design, fabrication and supply of the BLDC machines with various configurations required for this research work were entirely carried out by Raviprasad, Bhupal and Chandan. I am grateful to all of them. I cannot forget the help rendered by Vijaya during experimentation and documentation of the work. I am thankful to her for the continuous support especially during writing and reviewing of the thesis. I want to thank my friends in Applied Power Electronics Lab, IIT, Bombay for their help and support during the academic works. I thank Ramya B and Kavita for their help in providing all the literatures required for my research work. I could not have done this work without the help and cooperation of my wife Seetha and son Viveka. I am always thankful to them.

I always cherish the memory of my interactions with my teacher Prof. Ramanarayan who has taught the subject Power electronics to give an insight into the power electronics subject to me. I would like to attribute all my success, my achievements to my father and mother. My father and his rational thinking remains an inspiration to me all through my life. Finally I would like to thank Almighty for creating the opportunities for me to pursue the work of my interest.

Abstract

Concern of increasing energy demand, exhausting fossil fuel reserves and consequences of climate change, demands the necessity of design of energy efficient systems to conserve the existing energy resources. Energy storage is one of the area where there is a scope to improve the efficiency. A mechanism which stores the energy when it is available to utilize same later is called an Energy storage system. The three stages of any energy storing process are storing the energy in the device, retaining it and releasing it to the load. Energy loss should be as minimum as possible in all these processes. Out of many energy storage devices available, the flywheel has the merits like, environmental friendliness, long life, and limit less charge and discharge cycles. Advancement of Power Electronics technology and availability of fast switching high power semiconductors, high performance micro processors, high speed bearings, Permanent magnet machines has lead to widespread acceptance of Flywheels for the Energy Storage applications. The work presented in this thesis is pertaining to the power converters and their control schemes for efficient utilization of energy stored in a flywheel.

Target of this work was to design, develop, and build an efficient Flywheel Energy Storage (FES) system. The work carried out involved building and evaluating one FES system which consists of flywheel, PM-BLDC machine, bi-directional power converter and an electronic control system. Sources of various losses and their reduction techniques are studied in detail. Also detailed studies have been carried out to find the factors or which influence the quantity of energy harvested and new methods have been devised to enhance the harvested energy from the system.

Brushless DC (BLDC) motors are highly suitable for usage in high speed applications. A Bidirectional Power Converter (BDC) interfaces the DC power source to BLDC machine which is coupled to the flywheel. The BDC is operated as a boost converter for maintaining the constant dc bus voltage while energy being harvested from the flywheel. Source resistance seen by the boost converter plays an important role in its gain and hence harvestable energy. Dependency of this source resistance on machine parameters has been studied and modelled. It was important to model this source resistance to design an effective energy harvesting system. To understand the phenomenon of dependence of source resistance on machine parameters FEM/FFT analysis of a BLDC generator have been done. These were helpful in predicting source resistance and choose appropriate converter topology for maximizing the harvestable energy. Design and implementation of the controller has been carried out for BDC taking source resistance of the generator into consideration.

Between the flywheel (which stores the energy) and the load (which consumes the energy) there are different sub-systems like, electrical machine and bi-directional power converter. A portion of extracted energy from the flywheel is dissipated as loss in these subsystems before it is finally delivered to the load. These losses can be catagorized as mechanical losses (drag, Bearing friction), electrical losses (hys-

teresis, eddy current, copper) and power converter losses (switching, conduction). Magnitude of these losses depends on the operating conditions like, motor speed, dc bus voltage, switching frequency, load current etc. Finding out the sources of these losses and their quantification are done. This has helped in adopting suitable loss mitigation techniques.

A new BDC topology has been designed using a combination of fast turn off SCR and IGBT with a novel control logic implementation to achieve zero switching losses through Zero Voltage Transition (ZVT) and Zero Current Transition (ZCT) techniques. This new scheme ensures Zero Switching Power Loss (ZSPL) during turn-on as well as turn-off of transition of the devices in both buck and boost modes of operation of the BDC. This has resulted in improved efficiency, reduced EMI problems and reduced voltage stress on the power devices. A detailed design procedure has been evolved.

BDC is used as a boost converter to maintain dc bus voltage when energy is being harvested from the flywheel. One of the limitations of boost converter is dependency of its maximum achievable voltage gain on the ratio of its source resistance to load resistance ratio. This will limit the amount of harvested energy from a flywheel and reduces the energy efficiency at lower input voltages. This was the motivation for evolving a scheme/topology whose voltage gain is independent of its source resistance or load resistance leading to the development of novel scheme. This has been built which uses a novel unique combination of dual/multi armature winding permanent magnet BLDC machine and a buck converter. This resulted in 15 – 20% enhancement in the harvested energy from the flywheel in comparison with the existing schemes. This has also helped in overcoming the limitations of the boost converters. A detailed study and analysis has been carried out to find the effect of generator winding configurations, control strategies adopted in the proposed scheme.

Application areas of FES system includes the Pulse power supplies, Battery less UPS for short time back up, regenerative braking in transportation etc. Analysis and design of one proto type Capacitor Charging Power Supply (CCPS) using FESS as energy storage device done and presented.

This thesis has been prepared on each of these works and presented.

Contents

List of Tables

List of Figures

Nomenclature

Symbols	: **Definitions**
A_c	: Area of section of the pole face (m^2)
A_p	: Area under one pole arc (m^2) for one stamping of core
B	: Flux density produced in stator core (Weber)
B_a	: Flux density produced in stator core due to the armature current (Weber)
B_F	: Flux density produced in stator core by rotor magnet (Weber)
C	: DC Bus capacitor (F)
C_o	: Output capacitor (F)
C_r	: Resonant circuit capacitance (F)
D	: Duty cycle of the switching pulses
d	: Perturbed duty cycle
$\hat{d}$	: Perturbation in duty cycle
$D(t)$	: Instantaneous value of duty cycle of the buck converter
D_{max}	: Maximum duty cycle of the switching pulses
D_{min}	: Minimum duty cycle of switching pulses
e_b	: Armature instantaneous induced voltage/ phase (V)
E_b	: Armature peak induced voltage/ phase (V)
E_c	: Energy required to be stored in the capacitor per cycle (J)
E_h	: Harvestable energy from the flywheel (J)
E_u	: Useful energy from the flywheel (J)
E_{peak}	: Peak armature induced voltage (V)
e_R, e_Y, e_B	: Generated Voltage in each phase (V)
f_c	: Pulse power repetition frequency (Hz)
f_{max}	: Max frequency of operation (Hz)
f_{sw}	: Switching frequency of IGBT gate pulses (Hz)
G	: Gain of the Boost converter
G_{max}	: Maximum value of gain of Boost converter
I_a	: Peak armature current (A)
$I_a(t)$	: Instantaneous armature current (A)
$I_c(t)$	: Main device on- state current in Amperes
$i_c(t)$	: Instantaneous current through main device in Amperes
i_R, i_Y, i_B	: Instantaneous current through three phases in Amperes
$I_{cr}(t)$	: Instantaneous current through resonant capacitor in Amperes
I_{dc}	: DC Bus current (A)
$I_{m(av)}$	: Average motor input current (A)
I_L	: Load current in Amperes
I_{Lav}	: Average Load current (A)
I_o	: Output current in Amperes
I_{peak}	: Peak Armature current (A)
$\hat{I}_a$	: Perturbation in armature current (A)
J	: Moment of inertia of the flywheel (kg m^2)
K_e	: Voltage constant of the machine
K_v	: Voltage constant of the induced voltage (Volts/RPM)

K_x	: Proportionality constant relating I_a and B_a
L_a	: Armature Inductance / Phase (H)
L_B	: Inductor in series of the boost converter (H)
L_{crit}	: Critical armature leakage inductance/phase
L_r	: Resonant circuit inductance (H)
m	: No of slots/pole/phase
M	: Mass of the flywheel (kg)
N_c	: No of energy pulses in one cycle of flywheel discharge
N_{max}	: Maximum running speed of the motor (RPM)
N_r	: Running speed of the motor (RPM)
p	: No of poles of the machine
P_a	: Total anomalous losses (W)
P_{av}	: Average power input to capacitor per cycle (W)
P_{ave}	: Average generated mechanical power (W)
P_{cu}	: Armature copper loss (W)
P_{eF}	: Field flux dependent eddy power loss (W)
P_{ei}	: Armature current dependent eddy power loss (W)
P_{eiT}	: Total current dependent losses (W)
P_{eT}	: Total eddy current losses (W)
P_h	: Total hysteresis losses (W)
P_{in}	: Input power (W)
P_{Load}	: Electrical power available (Watts)
P_{Loss}	: Power loss (Watts)
$P_{m(av)}$	: Average input power to motor (W)
P_{mech}	: Generated mechanical power (Watts)
P_o	: Output power in Watts
P_p	: Peak pulse power (W)
P_s	: Armature current dependent loss (W)
P_{SW}	: Switching power loss in the power device (W)
p_R, p_Y, p_B	: Instantaneous power through three phases (W)
$\Re$	: Reluctance of the air gap flux path in the machine
R	: Radius of flywheel (m)
R_a	: Armature resistance / Phase (Ω)
R_{cu}	: Equivalent resistance for copper loss (Ω)
R_e	: Flux dependent eddy current loss component(Ω)
R_{eF}	: Equivalent resistance for field flux dep. eddy loss (Ω)
R_{ei}	: Equivalent resistance for current dep. eddy loss (Ω)
R_h	: Hysterisis loss components (Ω)
R_L	: Load resistance connected across dc bus (Ω)
R_s	: Equivalent Source resistance of boost Converter(Ω)
sp	: Slot pitch under one pole arc (m)
T	: Coasting down time of flywheel (s)
T_o	: Half of the resonance period (s)
T_{acc}	: Time taken by flywheel to reach rated speed (s)
T_{bu}	: Power back up time (s)
T_c	: Capacitor charge/discharge pulse period (s)
T_{excess}	: Time duration for which resonant current exceeds the load current (s)
ω	: Rotor mechanical speed in rad/sec

ω_{max}	:	Maximum rotor mechanical speed in rad/sec
ω_{min}	:	Minimum rotor mechanical speed in rad/sec
V_{dc}	:	DC Bus Voltage (V)
$\hat{V}$	:	DC Bus set Voltage (V)
V_g	:	Generator voltage (V)
V_{mg}	:	Motor/generator voltage (V)
$V_{CE}(t)$	:	Collector emittor voltage (V)
$V_{mg(min)}$	:	Minimum motor/generator voltage (V)
$V_{chop-in}$	:	Chopper input voltage (V)
v_R, v_Y, v_B	:	Instantaneous drive output voltage w.r.t. DC- (V)

Abbreviations

BDC	:	Bidirectional Converter
CCPS	:	Capacitor Charging Power Supply
DWBC	:	Dual Winding Buck Converter
FEM	:	Finite Element Method
FESS	:	Flywheel Energy Storage System
FFT	:	Fast Fourier Transform
IES	:	Intermediate Energy Storage
MWMC	:	Multi Winding Multi Chopper
MWSC	:	Multi Winding Single Chopper
PM-BLDC	:	Permanent Magnet Brushless DC
PMSM	:	Permanent Magnet Synchronous Machine
SSBC	:	Single Stage Boost Converter
TSBC	:	Two Stage Boost Converter
THD	:	Toltal Hormonic Distorsion
UPS	:	Uninterruptable Power Supply
ZCS	:	Zero Current Switching
ZCT	:	Zero Current Transition
ZSPL	:	Zero Switching Power Loss
ZVS	:	Zero Voltage Switching
ZVT	:	Zero Voltage Transition

Chapter 1

Introduction

1.1 Energy storage: Why and How

Most prevalent source of energy nowadays is Electrical energy. We get this energy from the power plants. One of the difficulties with power plants (and even more so with forms of renewable energy such as wind and solar power) is that they don't necessarily produce electricity constantly which precisely matches the rise and fall in demand over the course of a day. In many a time synchronizing the power generation with demand (by load) is rather difficult. To tide over this difficulty, a mechanism is required which stores the energy when it is available and releases the same later as and when it is demanded by the load. This system is called an Energy storage system. The electronic devices like communication networks, industrial process controllers, personal computers, electrical machinery and apparatus demand higher quality of electricity without any interruption. The energy storage devices can be utilized [1, 2] for protecting these equipments from momentary voltage dips, voltage sags due to overload, power failure caused by line faults. But electrical energy in an ac form cannot be stored in the same form.

However, it can be stored after converting it to dc in the form of electromagnetic energy (current, in inductors), electrochemical energy (Chemical bonding, in batteries), kinetic energy (angular velocity, in flywheels) or as potential energy (as voltage, in capacitors) form by using a power converter. Each of these methods has its own advantages and disadvantages [3]. Most important characteristics of these devices are the amount of energy that can be stored and rate at which the energy can be transferred to/from the energy storage device. The amount of energy that can be stored is the property of the storage device and the energy transfer rate depends mainly on the peak power rating of the power converter and the response time of the storage device. A comparision in terms of energy density, efficiency, cost of batteries, FES, ultra capacitor, compressed air etc are given in table table 1.1. It can be seen from this table that the energy density is lowest for ultra capacitor (2 W/kg), lead acid batteries (30 W/kg) and flywheels (50 W/kg) where as the efficiency about 95% for both ultra capacitors and FESS and for batteries it is 70% only.

The flywheel stores energy in the form of angular velocity of rotating the mass. Out of many energy storage devices available, the flywheel has the merits like, environmental friendly, long life, and limit less charge and discharge cycles. Flywheels compete with chemical batteries, presently the most common energy storage device, in terms of power, energy density, cycle life, charging time, operating temperature range, environmental friendliness, and maintenance needs [4, 5, 6]. Another advantage of flywheel is that, by a simple measurement of the rotating speed, it is possible to know the exact amount of stored energy and to absorb or provide large amounts of energy in a shorter time than with a traditional chemical battery [7]. Out of various devices, the flywheel is considered here.

Table 1.1: Comparision of various energy storage devices

Technology	η in %	Energy Density Wh/Kg	Power Density	Expected life in Years	Energy capital cost in \$/kWh	Cycle life (kCycles)
Lead Acid	70 - 80	20 - 35	25	5	200	0.2 - 2
Ni-Cd	60 - 90	40 - 60	14 - 180	10	-	0.5 - 2
Compressed Air	40 - 50	10 - 30	-	-	250	> 20 years
Flywheels	95	> 50	5000	30	800	> 20
Li-Ion	70 - 85	100 - 200	360	-	-	0.5 - 2
Pumped Hydro	65 - 80	0.3	Low	-	16.8	> 20 years
Capacitors	95	N/a	Low	Good	300	-

(Courtesy: "Energy Storage System for Transport Grid Applications", IEEE Trans. on Ind. Electron. Vol. 57, No. 12, December 2010.)

1.2 Historical background of Flywheel Energy Storage

The origin and use of flywheel technology for mechanical energy storage began over 100 years. These were solely to keep machinary running smoothly from cycle to cycle as in the case of automobile built [8]. The earliest form of a flywheel is a potter's wheel that uses stored energy to shape the earthen vessels. The wheel is a disc made of wood, stone or clay. It rests on a fixed pivot and can be rotated around its centre. The main disadvantages are friction and material integrity. Iron flywheels have greater material integrity than flywheels made up of wood, stone or clay. Flywheels have been used for a long time as mechanical energy storage devices. These flywheels were used mostly for smoothing torque pulses in steam engines [9]. Flywheels store energy in the form of angular velocity. Energy stored in a flywheel can be computed using the following relation.

$$E = \frac{1}{2} J\omega^2 \tag{1.1}$$

Where "E" is the amount of energy stored in a flywheel, "J" is the moment of inertia and "ω" is angular velocity. The moment of inertia is a physical quantity and can be computed using following relation.

$$J = \frac{1}{2}mr^2 \tag{1.2}$$

Where "J" is the moment of inertia, "m" is the mass and "r" is the radius of the flywheel. During the years after industrial revolution, for higher energy storage, the trend was mostly towards increasing mass rather than increasing speed. Large flywheels are made from cast iron, with heavier rims, were built for the largest engines. However, with the advent of the small internal combustion engine in the middle of 19^{th} century, the trend shifted towards high-speed flywheels with low inertia for automotive applications. More recently, the ability of a flywheel to deliver high power in a short time has been used in applications such as mechanical presses, lubrication or cooling pumps, mine locomotives, inertial friction welding and inertial starters [9]. The second part of 20^{th} century saw advances in the field of high-strength composite materials. Composite flywheels can operate at higher speeds and can store more energy for a given mass than a conventional steel flywheel. The concept of a flywheel for smoothing torque pulsation, energy storage system for electric vehicles and stationary power backup was proposed during early 1970's [8].

1.3 Flywheels of industrial revolution

The best known flywheels which are used in factory steam engines, traction engines etc are from the Industrial Revolution period. During 18^{th} or 19^{th} century almost every machine used in any industry had a huge flywheel somewhere in the mechanism. Though the origins and use of flywheel technology for mechanical energy storage began over 100 years ago, the real development of flywheel carried out during the Industrial Revolution [8]. The widespread availability of iron and steel during the Industrial Revolution made it possible to make high precision flywheels, which played a vital role to ensure the smooth and efficient operation of the engines. One of the first modern dissertations on the theoretical stress limitations of rotational disks (isotropic only) is the seminal work by Dr. A. Stodola [10] whose first translation to English was made in 1917. The next big milestones were during the 1960's and 1970's when NASA sponsored programs proposed energy storage flywheels as possible primary sources for space missions. However, it was not until the 1980's when microelectronics, magnetic bearing systems and high power density motor-generators became enabling technologies [8].

Meanwhile, road vehicles, ships, trains, and airplanes were using internal combustion engines powered by gasoline, diesel, and kerosene. Flywheels were generally large and heavy and had no place inside a small vehicle like a car. As a result, flywheel technology fell somewhat by the wayside as the 20^{th} century progressed [11].

1.4 Modern Flywheels

Since the mid-20^{th} century, interest in flywheels has picked up again, largely because people have become more concerned about the price of fuels and the environmental impact of using them [11]. Flywheels can be used for saving energy. Since 1950s, European bus makers such as M.A.N. and Mercedes-Benz have been experimenting with flywheel technology in vehicles known as gyro buses [11]. The basic idea is to mount a heavy steel flywheel between the rear engine of the bus and the rear axle, so that it acts as a bridge between the engine and the wheels. Whenever the bus brakes, the flywheel works as a regenerative brake, absorbing kinetic energy and slowing the vehicle down. When the bus starts up again, the flywheel returns its energy to the transmission, saving much of the braking energy that would otherwise have been wasted. Modern railroad and subway trains also make widespread use of regenerative, flywheel brakes, which can give a total energy saving of perhaps a third or more. Some electric car makers have proposed using super-fast spinning flywheels as energy storage devices instead of batteries [12].

One of the big advantages of this would be that flywheels could potentially last for the entire life of a car, unlike batteries, which need regular maintenance and very expensive replacement perhaps every 3-4years. In the last few years, race cars have also been using flywheels, though more to provide a power boost than to save energy [11]. This technology is called KERS (Kinetic Energy Recovery System) and consists of a very compact and high speed flywheel that absorbs energy which would have normally be lost as heat during braking. The driver can flick a switch on the steering wheel so the flywheel temporarily engages with the car's drive train, giving a brief speed boost when extra power is needed for acceleration. With such a high-speed flywheel, safety considerations become hugely important; the flywheel is fitted inside a sturdy container to stop it injuring the driver if it explodes [13]. Some forms of KERS use electric motors, generators, and batteries to store energy instead of flywheels, in a similar way to hybrid cars.

At times when there is more electricity supply than demand (such as during the night or on the weekend), power plants can feed their excess energy into huge flywheels, which will store it for periods ranging from minutes to hours and release it again at times of peak need. In Stephentown, New York, Beacon Power uses flywheels to provide 20 megawatts of power storage to meet temporary peaks in demand [11]. They are also used in places like computer data centers to provide emergency, backup power in case of outages.

1.5 Energy storage capacity of a flywheel

The energy stored in a flywheel can be increased either by increasing its moment of inertia or its running speed or both. Some FES designs utilize hollow cylinders for the flywheel allowing the mass to be concentrated at the outer radius of the flywheel to increase their moment of inertia for the given weight [14]. Running flywheels at higher speed will result in higher rotational losses due to air drag and bearing friction [15, 16]. This will result in significant self-discharge in no load condition. Therefore high-speed flywheels are provided with vacuum enclosure to reduce air resistance [16]. The use of magnetic bearings also helps overcome the problems with conventional high loss bearing [17].

1.6 Flywheel Energy Storage System(FESS)

The "Flywheel Energy Storage" or "Mechanical batteries" describes a system which consists of a flywheel, a motor/generator and power converter. The FESS taps the energy from an electric source, stores it as a kinetic energy of rotation, and delivers it to the load as electric energy. The electrical machine (working as motor) accelerates the flywheel to store the energy mechanical form. While the flywheel is decelerating, the same machine works as generator to deliver the energy to the load in the electrical form [18]. Block diagram of a typical FESS is shown in Fig. 1.1. As shown in the figure the flywheel is coupled to the electrical machine which is connected to the dc bus through a Bi-Directional Converter (BDC). The flywheel can be housed in a vacuum chamber to minimize the windage. A suitable controller is used for facilitating interface between the source and the flywheel [19].

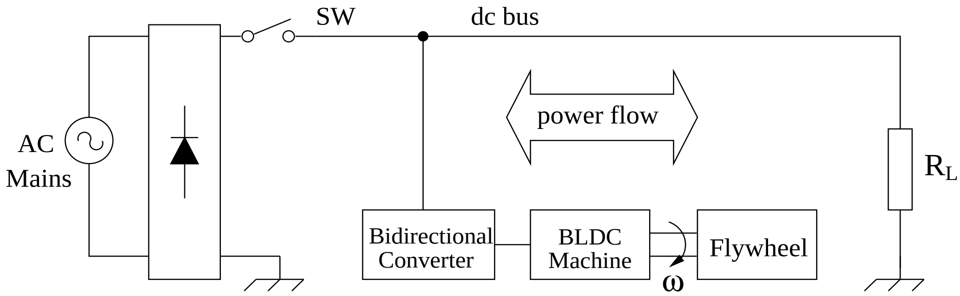

Figure 1.1: Block diagram of a typical FESS

1.7 Principle of working of an FESS

As shown in the Fig. 1.1, the bi-directional converter along with the electrical machine facilitates the energy flow to and from the flywheel. In such a system the energy is stored in the flywheel by accelerating it. The amount of energy stored depends on the moment of inertia and running speed of the flywheel. Energy delivered to the load (extracted from flywheel) when the flywheel is decelerating is given by,

$$E_h = \frac{1}{2} J(\omega_{max}^2 - \omega_{min}^2) \tag{1.3}$$

The energy can be utilized only if it is extracted at a constant dc bus voltage. Energy thus extracted at constant dc bus voltage and utilized is called as "harvestable energy" from flywheel. As the energy is extracted from the flywheel, speed of flywheel and induced voltage of the generator (thereby dc bus voltage) drops. This is shown in the Fig. 1.2. During this period the BDC is operated as a boost converter to boost the generator voltage for maintaining the dc bus voltage constant. It is clear from (1.3) that, for a given top speed, the harvestable energy depends on the lowest speed down to which the energy can be extracted from the flywheel at constant dc bus voltage.

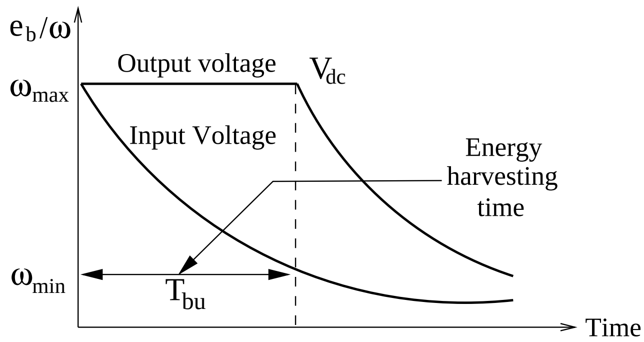

Figure 1.2: Voltage time characteristic of an FESS

1.8 Objective of this work

To understand the system we need to build one prototype FES system. This will help us to identify the source of the losses, apportion and analyse the losses in the system. From this we can find out the appropriate mitigation technique. Analysis of various BLDC machine parameters will help in developing techniques of maximizing the harvested energy from the flywheel. Losses due to switching of power devices at higher speed of flywheel contribute significantly to the total loss of the bidirectional converter particularly at lower generator speeds. Hence reduction of these losses will increase the overall efficiency of the FESS. The boost converter is part of an FESS and major limitation of this converter is the dependency of its maximum achievable voltage gain on its source resistance limiting the amount of energy harvested from the flywheel. Therefore, an alternate technique required to be adopted to overcome the limitations of boost converter. Finally evaluation of the designed FESS can be done using it in various different applications.

Taking above mentioned aspects into consideration the objectives of this work are as listed below:

- Selection of suitable topology and prototype development of FESS
- Investigation and analysis of the BLDC machine parameters and losses on the performance of the FES system
- Design of a new soft switching topology using ZVT/ZCT technique to achieve high efficiency bidirectional converter
- Analysis and design of novel dual winding BLDC machine and buck converter combination to overcome the limitations of conventional boost converter and extension of the same to the multi-winding BLDC machine
- Evaluation of the proposed design of FESS using the application such as UPS and pulse power source

1.9 Contributions from this work

One FES System was built, tested, performance parameters found out and limitations are brought out. Sources of various losses in the system are identified; new ZCT/ZVT switching technique is proposed for reducing switching losses in the power device; effect of BLDC generator parameters which influence the quantity of energy harvested are analysed. A novel scheme has been proposed which uses a unique combination of dual-armature winding permanent magnet brushless dc machine and a buck converter to overcome the limitations of conventional boost converter and the same has been extended to multi-winding BLDC machine. Proposed new topologies/schemes are simulated and validated experimental results.

1.10 Organization of the thesis

The thesis is organized as follows:

Chapter 2 covers the discussion on the key issues to be considered for the design of FESS, presentation of literature survey carried out, discussion on the latest developments in this field, design challenges involved in the selection of various subsystems and the applications of FESS.

Chapter 3 focuses on hardware design aspects of an FESS, analysis and design of the controller, study and analysis of the effects of generator parameters on the boost converter performance. The experimental results are included.

Chapter 4 covers the topic of identification, apportioning and analysis of the sources of various losses and their mitigation techniques.

Chapter 5 covers the identification of the sources of current dependent losses in BLDC machine, modelling them as a series resistances using FEM technique, study the effect of leakage inductance on the machine performance, validation of the studies through simulation and experimental results,the guidelines for the design of BLDC generator and selection of appropriate bidirectional converter topology for optimal energy harvesting.

Chapter 6 presents a novel FESS scheme using a multi winding BLDC generator combined with new switching topology for enhancing the harvested energy from a flywheel. This chapter also covers the presentation of the results obtained from experimental prototype and validation of the predictions

Chapter 7 covers the performance analysis of prototype model of the FESS based capacitor charging power supply.

Chapter 8 gives the conclusions made from the analysis, studies and experiments carried out and scope for the further work.

Appendix-A gives the computation of motor current, generator current, guidelines and procedure of selection of the generator and power converter required for building FES system.

Appendix-B gives the relationship between the flywheel speed and time during energy harvesting period.

Appendix-C gives the photographs of the prototype FES system.

Appendix-D gives the technical specifications of semiconductor.

Appendix-E gives the cost benefit analysis of adopting an FESS.

Chapter 2

Literature Survey

This chapter covers the brief report of the survey done for the literatures available in the field of Flywheel Energy Storage and its applications. Many researchers have published literatures on the design of the flywheel, selection and design of Bi-directional converter, ZVT/ZCT technique of switching; Multi/Dual Winding generators are covered in the literature survey. Detailed report of the literature survey carried out is presented in this chapter.

2.1 Challenges of designing an FES system: An over view of global research

The key issues considered in the design of an FESS are selection and design of various subsystems, power transfer, operating losses, harvestable energy, failure management, and manufacturability [14]. The design process of an FESS starts with the choice of the appropriate bearing suspension system, selection of the suitable electrical machine, design of the power converter and flywheel and finally making a control strategy. As per the available literature, the emphasis was given by the designers for increasing the energy density, overall energy efficiency and optimum energy harvesting. The literature survey carried out covers the topics related to the selection procedures and design considerations of various subsystems.

2.1.1 Flywheel

Size and shape of the flywheel are selected such that maximum energy storage should be possible for a given mass. A compact flywheel can be built by choosing higher value of angular velocity. Factors which limit the maximum possible angular velocity are, tolerable stress of the material, availability of bearings, flywheel balancing systems etc. Moment of inertia can be increased for the given mass by concentrating the mass at the periphery of the wheel. Flywheel can be built by using a rim and connected to the centre shaft by spokes. This will have highest possible moment of inertia for the given mass. Various other possible geometries for the flywheel are constant stress disc, conical disc, constant thickness disc, cylindrical shaped disc etc. Geometry of the flywheel shall be decided on the material and the operating speed. Generally either constant thickness disc or cylindrical shaped flywheel is used due their simplicity of design, ease of fabrication, maximum extent of material usage etc [14].

2.1.2 Bearings

Running the flywheel at higher speed results in higher rotational losses due to the air drag and the bearing friction [15, 17]. Therefore low loss bearings at the rated speed are required. The loss in the bearing is directly proportional to the operating speed and load on the bearing. Both the parameters are decided by the energy storage requirements. The bearing with lowest possible coefficient of friction shall be selected. Hybrid, Ceramic ball or Magnetic bearings are capable of running at higher speed with low frictional losses. Many researchers attempted to use the magnetic bearings in various configurations in the area of pumps, compressors, milling and grinding spindles, turbine engines and centrifuges [20, 21, 22].

2.1.3 Electrical machine

The electrical machine required for the FESS facilitates charging the flywheel coupled to its rotor and discharges the same as and when demanded by the load. The typical prime movers for the flywheel are Induction motors (IM) [23] or Switched/Synchronous Reluctance Motors (SRM) or Permanent Magnet synchronous Motors (PMSM)/ Brushless DC (BLDC) motor [20]. With the advent of high energy permanent-magnet material the PM machines are easily available [21]. Compared to the SRM or IM, the Permanent Magnet machines offer high torque densities combined with low rotor losses. The PM makes it suitable to use it as generator without any additional excitation source [20, 24]. Since the inertia and operating speed are very high, the machine shall have the features like, no moving contact (absence of friction or arcing), minimum torque ripple (to reduce the mechanical vibrations), and constant torque right from zero speed to full speed. The selected machine should be able to work as a generator in the absence of the mains supply. Hence, PM BLDC machine is attractive for this application due to their high efficiency, absence of EMI problems and mechanical reliability due to the absence of brushes [20, 21].

Lee et. al. [25] have analyzed and devised an elegant control scheme for maximizing power density and efficiency for BLDC generators. Other authors [26, 27] have discussed the control strategies of the BLDC generators. There are BLDC machines available with two armature windings called as "Dual armature wound BLDC (DW-BLDC) machines". In some applications [28], DW-BLDC machines have been used for achieving higher starting torque. Dual winding method of BLDC machine have also been proposed in [29] for driving the motor to high speed with large starting torque with an automatic changeover from dual to main winding to maximize the torque output. In some other applications, dual armature winding BLDC machines have been proposed for reducing the output voltage ripple [29, 30, 31] when the machine is used as a generator.

Over last two decades, the power density, efficiency and fault tolerance were of great importance such as electric propulsion applications, multiphase motor drives obtained recognition again. For a given output power, multiphase motor drives can reduce the stator currents per phase, which leads to the usage of semiconductor switches with lower power rating and by increasing the number of phases, the torque per ampere for the same volume machine also becomes higher. Multiphase BLDC motors are increasingly utilized in traction or propulsion applications due to the higher efficiency, power density and relatively easy control .

2.1.4 Bi-directional power converter

Bi-directional converter along with a controller serves as a drive for motoring action and acts as a voltage regulating system for generating action of the above mentioned electrical machine [32]. It facilitates the energy flow to and from the flywheel. When the BLDC machine is acting as a generator, the power can be drawn from the same using active rectifiers or boost converter. A standard six switch voltage source inverter topology can be used either as a 3-phase BLDC motor drive or as a boost converter by appropriately controlling the IGBT gate drive pulses. Most important aspect to be considered while selecting the BDC is that it will ensure maximum possible energy harvesting for a given top speed of the flywheel as well as controlled charging of the flywheel. Higher the voltage gain of boost converter, higher is the energy extracted from the flywheel for a given top speed of the flywheel [32]. However, the voltage gain of the boost converter is very sensitive to the ratio of its source resistance to load resistance [33]. Most important requirements of FESS in generating mode are, high voltage gain of the boost converter, high efficiency and optimal energy harvesting [34]. Some researchers have proposed a single stage boostconverter by integrating BLDC generators, diode rectifier to a "C"uk DC/DC converter for small wind power applications [35]. Advent of Fast processors, availability of high power semiconductors has enabled the designer to design the converter and controller for FESS with features like, ease of control, compact power circuit, high reliability [36].

Higher overall efficency of bidirectional converter can be achieved by reducing its losses. Losses due to switching of the power devices at higher frequencies contribute significantly to the total loss of the BDC particularly at lower generator speeds (lower induced voltage) in an FES system [37]. Switching power loss can be reduced either by Zero Voltage Switching (ZVS/ZVT) method or Zero Current Switching (ZCS/ZCT) method depending upon whether the voltage across the device is made zero during the turn ON or the current through the device is made zero during the turn OFF transition. It may be noted that in ZVS/ZCS, the resonant circuit comes in series with the main switch, whereas in the case of ZVT/ZCT, the resonant circuit doesn't come in series with the main switch - rather it comes into picture only during the transitions (ON to OFF and OFF to ON). This makes ZVT/ZCT topologies suitable for PWM applications. In ZCT technique, the current through the switching device becomes negative (i.e. anti-parallel diode conducts) during the switching transition, making it a "true" Zero Switching Power Loss (ZSPL).

Extensive research work has been carried out in the past three decades on ZCT [38, 39, 40, 41, 42], ZVT [43, 44, 45], ZCS [46, 47] and ZVS [46, 47, 48] schemes. Various topologies and configurations have been proposed to reduce switching losses. Out of these topologies some use ZCS [49, 50] and/or ZVS [49, 51, 52], while the others use low voltage turn on [47]. Topologies proposed in [46, 53] use snubber assisted turn off of the switching device, which helps in loss reduction but does not eliminate the losses completely. Major challenges of low cost, high efficiency dc-dc converters are given in [48]. Li et. al., [40] give an excellent comparison of the various ZCT schemes.

Some schemes proposed in the previously reported work, have zero voltage turn on and/or low current turn off while some others have low voltage turn on and/or zero current turn off. In the past, researchers have worked on a variety of topologies and control logic to achieve this. Low current turn off is generally implemented by connecting snubber capacitors parallel to the switch [51]. The low voltage turn on is achieved by connecting an inductor in series with the switch [52, 54]. If a converter circuit is required to be operated where the switching device is subjected to high dynamic stress only at turn on, then, only a series inductance need be provided [42]. Similarly, if the circuit is required to be operated where high dynamic stress occurs at turn off, then, only a shunt capacitance is necessary. When an IGBT is used as a switching device, this capacitor value should be large enough to take care of the tail current of the device, which demands large initial inductor current to discharge [52]making the snubber related circuits bulky and the snubber losses high. Therefore, in applications where IGBT is used, resonant transition switching technique (ZCT) is more desirable. To help the designers, some researchers have developed mathematical expression to determine the occurrence of soft-switching for a general topology of zero voltage transition (ZVT) converters for choosing appropriately the values of inductance and capacitance for the auxiliary resonant branch ensuring ZVT [53].

In the case of FES systems, the Bi-directional converter, where IGBT is the preferred switching device, is required to have ZCT switching in both buck and boost mode of operation to achieve true ZSPL operation. Even though many researchers in the past have proposed ZCT switching, soft switching and active clamp [41, 55, 56, 57, 58], they are for buck or boost converter as independent topologies. Some of the recent publications available in the area of medium power BDC are given in [34, 45, 52, 59]. Generally, the configurations used in these BDC include coupled inductors based converters, series resonant circuits and half-bridge circuits with PWM. Investigations into major families of isolated BDCs which employ soft-switching techniques are reported in [60]. One such resonant tank isolated BDC featuring ZVS for input side chopper and ZCS for output rectifier switches is proposed in [61] and another ZVS-PWM non-isolated bidirectional converter dc-dc converter with steep conversion ratio is proposed using auxiliary circuits [62]. In both the proposals, ZVS is achieved in both buck and boost modes of operation but only for turn on transition.

2.1.5 Controller

The motor is supplied with controlled ac current at the desired frequency through the bi-directional power converter. The controller generates the gate control pulses for the semiconductorswitches of BDC. This ac current generates the accelerating torque of the motor to charge the flywheel. During deceleration, the flywheel discharges through BDC to the DC bus. During this period the controller makes the BDC to operate as boost converter.

Armature current control in motoring mode and dc bus voltage control in generating mode operation is achieved by adopting a feed forward controller [63] or a feedback controller [64]. Feed forward controller is used for compensating the effect of reducing speed of the flywheel and feedback controller for maintaining the output dc bus voltage constant while energy is being extracted from the flywheel.

2.2 Past research work on applications of FESS

Lot of research work have been carried out on the applications of FESS in various areas like, storage, distribution and utilization of electrical energy. The applications of FESS vary from power smoothing in the grid to Transport/Hybrid vehicles to UPS applications [9, 12, 65, 66]

2.2.1 Power levelling in the grid

A flywheel stores energy very efficiently and has the potential for very high pulse power compared with a chemical battery [67]. In addition, a flywheel has a relatively long life and is not affected by ambient temperature as is a chemical battery. On the other hand the reduced cost of power electronic devices as well as the breakthrough of new technologies in the field of energy storage makes it possible to incorporate them in to power system [2]. FESS are used for power compensation in the energy sources which contain power fluctuations (such as wind energy). Power smoothing is achieved by operating the machine as a motor or generator to store or retrieve energy from a rotating flywheel [1]. Flywheel controlled by power electronics enables to exercise a dynamic control over the flow of active and reactive power. Therefore they have great potential for improving the dynamic operation of power system.

2.2.2 Transport/Hybrid vehicles

Flywheel systems are characterized by being able to deliver very high peak power; but it is limited by power converter [3]. FESS has high power and energy density. It can handle virtually infinite number of charge-discharge cycles. Therefore, they are typically employed in transportation and power quality applications that require compact energy storage system and large number of charge-discharge cycles [65]. The fuel efficiency and the performance of the vehicle is limited by the performance of the energy storage device [19].

The environment pre-occupation and directives related to the reduction of pollution and noise due to transport have contributed to the research activities in the field of clean vehicles to improve technology and architectures of hybrid vehicles [68]. Electrification of transportation sector is seen as an effective way to substantially reduce the overall use of hydrocarbons. Electrified vehicles with plug-in capability contain an energy storage element that is capable of storing power from the grid. If this power is produced using renewable energy sources, the overall reduction in the use of hydrocarbons is substantial [3]. Combination of a battery and an electro-mechanical storage system will enhance the available on-board energy. The basic principle is based on usage of high rotational speed flywheel to store kinetic energy. A high efficiency motor-generator and converter allow to supply and recover the energy in electrical form during the vehicle acceleration and braking respectively [68]. Though the flywheel has the advantages like, long life, free from depth of discharge effects, accepting and delivering large amount of energy in a very short time, due to the current cost of the flywheels they are initially being considered for large vehicles where the battery cost is inherently high [69].

2.2.3 Stationary power backup (UPS)

Flywheel energy storage systems are generally more reliable than batteries [16], so applicability is mostly an issue of cost-effectiveness. Batteries will usually have a lower initial investment than flywheels, but suffer from significantly shorter equipment life, higher foot print and higher operation/maintenance expenses. UPS batteries are sized to provide backup power for period ranges from about 5 minutes to around 1 hour. This is commonly about 15 minutes [16]. Flywheels, on the other hand, provide backup power for period about 60 seconds. This is enough time to allow the flywheel to handle power outages until a backup generator can come up to full power (generally in 30 seconds).

2.2.4 Pulse power

Applications such as Electromagnetic aircraft launch system, Electromagnetic guns, Electromagnetic welding etc require dc power source which need to supply large power to the load for very short duration. Typical capacitor charging power supply consists of a voltage booster with a current limiter. Switch mode power supplies are almost universally employed as capacitor chargers due to their compact size and high performance [70]. Selection of this capacitor charging system depends on pulse energy repetition rates and pulse to pulse repeatability as demanded by the load [71]. In contrast to conventional high voltage power supplies which delivers constant or near constant power to its load, CCPS with charging current limiter, supplies the output power which varies over a wide range [72]. The charging mode is characterized by high peak power. The instantaneous output power is almost zero at the beginning of the charging mode and highest at the end of the charging mode [72]. The characteristics of an ideal CCPS are, low charging time, high efficiency, high discharging rate, compact in size, good reliability, long life, lowest input power for a given pulse output power etc [73].

Charged capacitors can acts as power sources and ideally suited for such applications. Hence there is need for a dc power supply which can be used for charging this capacitor. This power supply requires high rated switchgears and power semiconductors devices at the input circuitry even though the average power drawn from the mains is low. To avoid high rated power components at input circuitry, an Intermediate Energy Storage (IES) device can be used. This IES device stores energy (drawing low average power from input mains) for longer duration and deliver same to the load in shorter time (higher power). This IES device should have capacity of high discharge rate to enable fast charging of the capacitor without deterioration of its own life. Flywheel is an ideal choice for IES device used in CCPS.

2.3 Summary

In this chapter overview of the research work carried out globally has been given. Design challenges of various subsystems used in the FESS are studied and presented. From this chapter we have found that following areas are not covered sufficiently by the researchers who have worked on the field of energy storage and harvesting:

- Analysis of various system parameters in detail which affect the performance of the FESS switching loss in the device
- True zero switching power loss schemes for BDC which makes both turn-off and turn-on losses in both buck and boost mode of operation
- Alternate topology/scheme to boost converter to overcome the limitation of its dependency on the maximum achievable voltage gain on the source resistance

Hence we have set following topics objectives in the work:

- Investigation and analysis of the BLDC machine parameters and the losses on the performance of the FES system.
- Investigation of new soft switching topology using ZVT/ZCT technique to achieve high efficiency bidirectional converter
- Analysis and design of novel dual winding BLDC machine and buck converter combination to overcome the limitations of conventional boost converter.

Design procedures for building an FESS and validation of the same with experimental results are dealt in the chapter-3.

Chapter 3

Selection of Topology and Prototype development

This chapter has focused on the hardware aspects of selection and designing of an FESS. Analysis and design of a controller for bi-directional converter to store the energy in the flywheel and extract an optimum energy stored in the flywheel is carried out. Physical design as well as prototype fabrication of the complete system has been carried out and is described in detail. Operating modes of FESS (motoring mode and generating mode) are identified; operating principle in motoring and generating mode is also explained in detail. Analysis of the experimental results is carried out and the limitations of the system are found out and presented.

3.1 Principle of operation and operating modes

The FESS is a device which stores the energy available from power grid in the mechanical form. Energy storage system stores the energy when it is available and releases the same for utilization as and when required. In any energy storage system, there are three processes namely storing the available energy in the device, retaining the same when idling and releasing the energy as and when required by the load. Flywheel is used for storing the energy in the form of angular velocity. The amount of energy that can be stored depends on the moment of inertia and running speed of the flywheel. It is coupled to the rotor of an electrical machine. This machine works as a motor for accelerating the flywheel to store the energy. The same machine works as a generator to discharge the flywheel while it is decelerating to return the energy back to the source. As the energy is extracted from the flywheel, the induced voltage (speed) of the generator drops. Hence there is a need for voltage boosting mechanism to maintain the output voltage constant.

A typical FESS is shown in Fig. 3.1. In this system dc bus which is backed by an energy storage device FESS and supplying power to the load R_L . This consists of a rectifier, a bi-directional converter (BDC), electrical machine and a flywheel. The flywheel is coupled to the rotor of the electrical machine supported by high speed bearings. The electrical machine is connected to the dc bus through a BDC. The BLDC machine coupled to a flywheel is hereafter called as “FES machine”. The bi-directional converter (BDC) along with the electrical machine facilitates the energy flow to and from the flywheel. In motoring mode the switch “SW” is

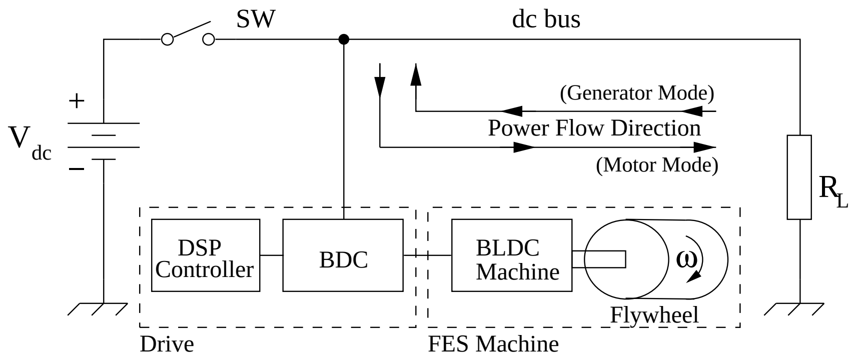

Figure 3.1: Block diagram of a typical FESS

closed; the machine draws the power from dc bus and accelerates the flywheel to store the energy; the BDC acts as a voltage buck converter. In generating mode the switch “SW” is opened; the same machine discharges the flywheel to return back the energy to the dc bus; the BDC acts as a voltage boost converter. The electrical machine may be either Permanent Magnet Brush-less DC (PMBLDC) machine or Permanent Magnet Synchronous Machine (PMSM). As the energy is extracted from the flywheel, speed and dc bus voltage drops. The BDC is operated as a boost converter to maintain the dc bus voltage constant. The input to output voltage relation of BDC (in boost converter mode) is given by [33]

$$\frac{V_o}{V_{in}} = \frac{1}{1-D} \times \frac{1}{1 + \frac{Rs/R_L}{(1-D)^2}} \tag{3.1}$$

Bi-directional converter used here is a conventional six-switch IGBT Bridge as shown in the Fig. 3.2. The BDC can be used either as a BLDC motor drive (motoring mode) or 3-phase boost converter (generating mode) by appropriately triggering a set of IGBT gates using control pulses. These two modes of operations are explained in the following sections.

3.1.1 Motoring mode (BLDC Motor drive; Storing energy in the flywheel)

There are three Hall Effect rotor position sensors mounted near the rotor shaft. Output signals of these sensors indicate the position of rotor at that instant with respect to stator windings. These signals are used for determining the instants of turning “ON” and turning “OFF” of appropriate combination of switches in the power converter to apply the dc voltage across the particular armature windings such that an average positive torque is produced to make the rotor to rotate. This makes the flywheel to accelerate and store the energy. The logic is implemented by generating six sets of waveforms to trigger the six switches in the bridge. These waveforms are ANDed with high frequency PWM pulses generated by the closed loop controller with armature current as feedback [19]. In this mode of operation the dc voltage is applied across the armature winding during the period when the induced voltage is flat in the trapezoidal waveform [Fig. 3.3]. The BDC functions as motor drive in this mode.

3.1.2 Generating mode (Boost converter; extracting energy from the flywheel)

In the absence of input power, the flywheel continues to run due to its inertia driving the machine which acts as a generator. If electrical load is connected across generator terminals, it draws current and utilizes this energy. The terminal voltage of the machine drops exponentially as the flywheel decelerates. It is desired that energy harvested (power drawn) from the flywheel during the deceleration is at constant voltage. Because the energy stored in a flywheel can be utilized only if it is extracted at constant dc bus voltage. Energy thus extracted and utilized is called as "harvestable energy" from the flywheel. It may be noted that the dc bus voltage (output) is required to be more than the generated voltage (input). Therefore the voltage boosting is required. The BDC functions as boost converter in this mode.

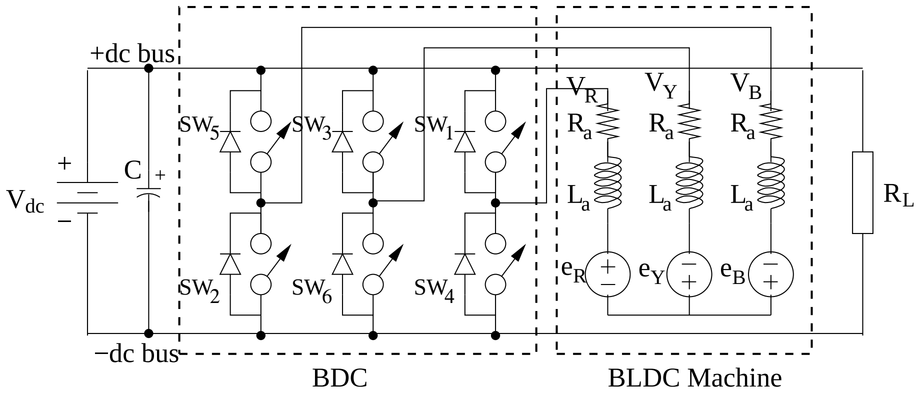

Figure 3.2: Bidirectional power converter

Operating principle in generating mode

The generator is connected to the dc bus through the BDC as shown in Fig. 3.2. Induced voltage waveforms in the armature winding of the generator are trapezoidal with the amplitude of the instantaneous voltage which is constant($= V_{dc}$) for a period of 120^o duration in both +ve and –ve cycles as shown in the Fig. 3.3

Phase voltages are shifted by 120^o with respect to each other. At any point of time during the full cycle, in first phase, the instantaneous induced voltage will be equal to dc bus voltage ($+V_{dc}$), in the next phase it will be $-V_{dc}$ and in the third phase, it will be sloping towards $+V_{dc}$ or $-V_{dc}$. If a load is connected across the generator terminals through power converter circuit (as shown in Fig. 3.2 the current will flow from the most positive potential point to the most negative potential point(i.e.$+V_{dc}$ to $-V_{dc}$). To operate the BDC as boost converter, the bottom switches [SW_2, SW_4, SW_6] are continuously gated with pulses at higher switching frequency f_s ; top switches [SW_1, SW_3, SW_5] are kept OFF permanently. When the bottom switches are made ON/OFF at switching frequency (keeping top switches off), energy flow takes place as follows:

(i) When any one of the SW_2, SW_4 or SW_6 (bottom switches) is ON:

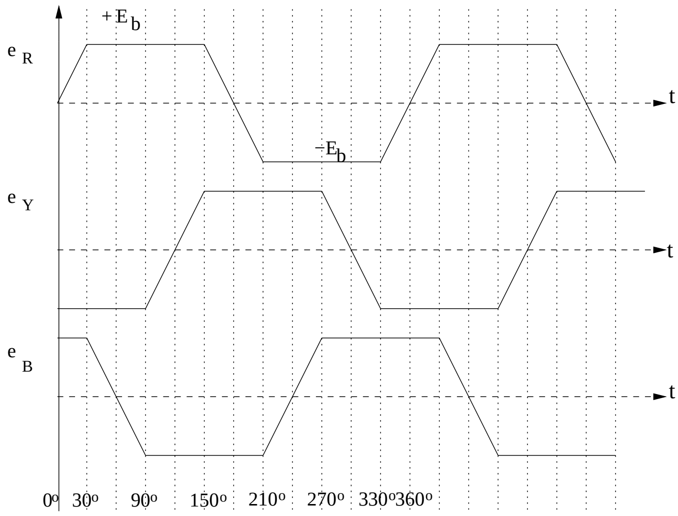

Figure 3.3: Generator induced voltage waveforms

Referring to Fig. 3.2, generator terminals are short circuited through one active "ON" switch, one diode and two series inductors ($2L_a$). For example, when SW_4 is made ON, current starts from +ve node of e_R of R phase, flows through L_a R_a of R phase, SW_4, D6, L_a R_a of Y phase and reaches – ve node of e_Y of Y phase. The machine current (inductor energy) increases and part of the stored energy in the flywheel is now transferred to the machine inductance causing the reduction in flywheel speed.

(ii) When any one of the SW_2, SW_4 or SW_6 (bottom switches) is OFF: When any one of the switch SW_2, SW_4 or SW_6 is made OFF, the generator terminals are connected to the dc bus through two diodes and two inductors in series. For example when SW_4 is made OFF, the inductor L a tries to maintain the current which will flow through D1, DC capacitor C (and Load resistor R_L), D6, L_a R_a of Y phase and ends at –ve node of e_Y of Y phase. The inductor energy is now transferred to the dc bus (DC bus capacitor and load R_L) and the inductor current ramps down. It may be observed from above discussion that the circuit functions as a voltage boost converter and voltage gain can be computed from the (3.1).

3.2 Selection of Electrical machine, Power Converter and Controller

The various subsystems of FESS such as electrical machine, bi directional power converter and controller selected should be able to deliver maximum energy for a given top speed of theflywheel. Storing and releasing energy from the FESS should be handled in an efficient way by the controller, power converter and other related systems. Therefore the selection of these systems plays an important role in building an efficient and reliable FESS.

3.2.1 Electrical machine

The electrical machine used in an FESS accelerates the flywheel during charging and discharge the same during deceleration. It is preferred to have a commutator-less machine, as it eliminates frequent maintenance problems, reduce the EMI and increase the efficiency. Permanent Magnet Synchronous Machines (PMSM) or Brushless DC (BLDC) machines can be used because they can be operated as generator or motor conveniently. PM machines use magnets to produce air-gap magnetic flux instead of field coils. This configuration eliminates rotor copper loss as well as the need for maintenance of the field exciting circuit. This has been made possible by the easy availability of high performance permanent magnets with high coercivity and residual magnetism, such as Samarium cobalt and Neodyum-Iron-Boron (NdFeB) magnets. The permanent magnet machines consist of a three phase stator windings similar to that of induction machine and a rotor with permanent magnets. The machine characteristics depend on the magnets used and the way they are located in the rotor. The permanent magnets (PM) are either mounted on the surface or buried in the interior of the rotor. Accordingly they are called as Surface Mounted PM machines or Interior PM Machines. PM machines can be broadly classified into two categories [74].

(i)Sinusoidal waveform machines: These machines have a uniformly rotating stator field as in induction machines. The stator winding is sinusoidally distributed or the magnets are shaped to get sinusoidal induced voltage waveforms. Hence sinusoidal stator currents are needed to produce ripple free torque.

(ii)Trapezoidal waveform machines: These are known as brushless DC or electronically commutated DC machines. Induced voltage is trapezoidal in its shape. The concentrated windings on the stator are the reason for the trapezoidal-shaped back emf waveform. The armature current is switched in discrete steps. The control of such motors is very simple. Only three discrete rotor positions per electrical revolution are needed in a three-phase machine to synchronize the phase currents with phase back emfs for effective torque production. A set of Hall Effect sensors are mounted on the armature to provide rotor position information. This eliminates the need for high-resolution encoder or position sensor required for the PMSM [6] [74]. The back emf waveforms are fixed with respect to rotor position. Square wave phase currents are supplied such that they are synchronized with the back emf peak of the respective phase. The controller achieves this by using the rotor position feedback information. From a control point of view such configuration makes the motor operates like a DC motor. Hence the motor is designated as a brushless DC motor.
There are several advantages of using PM for providing excitation in AC machines. Permanent magnets provide loss free excitation in a compact way without complications of connections to the external stationary electric circuits. These types of machines become very attractive option due to their high torque densities, high power density, excellent performance and with low rotor losses [74].The machine has to deliver rated power only for a short time during charging and discharging of flywheel. In the interval between end of charging and start of discharging the machine will be idling. During idling, the machine is required to provide only the

losses. In other words, the machine is used for intermittent operation only. A low loss short time rated permanent magnet machine is the best choice.

3.2.2 Bi-directional power converter

The bi-directional converter is required to interconnect source and storage device. This bi-directional converter along with a controller serves as a drive for motoring action and acts as a voltage regulating system for generating action of the electrical machine mentioned earlier [19]. It facilitates the energy flow to and from the flywheel. When the BLDC machine is working as a generator, the power can be drawn from the same using boost converter. A standard six switch voltage source inverter topology can be used either as a 3-phase BLDC motor drive or as a boost converter by appropriately controlling the IGBT gate drive pulses. Most important aspect to be considered while selecting the BDC is that it will ensure maximum possible energy harvesting for a given top speed of the flywheel as well as controlled charging of the flywheel. Higher the voltage gain of the boost converter, higher is the energy extracted from the flywheel for a given top speed of the flywheel [19].

3.2.3 Controller

Realization of control algorithm gives an option of choosing between analog and digital modes of implementation. Relative merits and demerits are mentioned below.

Analog Controller

Analog controllers are fast and signal transmission delay within the circuit is negligible in comparison with lowest time constant electromechanical components. These are, subject to parameter variations due to aging and drift of physical circuit components. Moreover, adjustment of control parameters requires replacement of circuit components and every new control strategy demands fresh circuit designs and fabrication.

Digital Controller

Digital controllers are realized using fast microprocessors or Digital Signal Processor. These enable implementation of complex control algorithm and easy parameter adjustment on account of their software programmability. Their main handicap is the finite and rather large signal sampling time which forces the controller to be effective for signals whose frequencies are equal to or less than half the sampling frequency. These controllers are much slower in comparison with analog controllers. In the present work, a digital controller has been adopted because of its easy programmability.

3.3 Harvestable energy

It is well known that all the available electrical equipments are designed to work at constant rated supply voltage. They function in the intended way only when the supply voltage is within the tolerable limits. Therefore the energy can be utilized only if it is extracted at constant output voltage. Energy thus extracted from flywheel and utilized is called as 'harvestable energy'. The process of energy extraction from a flywheel can be explained by referring the Fig. 3.4. This figure shows the voltage-time and speed-time characteristics of the generator. Various technologies related to energy harvesting process are defined as given below.

3.3.1 Harvestable energy

Harvestable energy can be obtained by subtracting the "Energy left behind in the flywheel at minimum speed" (up to which output voltage V_{dc} that can be maintained constant) from the Energy that was stored at maximum speed. The harvestable energy can be computed from the following equation

$$E_h = \frac{1}{2} J(\omega_{max}^2 - \omega_{min}^2) \tag{3.2}$$

3.3.2 Energy losses

The energy flows from flywheel through the generator and boost converter before it reaches load. When energy is transferred from flywheel to the load, the losses take place in mechanical components, generator and boost converter.

3.3.3 Backup time

Backup time is the duration for which power converter is able to maintain the output voltage V_{dc} constant with falling generator voltage. Higher output power can be drawn for a shorter backup time (T_{bu}) and the output power energy is low if it is drawn for a longer duration.

$$T_{bu} = \frac{E_h}{[V_{dc} \times I_{dc} + P_{Loss}]} \tag{3.3}$$

3.3.4 Useful energy

Useful energy can be calculated by subtracting the total losses in the system from harvested energy. A part of harvested energy is lost in flywheel generator and boost converter.

$$E_u = E_h - P_{loss} \times T_{bu} \tag{3.4}$$

3.3.5 Energy Efficiency

It is the ratio of useful energy to harvested energy. Overall energy efficiency of the system can be calculated by the following relation:

$$\eta = \left[\frac{P_o T_{backup}}{\frac{1}{2} J(\omega_{max}^2 - \omega_{min}^2)} \right] = 1 - \left[\frac{P_{loss} T_{backup}}{\frac{1}{2} J(\omega_{max}^2 - \omega_{min}^2)} \right] \tag{3.5}$$

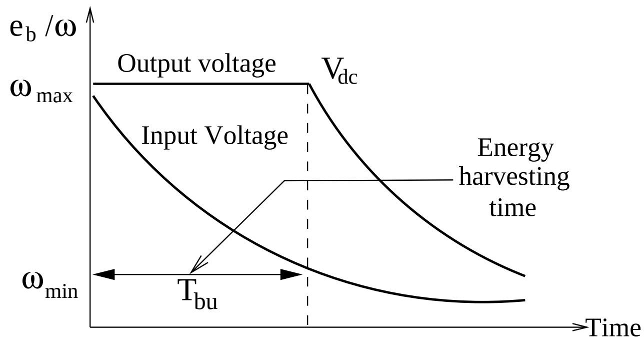

Figure 3.4: Flywheel speed / Induced voltage as a function of time

3.4 Modeling and controller design

In the absence of input power, the flywheel starts decelerating. When the flywheel is decelerating, the machine works as a generator. The generator voltage drops as the speed of the flywheel reduces. Energy is required to be harvested at constant DC bus voltage. It is required to design a voltage controller to boost the induced voltage to maintain the DC bus voltage constant. A mathematical model of the total system is also carried out.

3.4.1 Modeling of the system in motoring mode of operation

In this mode of operation the dc voltage is applied across the armature winding during the period when the induced voltage is flat in the trapezoidal waveform [Fig. 3.3]. BDC works as motor drive in this mode and the armature current is controlled by adjusting the duty cycle of the applied voltage. Simplified equivalent circuit of the converter in the motoring mode of operation is given in Fig. 3.5 The

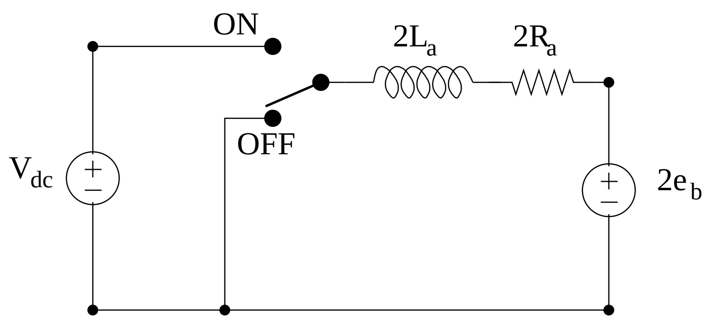

Figure 3.5: Simplified equivalent circuit in motoring mode

dynamic equations are given by,
(i) Period DT_{sw} ; Switch is ON:

$$2L_a \frac{di_a}{dt} = V_{dc} - 2i_a R_a - 2e_b \tag{3.6}$$

(ii) Period (1 − D)T_{sw} ; Switch is OFF:

$$2L_a \frac{di_a}{dt} = -2(i_a R_a + 2e_b) \tag{3.7}$$

3.4.2 Small signal modeling in motoring mode

Averaged equation is given by,

$$2L_a \frac{di_a}{dt} = V_{dc}\ D - 2i_a R_a - 2e_b \tag{3.8}$$

Assume that the current controller response time is much smaller compared to the mechanical time constant. Consider the perturbations; $i_a = I_a + \hat{i_a}$; $d = D + \hat{d}$; $e_b = E_b$; (Mechanical time constant is high; a Speed change takes place slowly). The small signal model becomes,

$$2L_a \frac{di_a}{dt} = V_{dc}\widehat{d} - 2i_a R_a \tag{3.9}$$

Current control transfer function of the system is,

$$\frac{i_{a(s)}}{d(s)} = \frac{V_{dc}}{2(R_a + sL_a)} \tag{3.10}$$

3.4.3 Modeling of the system in generating mode of operation

The generator is connected to the dc bus through the BDC as shown in Fig. 3.2. BDC is operated as a boost converter by continuously gating the bottom switches [SW_2, SW_4, SW_6] with switching frequency f_{sw} keeping the top switches [SW_1, SW_3, SW_5] OFF permanently. The control objective is to keep the dc bus voltage constant inspite of input voltage variation. Hence it is necessary to obtain the dc bus voltage controller transfer function. The power is transferred to the dc bus at constant voltage during deceleration of the flywheel. Constant dc voltage is achieved by adjusting the duty cycle of the active switches. By referring the Section-3.1.2 (i) and (ii) the simplified equivalent circuit of the machine in the generating mode can be written as shown in Fig. 3.6

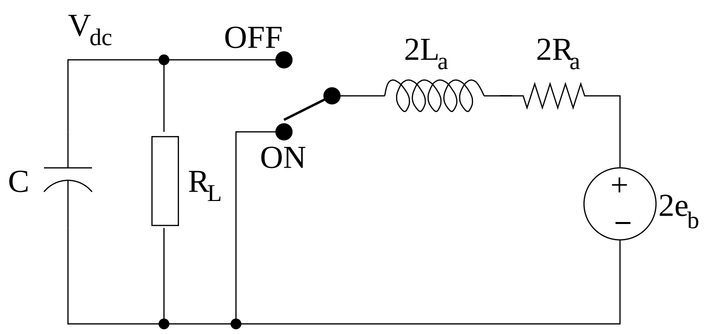

Figure 3.6: Simplified equivalent circuit in generating mode

(i) Period: DT_{sw} (Switch is ON) The dynamic equations for this period are given by

$$C\frac{dV_{dc}}{dt} = -\frac{V_{dc}}{R_L} \tag{3.11}$$

$$2L_a\frac{di_a}{dt} = 2e_b - 2i_aR_a \tag{3.12}$$

(ii). Period: (1-D)T_{sw} (Switch is OFF) The dynamic equations for this period are:

$$C\frac{dV_{dc}}{dt} = i_a - \frac{V_{dc}}{R_L} \tag{3.13}$$

$$2L_a\frac{di_a}{dt} = 2e_b - V_{dc} - 2i_aR_a \tag{3.14}$$

Time averaged equation can be obtained by multiplying equation (3.11) by DT_s and equation (3.13) by (1-D)T_{sw}, adding both and then dividing by T_{sw}.

$$C\frac{dV_{dc}}{dt} = i_a(1-D) - \frac{V_{dc}}{R_L} \tag{3.15}$$

Time averaged equation can be obtained by multiplying equation (3.12) by DTs and equation (3.14): by (1-D)T_{sw}, adding both and then dividing by T_{sw}.

$$2L_a\frac{di_a}{dt} = 2e_b - V_{dc}(1-D) - 2i_aR_a \tag{3.16}$$

3.4.4 Small signal modeling in generting mode

We may consider that the speed (and back emf) changes are relatively slow on account of high mechanical time constant. With small perturbations, $I_a = I_a + \hat{i_a}; d = D - \hat{d}; V_{dc} = V_{dc} + \hat{V_{dc}}; e_b = E_b$ to the system, the perturbed equations are,

$$C\frac{d\hat{V_{dc}}}{dt} = \hat{i_a}(1-D) - I_a\hat{d} - \frac{\hat{V_{dc}}}{R_L} \tag{3.17}$$

$$2L_a\frac{d\hat{i_a}}{dt} = V_{dc}\hat{d} - \hat{V_{dc}}(1-D) - 2\hat{i_a}R_a \tag{3.18}$$

Using equations (3.17), (3.18) the transfer function of the system becomes,

$$\frac{\hat{V_{dc}}(s)}{\hat{d}(s)} = \frac{2E_b}{(1-D)^2} \times \frac{(1 - \frac{2sL_a}{R_L(1-D)^2})}{1 + \frac{2L_a}{R_L(1-D)^2}s + \frac{2L_aC}{(1-D)^2}s^2} \tag{3.19}$$

The transfer function of the system is of the second order and the corner frequencies ω_p(pole), ω_z (zero) can be obtained by following relations.

$$\omega_p = \frac{(1-D)}{\sqrt{2L_aC}} \tag{3.20}$$

$$\omega_z = \frac{(1-D)^2R_L}{L_a} \tag{3.21}$$

A controller response time of 0.5 seconds (which is 2% of the power supply back up time) is considered. With a controller bandwidth of around 50 rad/s (corresponding to 0.5 sec backup time), dynamics due to the poles and zeros of the transfer function can be neglected and it is possible to approximate the transfer function, simply by a gain as given below.

$$\frac{\hat{V_{dc}}(s)}{\hat{d}(s)} = \frac{2E_b}{(1-D)^2} \tag{3.22}$$

A PI controller is employed for maintaining the dc bus voltage constant.

3.5 Design Specifications

Following are the specifications of the proposed prototype system:

- Supply voltage: 300 V DC, 1000 W,
- Flywheel: Speed=10.0 kRPM, Mass=15 kg, J=0.075 kgm^2
- Backup time: 30 seconds
- Values of components used: C=1650μF, L_a=0.97mH, R_a=1.2Ω , R_L=100Ω

3.6 Experimental setup

The complete system has been built (with the configuration shown in Fig. 3.2 using a 3-phase, 4-pole, 1.0 kW, PM BLDC machine, 6-Switch IGBT based BDC with 4.0 kHz switching frequency and a mechanical flywheel. Motorola make Digital Signal Processor chip DSP56F805 is used as the controller. Motor current, rotor position and dc bus voltage are sensed using Hall Effect sensors and fed back to the DSP. These signals are used by DSP for the generation of gate control pulses for IGBTs and for the dc bus voltage regulation. The programming of DSP is done using “C” language. The control algorithm for PI voltage controller software is implemented. User interface is achieved using LCD/Display devices through the serial port of DSP chip.

3.6.1 Motoring Mode (BLDC Motor drive)

The various tasks like sensing of rotor position, generation and control of pulses to IGBT gates, conversion and conditioning of analog signals are carried out in the DSP chip. Three numbers of Hall effect sensors are fixed near armature coils with the angular distance of 120^o (electrical) between any two them. The sensor output goes high when noth pole of rotor comes near to it and low when south pole of the rotor comes near to it. Logic is built in the DSP to switch ON the appropriate pair of IGBT of the BDC to drive the current through the armature coil for producing the average positive torque.

3.6.2 Generating mode (Boost converter)

The rotor position sensor signals are ignored and top side IGBTs of the BDC are kept permanently OFF in this mode. Bottom side IGBTs are switched asynchronously with controlled pulse width through a PI controller at a switching frequency of f_{sw}. The controller adjusts the pulse width of the switching signal depending upon the error signal (difference between the reference and dc bus feed back voltage). The control circuit monitors the input power supply conditions like failure, dip, blackouts, brownouts, sags etc and take appropriate actions. The controller accepts the voltage set point from a user interface keypad and the feedback from the dc bus voltage.

3.7 Experimentation and tabulation of results

Experiments were conducted to verify and validate the proposed design methodology for FESS and an associated controller. Following tests were conducted to find various performance parameters like backup time, boost converter gain, maximum energy extracted.

3.7.1 Power backup time test

The input supply is switched off and the flywheel is allowed to decelerate. The induced voltage waveform obtained from the generator at the speed of 10,000 rpm is recorded and shown in the Fig. 3.7

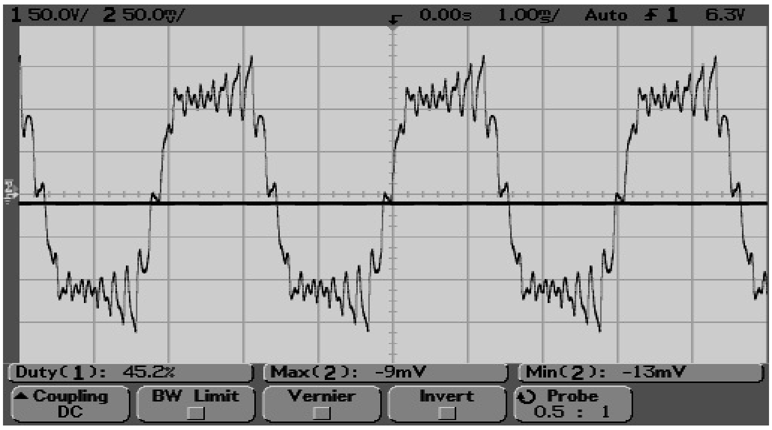

Figure 3.7: Induced voltage waveform of generator at 10,000 RPM

The time up to which the dc bus voltage is maintained constant at 300V is recorded. BDC has delivered output power of 818W for duration of 19 sec as shown in Fig. 3.8. It is also observed that the minimum induced voltage up to which system maintains 300V dc voltage is 185 volts at 818W output power and 127 volts at 450W output power.

3.7.2 Energy efficiency test

In this test, the flywheel was allowed to decelerate and the energy is extracted with various values of load resistance connected across the dc bus. Backup time, energy

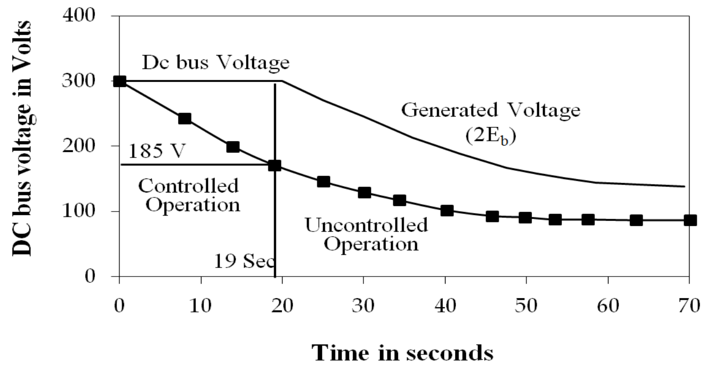

Figure 3.8: DC bus voltage versus time at 818W output power

harvested are recorded and efficiency is computed which are given in table 3.1 Quantity of harvested energy is plotted as function of backup time as shown in

Table 3.1: Energy harvested and Efficiency at various loads

Output power in Watts	Backup Time in sec	Energy Harvested in Joules	Efficiency in Percentage
818	19	16359	78
450	41	18953	62
338	53	17937	56

Fig. 3.9. It is evident from this plot that the energy harvested has maxima that vary as a function of power and backup time.

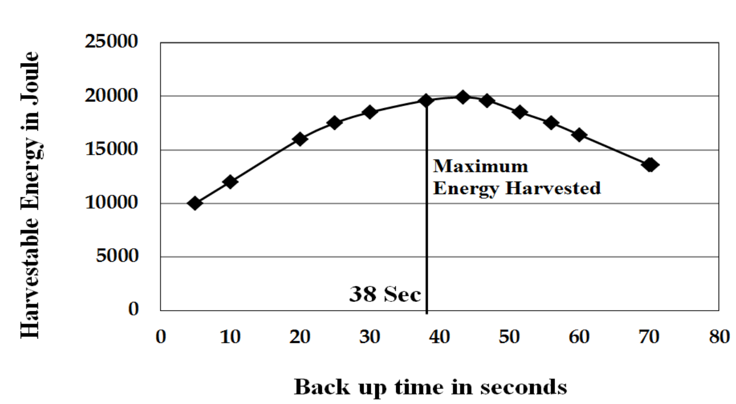

Figure 3.9: Harvested energy versus backup time

3.7.3 Boost converter performance test

In this test, top speed of the flywheel, load voltage, output power and back up time are recorded with various loads connected across the dc bus. The readings taken from this test are tabulated which is shown in the table E.1

Table 3.2: Voltage gain as a function of load current

Output power in Watts @300 V DC	Output current in Amps	Minimum speed in RPM	Measured Voltage gain	Estimated voltage gain
818	2.72	6894	1.6	3.23
450	1.50	4691	2.36	4.33
338	1.13	4291	2.52	4.97

It is observed from the table E.1 that the voltage gain of the boost converter has reduced as the load current is increased. This results in the increase of the minimum speed (induced voltage) up to which the boost converter maintains the output dc voltage.

3.8 Summary

Basic requirements of the FESS are studied; Selection of various subsystems is done; Analysis, modeling, design, fabrication and evaluation of an FESS have been carried out. From studies it is concluded that a low loss, short time rated two-quadrant Permanent Magnet machine is the best choice for this application. It is observed that the generator current increases as the flywheel slow down. Therefore the current rating of the converter is decided based on the output power requirement, at lowest operating speed of the flywheel.

Experiments have been conducted on the prototype FESS built for evaluating the performance of the system. The system was run up to a speed of 10,000 RPM. The system was able to maintain the dc bus voltage at 300V for a period of 19sec at 818 W power and 41sec at 450 W power delivery to the load. The plot of energy harvested as a function of time shows that the harvested energy has maxima. For a given system, there is clearly a peak energy point, where the energy extracted was maximum. It is observed from these experimental results that, at higher armature currents of the generator the energy efficiency and voltage gain of the boost converter are low. Lower boost converter voltage gain at higher armature currents limits the total energy that can be extracted for a given top speed. This becomes a serious limitation of this system. Analysis of the experimental results, limitations of the system and possible solutions are discussed in Chapter-4.

Chapter 4

Investigation and Analysis of result

This chapter is focused on the identification of the source, apportioning, analysis and various mitigation techniques of the losses in an FESS. First part of the chapter deals with the quantification of various losses in the system. Second part covers the new BDC topology which is proposed using a combination of fast turn off SCR and IGBT with a novel control logic implementation to achieve zero switching power loss (ZSPL) through zero voltage transition (ZVT) and zero current transition (ZCT) techniques. The basic principle of operation, analysis, and design procedure of the topology are presented for both voltage buck and boost modes of operation of the proposed BDC topology. A design example is also presented. Tests are conducted to find the various performance parameters of FESS subsystems and results are presented. Limitations of the system are highlighted.

4.1 Investigation of various losses

The FESS is connected in parallel to the DC voltage source which is feeding the DC load as shown in Fig. 3.1 of Chapter. 3.

4.1.1 Identification of sources of losses in FESS

Between the flywheel (which stores the energy) and load (which utilize the energy) there are different devices like, bearing, electrical machine and BDC. Various losses take place in the FESS are shown schematically in the Fig. 4.1. A portion of energy

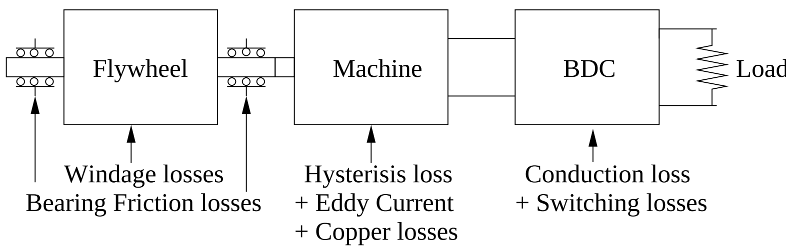

Figure 4.1: Representation of various losses in an FES System

which is extracted from the flywheel is dissipated as loss in these subsystems. It is possible to find the sources of losses, quantify them by computation and their relative contributions to the total loss. By knowing the sources and their contribution to total losses, different loss reduction techniques can be adopted.

4.1.2 Experimental setup

An FESS has been built using a Permanent Magnet Brushless DC (PM-BLDC) machine, IGBT based BDC, a mechanical flywheel and a boost converter. The ac voltage from the generator is converted into required dc voltage in two stages. In the first stage low voltage ac is converted to dc voltage using BDC as rectifier. In the second stage this low voltage dc is boosted to required higher voltage dc using a boost converter. This is the arrangement used in the experimental setup and is called as Two Stage Boost Converter (TSBC). The power circuit diagram of this TSBC used in the test setup is shown in Fig. 4.2

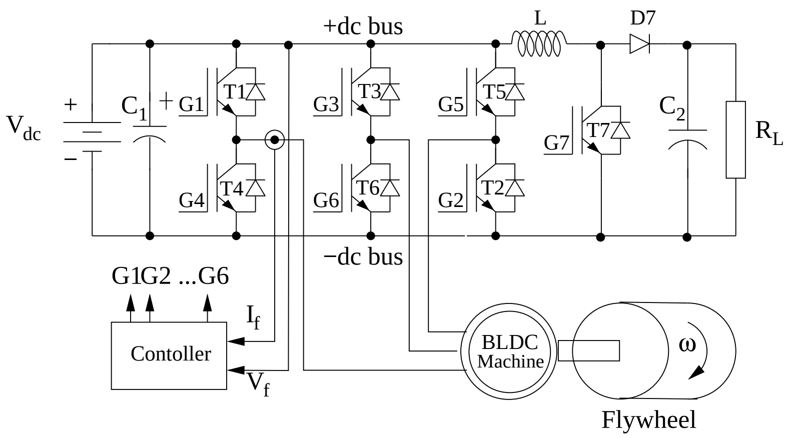

Figure 4.2: Power circuit diagram of a typical FES System

Specifications of the system built were as given in table 4.1

Table 4.1: Specifications of the FESS

Parameter	Specifications
Input voltage	550 Volts DC
Output power	5.0 kW
Rated speed	15000 RPM
Machine Type	3ϕ, 4 Pole, PM-BLDC
Weight of the flywheel	45.3 kg
Moment of Inertia (J)	0.681 Kgm^2
Backup time	60.0 seconds
Controller	Motorola DSP56F805
Power Switch (IGBT)	SKM100GB123D
Switching Freq(f_{sw})	16 kHz

4.1.3 Basis of conducted experiments

Motor coupled to the flywheel is made to accelerate to the rated speed using input dc power and the power supply to the motor is switched off; the flywheel continues to run due to its inertia driving the machine as generator till all stored energy is consumed. If an electrical load is connected across the generator it draws current and absorbs the energy stored in the flywheel. This makes the flywheel to decelerate. If electrical load is not connected, the stored mechanical energy in the flywheel is dissipated as losses in mechanical components, electrical machine and the powerconverter. Total power input to the system during the acceleration and running is computed by multiplying the dc bus voltage and dc bus current.
When the flywheel is not coupled to the motor, mechanical losses are assumed to be negligible as compared to it when flywheel is coupled to the motor. This assumption is made because, in the experimental setup used the mass of the rotor (8.8 kg) is $1/5^{th}$ as compared to mass of the flywheel (45.3 kg) and surface area of rotor is only $1/8^{th}$ (0.036 m^2) as compared to the surface area of flywheel (0.2883 m^2). Hence, when the flywheel is not coupled to the motor, measured loss is attributed to the iron loss of the electrical machine used after neglecting the loss due to the drag and the bearing friction. Two sets of experiments are conducted on the FESS. They are Loss Analysis Test (LAT) to analyse the system losses and Performance Analysis Test (PAT) to evaluate the performance of the system.

4.1.4 Loss analysis tests

In order to find out the mechanical losses in the machine the classical retardation test is done. The machine is made to accelerate up to a speed of 15000 RPM. Speed, dc bus voltage and dc bus current are measured at regular intervals of time and plotted. Tests conducted are given below:

- Acceleration test without flywheel
- Acceleration test with flywheel, without load

No-load test of machine is conducted without flywheel and hence the mechanical losses are negligible. Iron loss of the machine is computed using this no load test data. The input power measured during the acceleration test with flywheel will give the total power loss which includes the mechanical and electrical losses. These losses are plotted as a function of speed as shown in Fig. 4.3

4.1.4.1 Analysis of the power loss data

(i) Testing without flywheel
As explained earlier, when the flywheel is not coupled to the rotor shaft, the loss due to the drag and bearing friction can be neglected. Therefore, the measured loss during this test can be entirely due to the iron loss of the machine.
(ii) Testing with flywheel
As explained earlier, when flywheel is coupled to the rotor shaft, loss computed is the sum of the losses due to bearing friction, drag, hysteresis and eddy current.

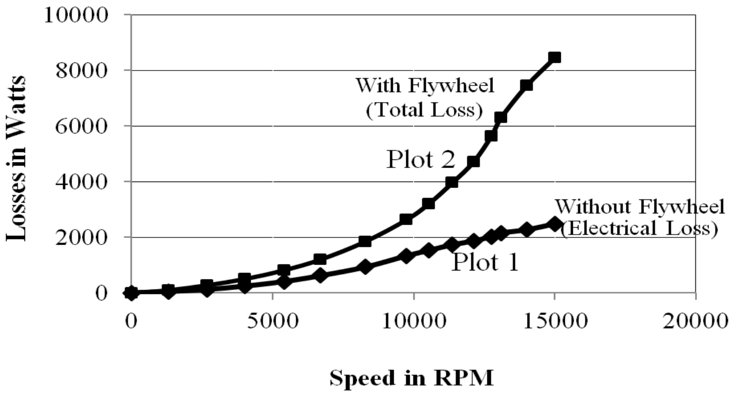

Figure 4.3: Losses with and without flywheel as a function of Speed

4.1.4.2 Relationship between the flywheel speed and various losses

The relation between various losses as a function of speed is found out using curve-fitting method. If P_{Loss} is the total loss in the system and "N" is the operating speed of the machine in RPM, then the equation thus obtained are given as below:
(i) Without flywheel (Plot-1 of Fig.4.3)

$$P_{Loss} = 0.00000862464N^2 + 0.0388244N \tag{4.1}$$

(Eddy current loss) (Hysteresis loss)

(ii) With flywheel (Plot-2 of Fig.4.3)

$$P_{Loss} = 0.000011N^x + 0.0498244N \tag{4.2}$$

(Drag+Eddy loss) (Bearing Friction + Hysterisis loss)

("x" varies from 1.91 to 1.985 as "N" varies from 0 to 15000 RPM).
It is found that the right hand side of the equation contains two terms, one is proportional to the speed and the other is proportional to the square of speed. This is in the expected lines. From the theory, it is known that the bearing friction loss in the flywheel and hysteresis loss in machine are proportional to speed and Drag loss in the flywheel and eddy current loss in the machine are proportional to square of the speed. In case of drag loss, it may be noticed that the power of speed is not constant "2", but it varies from 1.9 to 1.985 as the speed varies from 0 to 15000 RPM. Therefore, subtracting the square component of loss obtained from test "without flywheel" from square component of loss obtained from the test "with flywheel" gives the drag loss in the system and subtracting the linear component of loss of test "without flywheel" from the linear component of loss obtained from the test 'with flywheel' gives the bearing friction loss of the machine.

4.1.4.3 Apportioning of various losses in generating mode

The individual losses are computed at various speeds using (4.1), (4.2) and as explained in the previous subsection. These values have been tabulated in table 4.2

and plotted as a function of rotor speed as shown in Fig. 4.4 and Fig. 4.5

Table 4.2: Various losses of the system

Speed in kRPM	Total Input power Loss	Mechanical Loss (watts)		Electrical machine Loss (watts)			Power converter Loss (watts)	
		B/F Loss	Drag Loss	Hyst Loss	Eddy Loss	Copper Loss	S/W Loss	Cond. Loss
1.3	185	15	24.3	51	12	0.3	71.6	11.2
4.0	578	44	219	156	113	1.0	23.9	20
8.3	1923	91	978	321	479	3.4	11.9	37
12.1	4723	133	3005	470	1028	11.2	8.4	66
15.0	8670	165	6216	582	1575	24.9	7.0	99

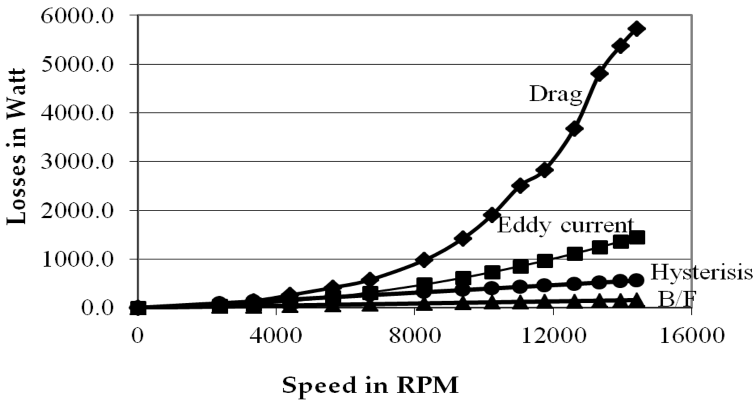

Figure 4.4: Electro-mechanical losses in the system as a function of speed.

4.1.4.4 Observations made from the LAT and contributions of various losses to the total loss

Various losses and their contributions to the total loss at different speeds are given in table 4.3. Following observations are made from the analysis of experimental results:

Table 4.3: Various losses and their contributions to the total loss

Speed in RPM	Types of losses in percentage(%)						
	Drag Loss	B/F Loss	Eddy Loss	Hyst Loss	S/W Loss	Cond. Loss	Copper Loss
2670	28	9	15	32	11	3	0.20
5400	43	7	23	23	2.0	2	0.17
10530	60	3	23	12	0.28	1.5	0.20
15000	72	2	18	7	0.10	1	0.30

- Bearing friction and hysteresis losses are proportional to the rotor speed; Drag and eddy current losses are proportional to the square of rotor speed.

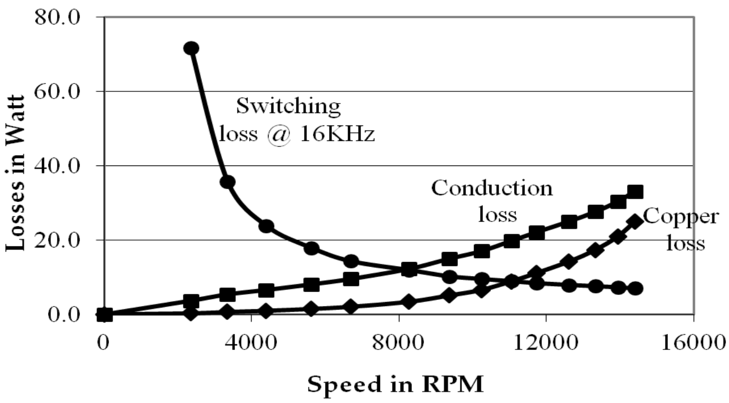

Figure 4.5: Power converter losses in the system as a function of speed

- Loss due to drag and eddy current dominates at higher rotor speeds.
- At higher rotor speeds the overall loss can be reduced to the large extent by reducing the drag and eddy current losses as they dominate at higher rotor speeds.
- Switching losses are high at low speed due to high input current.

4.1.5 Performance analysis tests

In these tests the input power supply is switched off and the flywheel is allowed to decelerate. The time duration for which the dc bus voltage is maintained constant at 400V is recorded at various loads. Following tests were conducted to find various performance parameters like backup time, maximum energy extracted from the flywheel, lowest required generator voltage.

4.1.5.1 Power backup test

The power backup test was conducted to find out the backup time and lowest speed (or generator voltage) up to which the system maintains the output dc bus voltage constant. In this test the flywheel was allowed to decelerate by switching off the input supply. As the flywheel speed is reduced, the generator voltage also drops. The time up to which the dc bus voltage is maintained at 400V in spite of reduction of generator voltage is recorded. The test is conducted with various load currents, at constant dc bus voltage 400V. Fig. 4.6 shows the variation of generator and output voltages with time.

It may be noted that, even though the generator voltage reduces with time, the dc bus voltage is maintained constant at 400V for a duration depending on the load. It is also observed that the minimum speed (induced voltage) up to which the system maintains the output dc voltage constant is a function of ratio of source resistance to load resistance.

4.1.5.2 Power and Energy balance tests

These tests was conducted to verify energy balance and power balance equations.

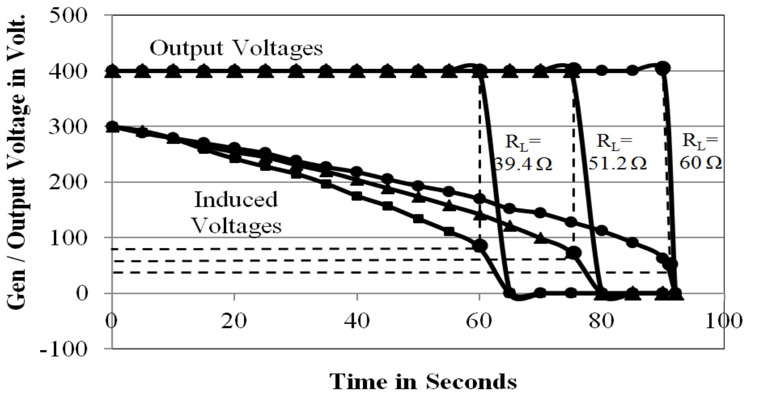

Figure 4.6: Output voltage at various loads as a function of time

(i)Power balance equations :

When input power is not available, flywheel continues to run and driving the generator. Load power will be equal to generated power (from flywheel) minus the losses in the system. The losses are taking place in flywheel, machine and power converter. Mechanical power generated by flywheel, Power drawn by the load and the power lost in the conversion process are computed as given below:

$$P_{mech} = J\omega\frac{dw}{dt} \tag{4.3}$$

$$P_{load} = V_{dc}I_{dc} \tag{4.4}$$

$$P_{Loss} = 0.000011N^{x} + 0.0498244N \tag{4.5}$$

In this test the input power was switched off allowing the flywheel to decelerate. A 4.0kW power was drawn continuously from the dc bus by connecting resistive load of 39.2Ω. Speed and load power are measured at regular interval of time as the flywheel is decelerated. Power generated from the flywheel and total system losses is also computed from the retardation test data for this period. All these values are tabulated and plotted as given in the Fig. 4.7

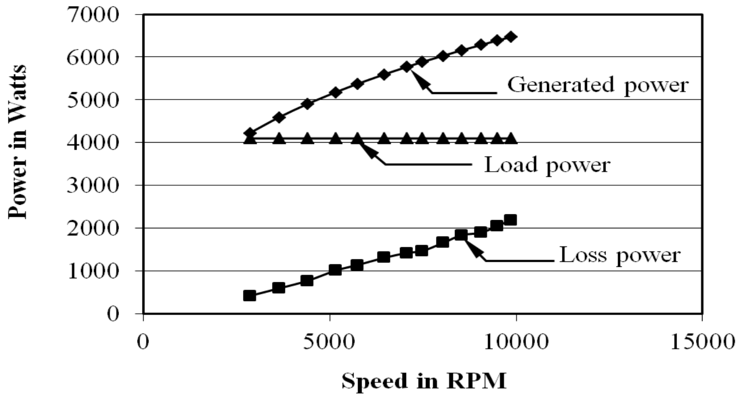

Figure 4.7: Power as a function of speed

(ii)Energy balance equations :
Mechanical energy extracted from the flywheel (E1), averaged generated energy (E2), energy lost in the various power processing components (E3), energy delivered to the load (E4) and energy efficiency (η) during the energy extraction process are computed as follows

$$E_1 = \frac{1}{2}J(\omega_{max}^2 - \omega_{min}^2) \tag{4.6}$$

$$E_2 = J\omega\frac{dw}{dt}T_{bu} \tag{4.7}$$

$$E_3 = P_{Loss}T_{bu} \tag{4.8}$$

$$E_4 = V_{dc}I_{dc}T_{bu} \tag{4.9}$$

$$\eta = \frac{E4}{E1} \tag{4.10}$$

When the flywheel is supplying power to the load, the measurement and computation of energy at various subsystems are carried out. They are shown in the table 4.4 given below. The measured value and the computed values are in expected lines.

Table 4.4: Measured energy at various stages

Sources of Energy	Energy in Joules
Extracted Mechanical Energy (E1) (By computation)	327882
Generated Mechanical Energy (E2) (By computation)	336227
Energy Lost by in various levels (E3) (By Measurement)	82086
Electrical Energy available at load (E4) (By measurement)	246000
Energy efficiency (η)	75 %

There is a slight difference in values between total energy generated and sum of energy lost and the energy utilized by the load. This might be due to measurement errors and the assumptions made.

4.2 New ZSPL topology for the reduction of switching losses

The losses due to switching of devices at higher frequencies contribute significantly to the total loss of the BDC particularly at lower generator speeds (lower induced voltage) in an FES system. Causes and mechanism of switching power loss in a semiconductor device are already well documented in the text books on power electronics. Switching power loss can be reduced either by Zero Voltage Switching (ZVS/ZVT) method or Zero Current Switching (ZCS/ZCT) method depending upon whether the voltage across the device is made zero during the turn ON or the current through the device is made zero during the turn OFF transition. It may be noted that in ZVS/ZCS, the resonant circuit comes in series with the main switch, whereas in the case of ZVT/ZCT, the resonant circuit doesn't come in series with the main switch - rather it comes into picture only during the transitions (ON to OFF and OFF to ON). This makes ZVT/ZCT topologies suitable for PWM applications. In ZCT technique, the current through the switching device becomes negative (i.e. anti- parallel diode conducts) during the switching transition, making it a "true" Zero Switching Power Loss (ZSPL) as compared to ZVS/ZCS.

Desired features of an ideal BDC in respect of switching loss and control logic are as follows:

- ZSPL shall be implemented using minimum no. of additional devices
- BDC shall have ZSPL feature in both buck and boost operating modes.
- Control Logic implementation shall be simple.
- Energy stored / consumed in the resonant circuit to achieve ZSPL shall be as low as possible.

The new topology, proposed in the next section meets all of the above requirements of BDC.

4.2.1 New ZSPL topology for bi-directional converter

The devices used in this topology are, IGBT as main devices for carrying the load current and SCR as auxiliary devices. Bidirectional converters which are used in energy storage systems are basically DC–DC converters and may be isolated or non isolated type. A typical BDC consists of two switches. While, one switch is used for stepping down the voltage and making the power flow from the dc bus to FES machine, the other switch is used for boosting the voltage making the power flow from FES machine to the dc bus as shown in the Fig. 4.8.

4.2.2 Proposed scheme

The circuit configuration used here is a modified version of the McMurray Bedford circuit [40] which is used as one leg of forced commutated 3-phase thyristorised inverters using SCR as switching devices. The new topology uses IGBT as the main device and a fast turn off SCR as the auxiliary device. Since the current impulse in the resonant circuit has a natural zero crossing, SCR is the good choice for the auxiliary device used in the considered application. Use of SCR as auxiliary device reduces the conduction and switching losses in the auxiliary devices. This also makes the triggering circuit and control logic simple due to short gate pulses and the natural current commutation of the SCR. The design approach, control logic implementation, and selection of values of resonant circuit (inductor and capacitor) are explained in the later part of this chapter. The proposed topology, in conjunction with developed control logic, is able to achieve ZSPL for both buck and boost mode of operation.

4.2.3 Working principle

Fig. 4.8 shows the equivalent circuit of the system depicted in Fig.3.1 of Chapter-3. For the sake of simplicity, only one phase of the 3-phase FES machine and BDC is shown. The dc bus is energized from the voltage obtained by rectifying the ac mains voltage. The FES machine is connected to the dc bus through the switches S_1 and S_2 as shown in Fig. 4.8. In motoring mode, the switch S_1 along with D_2 is used for bucking the voltage of dc bus to drive the FES machine. Similarly, in generating mode, the switch S_2 along with D_1 is used for boosting the voltage output of the FES machine. Switching assisted by ZCT is realized through the

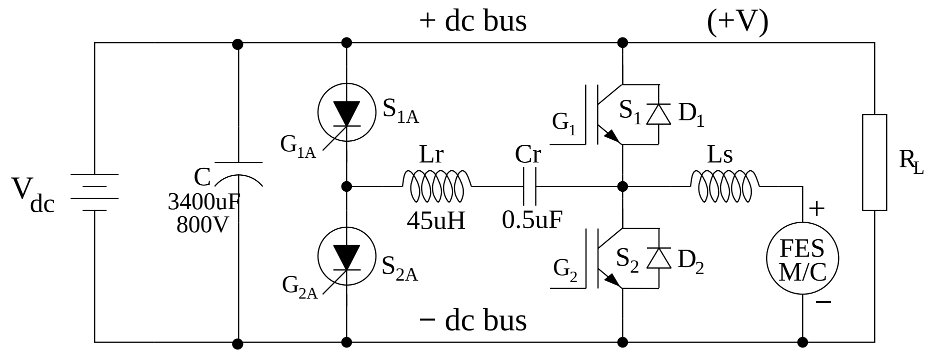

Figure 4.8: Equivalent circuit diagram of one phase of the new ZSPL topology for BDC

oscillating action of an LC circuit which is triggered by an auxiliary switch. S_1, S_2 are the main switches and S_{1A}, S_{2A} are the auxiliary switches as shown in Fig. 4.8. Also, there are anti-parallel diodes D_1 and D_2 for the switches S_1 and S_2 respectively. The trigger control logic for these four switches is implemented in such a way that, the current is made to flow through the diode which is connected anti parallel to the main device whenever the main device is required to be turned on or turned off. This makes the main device to go from OFF state to ON state when the voltage across it is zero and from ON state to OFF state when the current through it is zero. This results in an ideal ZSPL switching of the device. This topology can be used for energy transfer from dc bus to FES machine (known as buck mode) as well as from FES machine to dc bus (known as boost mode).

4.2.4 Advantages of new scheme

The BDC built with this topology has all the desired features mentioned in the section 4.2. The advantages are summarized below:

- This topology uses IGBT for the main device and SCR for the auxiliary device. This helps in reducing the power loss and cost of the auxiliary device and makes the triggering circuit simple.

- This topology renders a zero switching loss solution both during turn on and turn off, thereby improving the overall efficiency, reducing the thermal stress on the devices (which implies enhanced reliability), and reducing EMI problems.

- The auxiliary circuit inductor or capacitor does not come in series or parallel with the main system when they are in operation (these components are totally isolated from the main circuit). As these components don't carry the load current, they will neither affect the wave shape or the magnitude of load circuit voltage/current or the response time of load circuit.

4.2.5 Analysis and design of the proposed scheme

Detailed analysis of turn ON and turn OFF commutation for buck and boost modes of operation of proposed topology is carried out in this section.

4.2.5.1 Switching Waveforms and analysis in buck mode

In this mode the power flows from the dc bus (at higher voltage) to the FES machine (at lower voltage). The switch S_1 is gated with high frequency pulses whose width is adjusted to get the required voltage at the input of FES machine. Control pulses and anticipated waveforms across the power components are shown in Fig. 4.9. By referring to Figs. 4.8 and 4.10, analysis of the circuit in buck mode is carried out as follows:

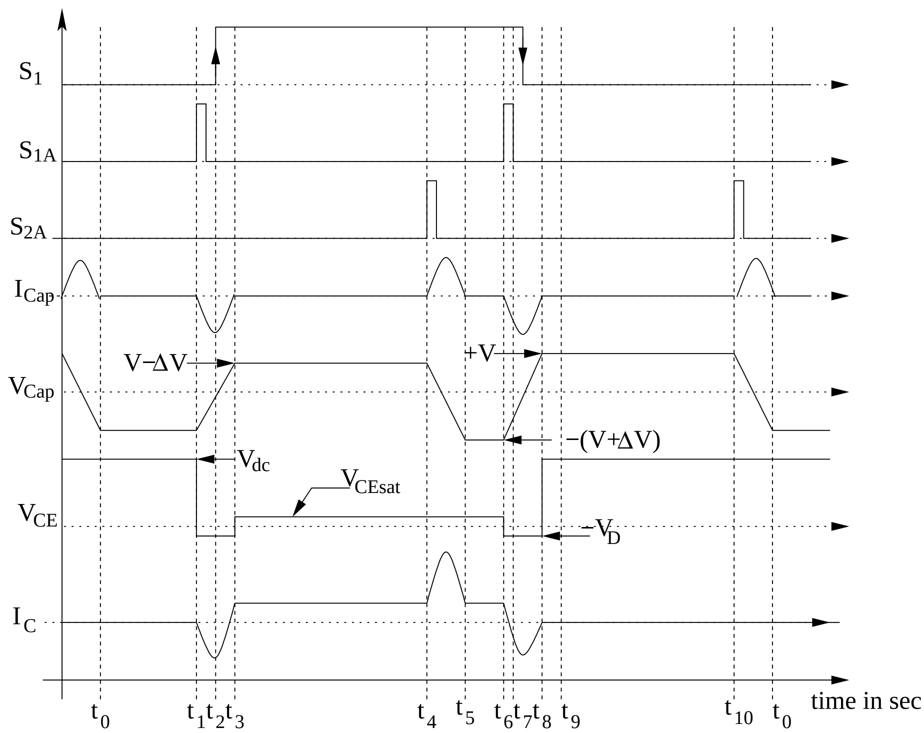

Figure 4.9: Control pulses, Current and voltage waveforms in buck mode

Mode 1 $[t_0 - t_1]$
The capacitor C_r is kept charged to voltage "V" with the polarity as shown in Fig. 4.10(a).

Mode 2 $[t_1 - t_2]$
The auxiliary switch S_{1A} (SCR) is turned on (at instant t_1) before the switch S_1 is turned on (at instant t_2) to make the capacitor start discharging through the devices, D_1 , auxiliary switch S_{1A} and resonant inductor L_r as shown in Fig. 4.10(b).

Mode 3 $[t_2 - t_3]$
At the end of the discharge at instant t_3, the polarity of the voltage across the capacitor C_r reverses. While D_1 is still carrying current, the gate signal of the main device S_1 is made high (at instant t_2) and the device goes to ON state. The load current in the main switch starts flowing when the voltage drop across it is zero. Resonance phenomenon completes at instant t_3 with capacitor, C_r attaining the voltage polarity as shown in Fig. 4.10(c).

Mode 4 $[t_3 - t_4]$
The resonant capacitor voltage polarity will continue to be in the same state as shown in Fig. 4.10(c) during this period. Since S_1 is ON, the current flows from dc bus to FES machine as shown in Fig. 4.10(c).

Mode 5 $[t_4 - t_5]$
The auxiliary switch S_{2A} is turned ON at instant t_4. The capacitor voltage changes its polarity as the charging current flows from dc+ through S_1 , L_r , S_{2A} and back to dc- as shown in Fig. 4.10(d). This makes the capacitor voltage polarity appropriate to make it ready for turning OFF the main switch S_1 as shown in Fig. 4.10(e).

Mode 6 $[t_5 - t_6]$
The resonant capacitor voltage polarity will continue to be in the same state as shown in Fig. 4.10(e) during this period. Since S_1 is ON, the current flows from dc bus to FES machine as shown in Fig. 4.10(e).

Mode 7 $[t_6 - t_7]$
Just before the switch S_1 is required to be turned off, the auxiliary switch S_{1A} is turned on again. This makes the current through the main switch S_1 to reduce as the load current is shared by the capacitor C_r as shown in Fig. 4.10(f). Once the capacitor current becomes equal to the load current, the current through the main switch becomes zero as shown in Fig. 4.9 at t_7.

Mode 8 $[t_7 - t_8]$
Capacitor discharges its remaining charge through D_1 as shown in Fig. 4.10(g). At the end of the discharge at instant t_8 , the polarity of the voltage across the capacitor C_r reverses. Any instant during the interval t_7 to t_8 the gate signal to the main device S_1 is removed, when the current through this is already zero. The current through D_1 becomes zero at t_8.

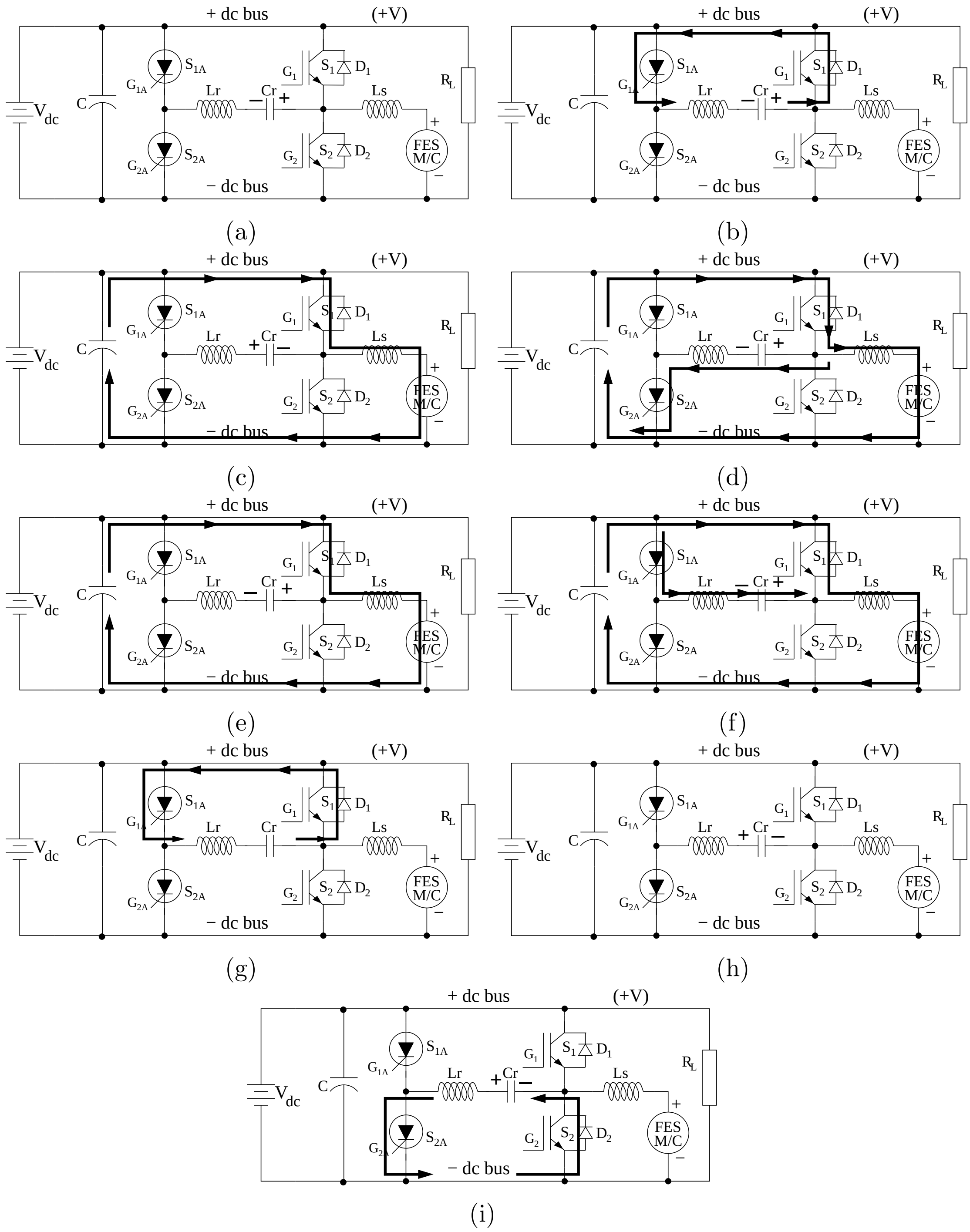

Figure 4.10: Current paths and device status in buck mode

Mode 9 $[t_8 - t_9]$
At the beginning of this mode, the capacitor has a voltage with a polarity as shown in Fig. 4.10(h). This is not the desired polarity of C_r and is required to be reversed for the next turn ON operation of S_1 .

Mode 10$[t_9 - t_{10}]$
No change in the status of circuit in this mode. The capacitor voltage continues with the polarity as shown in Fig. 4.10(h).

Mode 11 $[t_{10} - t_0]$
The auxiliary switch S_{2A} is tuned ON at instant t_{10}. The resonant capacitor voltage changes its polarity as the discharge current flows from C_r + through L_r, S_{2A}, D_2 and back to C_r- as shown in Fig. 4.10(i). At the instant, t_0 the capacitor acquires voltage with proper polarity required to make it ready for the next cycle as shown in Fig. 4.10(a).

4.2.5.2 Switching Waveforms and analysis in boost mode

In this mode, the power flows from the FES system (at lower voltage) to the dc bus (at higher voltage). The switch S_2 is gated with high frequency pulses whose width is adjusted to get therequired boosted dc bus voltage. Control pulses and anticipated waveforms across the power components are shown in Fig. 4.11. By referring to Fig. 4.8 and 4.12, analysis of the circuit in boost mode is carried out as follows:

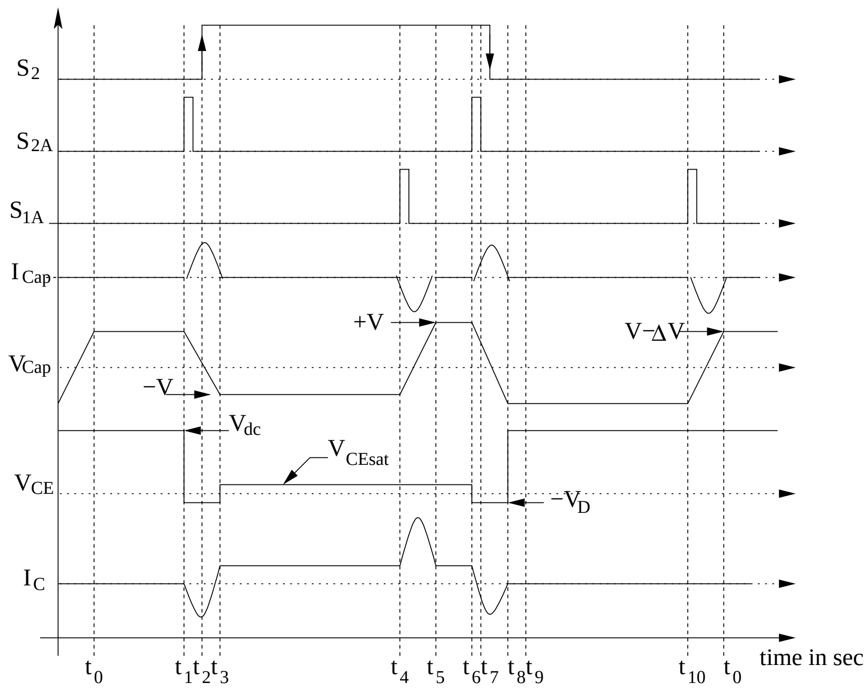

Figure 4.11: Control pulses, Current and Voltage waveforms in boost mode

Mode 1 $[t_0 - t_1]$
The resonant capacitor C_r is charged with the voltage polarity as shown in Fig. 4.12(a).

Mode 2 $[t_1 - t_1]$
Just before the switch S_2 is turned on, the auxiliary device S_{2A} is turned on at instant t_1 and the resonant capacitor discharges through the devices L_r , S_{2A} and D_2 as shown in Fig. 4.12(b).

Mode 3 $[t_2 - t_3]$
At instant t_2, gate pulse of the main device S_2 is made high, while freewheeling diode is still carrying the current. Current through the main device S_2 increases, shorting the source through the inductor L_s to ground as shown in Fig. 4.12(c). The capacitor C_r supplies part of this current as shown in Fig. 4.12(c). At the end of discharge (at instant t_3), the resonant capacitor current becomes zero and its voltage polarity reverses as shown in Fig. 4.12(d) with the magnitude equal to $V - \Delta V$. Main device S_2 continues to conduct.

Mode 4 $[t_3 - t_4\ ]$
During this period the resonant capacitor voltage polarity will continue to be in same as shown in Fig. 4.12(d). Since S_2 is ON, the current flows from positive of FES machine to series inductor L_s, S_2 and back to negative of FES machine as shown in Fig. 4.12(d). Some part of the energy of FES machine is transferred to the inductor L_s.

Mode 5 $[t_4 - t_5]$
Load current continues to flow through the main switch S_2 . The auxiliary switch S_{1A} is tuned ON at instant t_4 . The capacitor voltage changes its polarity as the charging current flows from +dc bus through S_{1A} , L_r , S_2 and back to - dc bus as shown in Fig. 4.12(e). This makes the resonant capacitor change its polarity and makes it ready for turning OFF the main switch S_2 as shown in Fig. 4.12(f).

Mode 6 $[t_5 - t_6]$
No change in the device state takes place in this period. The generator current continues to flow through the main switch S_2 .

Mode 7 $[t_6 - t_7]$
Just before the switch S_2 is required to be turned OFF, the auxiliary device S_{2A} is turned on again. This result in reduction of current through S_2 as the inductor current L_s is shared by the capacitor C_r as shown in Fig. 4.12(g). Once the capacitor current reaches the value of inductor current, the current through the switch S_2 becomes zero at t_7 as shown in Fig. 4.11.

Mode 8 $[t_7 - t_8]$
Resonant Capacitor C_r will discharge its remaining charge through D_2 as shown in Fig. 4.12(h). At the end of the discharge (at instant t_8) the polarity of the voltage across the resonant capacitor C_r reverses as shown in Fig. 4.12(c). At any instant during the period t_7 to t_8 the gate signal to the main switch S_2 is removed, when the current through the switch is already zero.

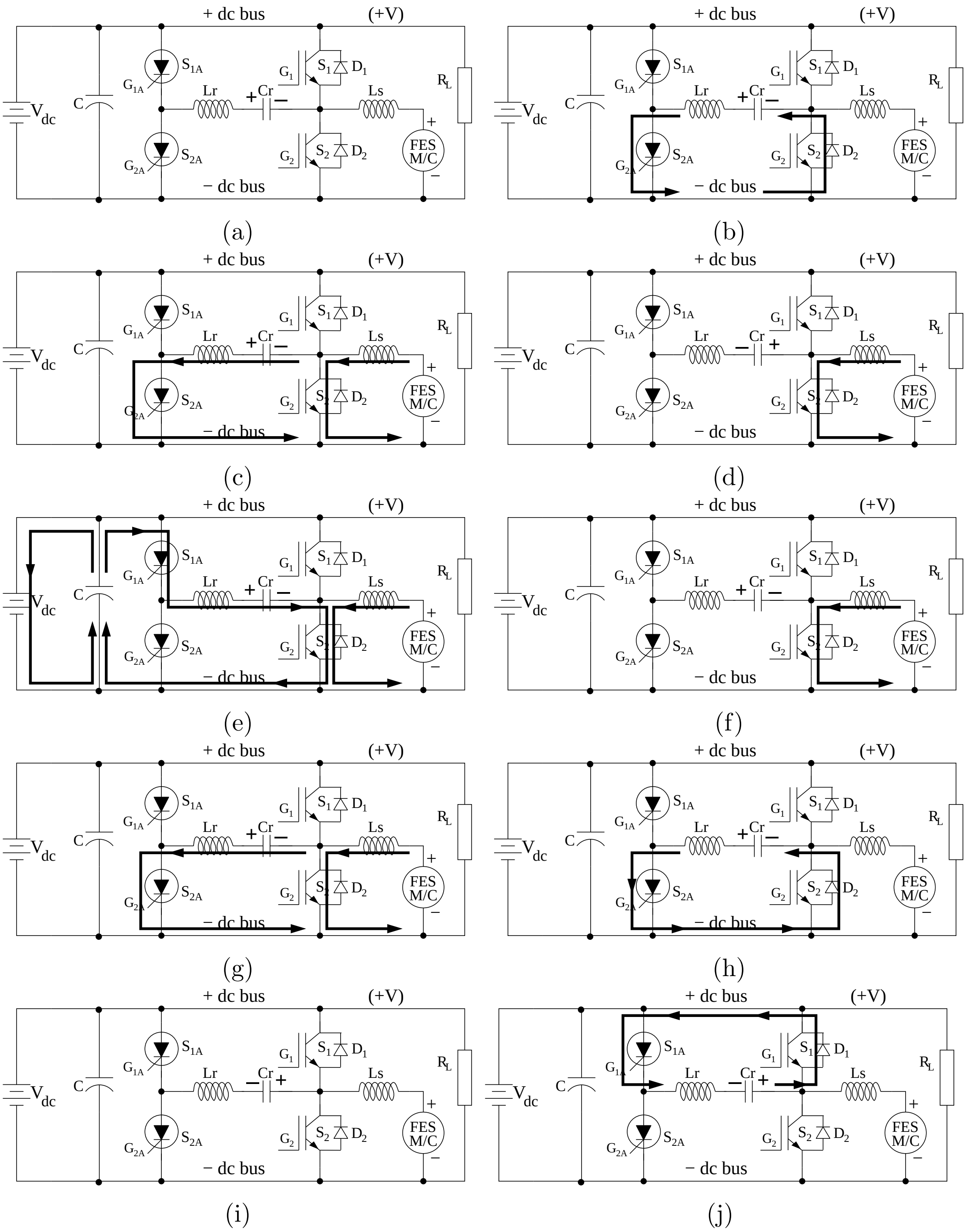

Figure 4.12: Current paths and device status in boost mode

Mode 9 $[t_8 - t_9]$
Resonant Capacitor C_r will have the polarity as shown in Fig. 4.12(i).

Mode 10 $[t_9 - t_{10}]$
Resonant Capacitor C_r will have the polarity as shown in Fig. 4.12(i).

Mode 11 $[t_{10} - t_0]$
The auxiliary switch S_{1A} is tuned ON at instant t_{10}. The resonant capacitor voltage changes its polarity as the discharge current flows through D_1 and S_{1A} as shown in Fig. 4.12(j). At this instant the resonant capacitor will acquire the voltage with proper polarity required to make it ready for the next cycle as shown in Fig. 4.12(a).

4.2.5.3 Design approach for ZVT/ZCT Transition circuit

It is desired that ZSPL be achieved for all operating conditions of the power converter i.e. resonant circuit should be designed to achieve ZCT/ZVT switching with rated load current through the main switch while power loss in the auxiliary switches/circuit is maintained as low as possible. The shape of a typical resonant current pulse is shown in Fig. 4.13. Design of the resonant circuit is nothing but-deciding the width and the peak value of this current pulse depending upon the power device characteristics and the magnitude of load current.

(i) Resonance period (Pulse width):
The resonant current exceeds the main switch current for duration T_{excess} as shown in Fig. 4.13. Choice of this time duration is device dependent. It should be long enough for the most stored charge of the main device to recombine. Generally T_{excess} should be at least twice longer than the t_{off} (sum of the storage time and current fall time of the main device).

(ii) Peak current (Pulse height):
Energy loss per cycle for achieving ZSPL must be as low as possible. Additional conduction loss takes place in the main switch due to the resonant current pulse. This is because in addition to the load current, the main device will have to carry an extra amount of resonant current pulse. Additional conduction loss due to this is caused only by that portion of resonant [40] current which is higher than load current in magnitude as shown in Fig. 4.13. Therefore, this peak current must be limited through proper selection of L_r and C_r . The values of L_r and C_r shall also be such that the required minimum duration of T_{excess} is twice as that of t_{off}. The additional conduction loss in the device should be kept as low as possible. T_{excess} can be increased either by increasing I_{peak} or by increasing T_o.

(iii)Maximum frequency of operation:
Turn off time of SCR (auxiliary device) and the off time (t_{off}) of main switch (IGBT/ MOSFET) put a limitation on the maximum frequency of operation. It can be seen from the following relation: Minimum gate control pulse width:$T_{min} = t_{10} - t_0$, Minimum time between two adjacent resonant current pulse is $T_r =$

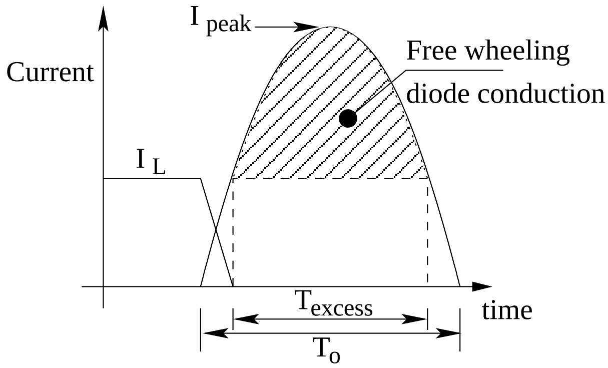

Figure 4.13: Resonant circuit current pulse

$2(t_{off} + t_q)$ time between t_3 and t_4 or t_5 and t_6[Fig. 4.11]

Note: Auxiliary device has to turn ON/OFF two times for each ON or OFF operation of the main device; Therefore two times the turn off time of the device is the minimum time. Four resonant current pulses are required in a cycle - two each for rising edge and falling edge respectively of the gate pulse of the main device. Therefore minimum gate pulse width is given by

$$T_{min} = 4(3t_{off} + t_q) \tag{4.11}$$

Maximum frequency of operation is given by,

$$f_{max} = \frac{1}{4(T_o + t_q)} \tag{4.12}$$

(iv) Design equations:

$$T_{excess} = 2t_{off} \tag{4.13}$$

$$T_o = 1.5T_{excess} = 3t_{off} \tag{4.14}$$

$$I_{peak} = 1.5I_L \tag{4.15}$$

$$Z_a = \frac{V_d}{I_{peak}} = \sqrt{\frac{L_r}{C_r}} \tag{4.16}$$

$$\sqrt{L_r C_r} = \frac{3t_{off}}{\pi} \tag{4.17}$$

From (4.15), (4.16) and (4.17), we get;

$$C_r = \frac{4.5t_{off} I_L}{\pi V_{dc}} \tag{4.18}$$

$$L_r = \frac{2t_{off} V_{dc}}{\pi I_L} \tag{4.19}$$

(v) A design example:
To test and validate the design approach explained in the previous section, design

Table 4.5: FES System specification and switching circuit parameters

FES Parameter		Resonant circuit parameter	
Output power	5.0 kW	L_r	1.2 μH,
DC bus voltage	550 V	C_r	0.159 μF
Peak load current (I_{peak})	150 A	f_{max}	16.18 kHz
Maximum speed of flywheel	15000 RPM	Power Devices parameter	
		t_{off}	445 ns
Minimum speed of flywheel	2500 RPM	(IGBT, SKM200GB125D)	
		t_q	15 μs
Backup time	60 s	(SCR, NTE5380)	

of a resonant circuit to achieve ZVT/ZCT of the power devices was carried out. The specifications of the FES system built are given in table 4.5

Design of resonant circuit for ZVT/ZCT was carried out using (4.18) and (4.19). The device parameters t_{off} (445 ns) and t_q (15 μs) are taken from the device data sheet of the respective manufacturer. Maximum value of dc bus voltage and currents (400 V, 100 A) are taken for computing L_r and C_r from the system specification sheet of the FES system built. The values of resonant components and max frequency of operation are given in table 4.5

4.2.6 Simulation and Experimentation

The simulation of the new topology using the values of components computed in the previous section was carried out using MATLAB/Simulink software and the results are recorded. Assumptions made in the simulation are,

- The capacitors and inductors used are ideal/lossless components
- Stray inductance of the connecting wires/bus bars equal to zero and there no stray capacitance in the circuit path.
- Due to above the voltage spikes and current surges during switching is absent.

4.2.6.1 Simulation result in boost and buck modes

It may be noted from the waveforms (obtained from simulations) which are given in Figs. 4.14(a) (iii), 4.14(a)(iv), 4.14(b)(iii) and 4.14(b)(iv) that the voltage across the switching device becomes zero before collector current starts flowing during switch ON transition of the device. Similarly, same figures show that the current through the switching device becomes zero before the voltage across the device starts increasing during switch OFF transition of the device. It is very clear from the simulation results given in Figs. 4.14(a) and 4.14(b) for buck and boost mode of operation respectively that the proposed topology will give definite advantage over the previous schemes.

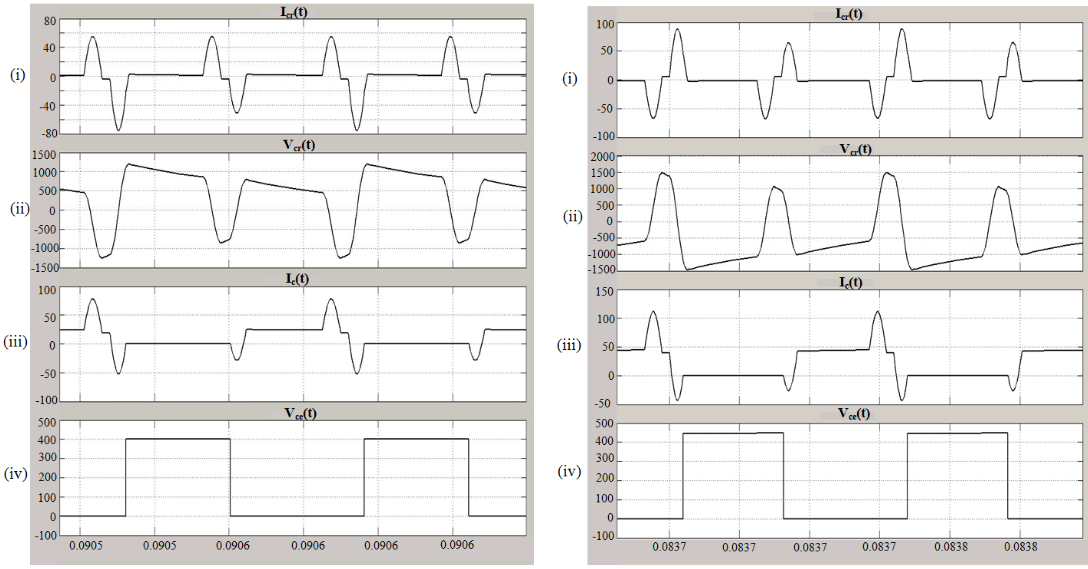

(a) Buck mode simulation (b) Boost mode simulation

Figure 4.14: Simulation results of the BDC showing the voltages across and current through the resonant components and power devices

4.2.6.2 Experimental results

A lab prototype of the bi-directional converter with ZCT switching technique was built using IGBT as the main switching device and the SCR as the auxiliary device. IGBT SKM200GB125D (200 A, 1200 V) of SEMIKRON make, which is easily available and best suited for high frequency application, was used. Maximum frequency of operation for this device for PWM application is 20 kHz. The converter is designed and tested for a reasonable maximum switching frequency of 15.4 kHz. The control logic was implemented and tested at various power levels.

The experiments have been conducted with various switching frequencies like 15.4 kHz, 7.5 kHz etc. The waveforms are recorded in a digital storage oscilloscope. The control pulses, device current/voltage waveforms in both buck and boost modes operations which are recorded are shown in Fig. 4.15 and Fig. 4.16. Plots of converter efficiency as a function of frequency in both buck and boost modes are given in Fig. 4.17 and Fig. 4.18 respectively . It is clear from Figs. 4.15 and 4.16 that in both buck and boost mode of operation of the topology, the voltage across the switching device becomes zero before collector current starts flowing and also the current through the switching device becomes zero before the voltage across the device started increasing. The waveforms recorded are not so close to ideal case, which can be attributed to the parasitic ringing in the current. It may also be observed that the waveforms at 7.5 kHz are much closer to the ideal waveform. Fig. 4.17 shows that there is a saving of 1.75% – 2.1% of power in buck mode of operation by adopting the proposed ZSPL topology and control logic for the converter. This resulted in an increase of energy back up time to 61.38s from 60.0s. Fig. 4.18 shows that there is a saving of 1.5% – 2.6% of power in boost mode by adopting the proposed ZSPL topology and control logic. This resulted in an increase of energy back up time to 62.25s from 60.0s.

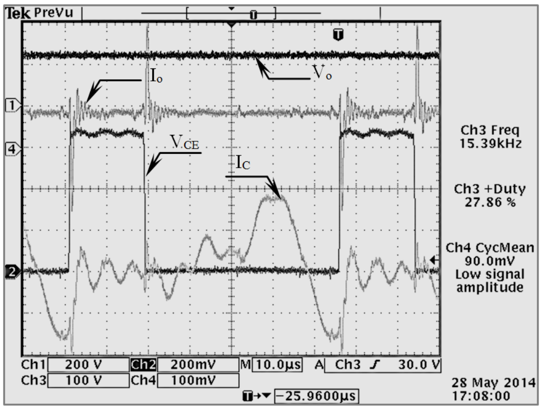

(a)

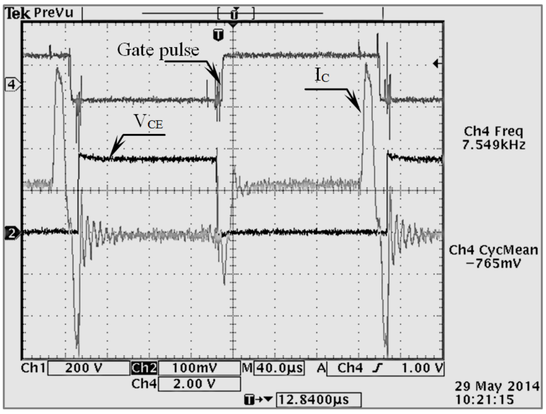

(b)

(a) Collector emitter voltage ($V_{ce(off)}$ = 340 V), collector current ($I_{c(on)}$ = 20 A), output voltage (V_o = 250 V) and output current(I_o = 10 A) waveforms with dc-bus voltage = 340 V, f_{sw} = 15.4 kHz,and with LC filter at output. (b) Collector emitter voltage ($V_{ce(off)}$ = 340 V), collector current ($I_{c(on)}$ = 10 A), output voltage (V_o = 250 V) and output current (I_o = 10 A) waveforms with dc-bus voltage = 340 V, f_{sw} = 15.4 kHz and without LC filter at output.

Figure 4.15: Experimental results in buck mode of operation of BDC

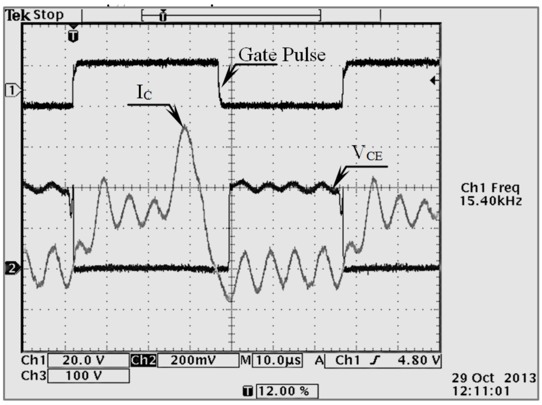

(a)

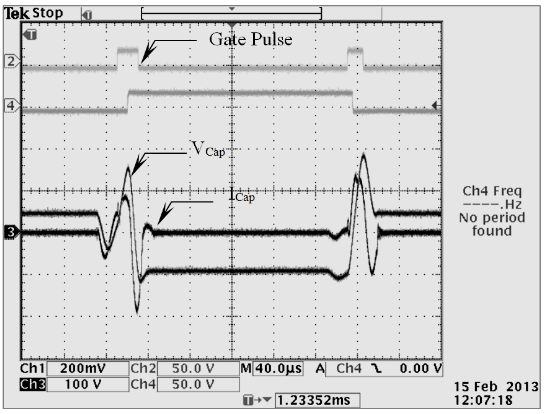

(b)

(a) Collector emitter voltage ($V_{ce(off)}$ = 200 V) and collector current ($I_{c(on)}$ = 40A) waveforms with dc-bus voltage = 200 V, f_{sw} = 15.4 kHz. (b) Capacitor voltage and capacitor current waveforms with f_{sw} = 2.2 kHz, R_L = 10 Ω.

Figure 4.16: Experimental results in boost mode of operation of BDC

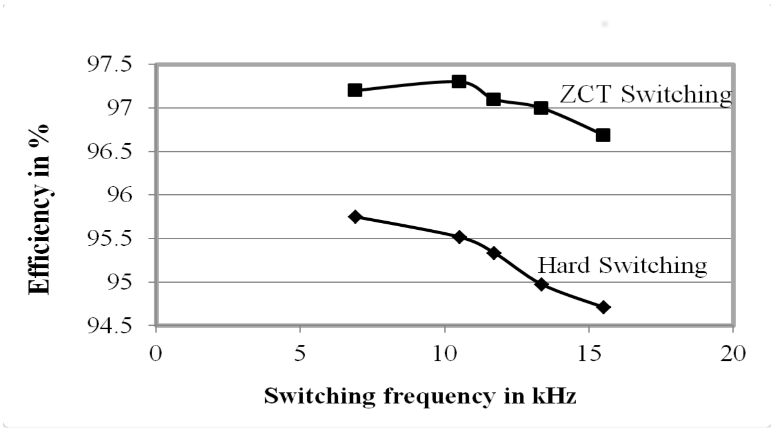

(At P_o = 4.3 kW, dc-bus voltage = 340 V)

Figure 4.17: Efficiency curves in buck mode as a function of switching frequency

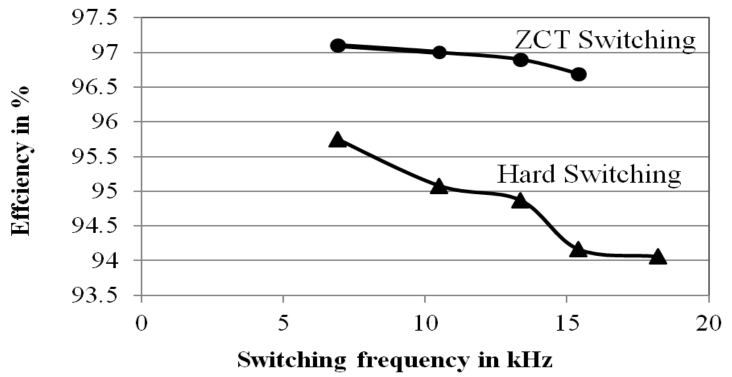

(At P_o = 4.3 kW, dc-bus voltage = 340 V)

Figure 4.18: Efficiency curves in boost mode as a function of switching frequency

4.3 Other loss reduction techniques

Drag loss can be reduced by providing the vacuum enclosure [76] for the rotating parts of the system. Both eddy current and hysteresis loss can be reduced by the using a two pole machine (with this the supply frequency becomes half) as well as by using low specific loss core material [21]. Bearing friction loss can be reduced by using an active magnetic bearings or ceramic/hybrid bearings [77]. With magnetic bearings, the system will become complicated and very expensive. Using a twopole machine will be a cheaper option compared to costly low specific loss core material. Usage of two pole machine will reduce the flux dependent loss as well as armature current dependent eddy current loss. As per the available literature [19], keeping the rotating parts in a enclosure with vacuum of 0.1mb, the loss due to drag will get reduce to the extent of 75% (compared to atmosphere)

4.4 Summary

After analysing the various losses it is found that drag loss and eddy current losses are dominant at higher speeds. Hence the easy solutions for improving the efficiency of the system are vacuum enclosure for rotating parts and usage of two-pole machine. With these techniques the efficiency can be increased to a large extent. Among other losses the switching loss in the boost converter which is due to the higher input current is improved by adopting a newly proposed topology which uses ZVT/ZCT switching technique. A BDC was built using this new proposed topology and tested with an output power level of 4.3kW at 340V input. The results were compared with those of hard switched topologies. It is observed that by using the proposed topology there is a saving of power to the extent of 1.5% to 2.6% resulting in an increase of the backup time from 60 seconds to 62.5 seconds. Interestingly, the saving in power is found to be higher in boost mode as compared to that in buck mode. This is due to the fact that in boost mode of operation the device current will be higher as compared to buck mode for the same output power leading to higher losses. It may be noted here that this is a desirable feature for an FES application because the energy stored in the flywheel is harvested during the boost mode operation of BDC.

Quantity of energy harvested depends on highest running speed of flywheel and the maximum voltage gain of boost converter. To enhance the harvested energy, the maximum achievable gain of the boost converter should be as high as possible which depends on the ratio of source resistance of generator to load resistance. Current dependent losses of the generator appear as a series resistance at the input of the boost converter. Detailed analysis and modelling of the current dependent losses in the generator reflected as series source resistance is carried out in the Chapter-5.

Chapter 5

Analysis of generator parameters for Optimal energy harvesting

This chapter focussed on various parameters which affects the amount of harvested energy. First part of chapter covers the study, analysis and modeling of the generator source resistance caused by current dependent losses in its core. Analysis of the BLDC machine using FEM and armature current waveforms using FFT been done to understand this phenomenon. The losses in a BLDC generator which appear as series source resistance to the boost converter (BDC) have been quantified. Results obtained from FEM/FFT analysis and circuit simulation are presented. The guidelines for the design of BLDC generator and the selection of a bi-directional converter topology for optimal energy harvesting from a FESS are given. Second part of this chapter covers the study of the effect of leakage inductance of the machine in motor and generator mode of operation on the dynamic performance, torque pulsation and peak armature current. Simulation and experimental results are also presented in this chapter.

5.1 Effect of source resistance

The value of source resistance decides the quantity of energy harvested from a flywheel. Therefore it is necessary to understand various parameters related to energy harvesting and their dependancy on the source resistance. This is carried out in the subsequent sections.

5.1.1 Dependency of Harvestable energy on boost converter gain

Maximum achievable gain G_{max} of the boost converter by substituting $D = D_{max}$ in (3.1) of chapter 3.

$$G_{max} = \frac{1}{1 - D_{max}} \times \frac{1}{1 + \frac{R_S/R_L}{(1-D_{max})^2}} \tag{5.1}$$

The voltage gain of the boost converter is the ratio of output voltage to input voltage. It is desired that this gain should be maximum when the input voltage is minimum to maintain the dc bus voltage constant. Therefore,

$$V_{min} = \frac{V_{dc}}{G_{max}} \tag{5.2}$$

As explained in the earlier chapters the energy harvested from a flywheel is given by [34],

$$E_h = \frac{1}{2} J(\omega_{max}^2 - \omega_{min}^2) \tag{5.3}$$

It is clear from (5.3) that, for a given top speed, the harvestable energy depends on ω_{min}. The induced voltage in a generator thereby dc bus voltage is proportional to the speed as per the following relation:

$$V_{min} = K_v \omega_{min} \tag{5.4}$$

Combining (5.2) and (5.4) we get,

$$\omega_{min} = \frac{V_{dc}}{K_v G_{max}} \tag{5.5}$$

It is clear from (5.1) to (5.5) that harvestable energy is proportional to the gain which in turn inversely proportional series source resistance of the generator. Detailed analysis is given in next section.

5.1.2 Effect of Source resistance on the voltage gain

Voltage gain of the boost converter is related to the duty cycle and ratio $\frac{R_S}{R_L}$ as given by (3.1). This shows that the voltage gain deteriorates with an increase in the value of $\frac{R_S}{R_L}$.

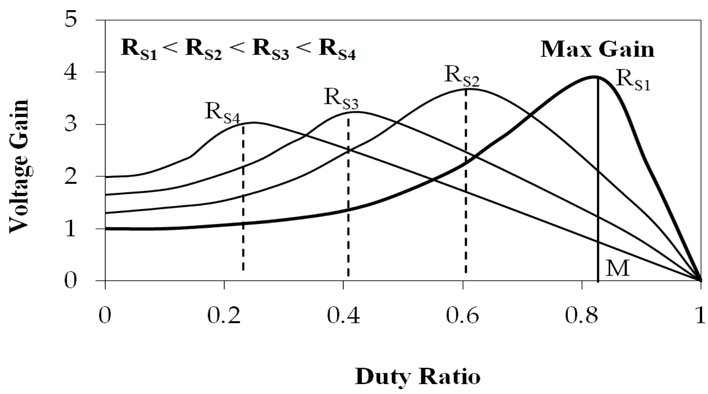

Figure 5.1: Voltage gain versus duty cycle

In Fig. 5.1, the voltage gain is plotted as function of duty cycle with various values of source resistance for a given R_L. It is clear from this graph that as the ratio of $\frac{R_S}{R_L}$ increases, the maximum voltage gain and the range of operating duty cycle decreases. Higher voltage gain can be achieved by keeping the ratio of $\frac{R_S}{R_L}$ as low as possible. In addition to this, higher efficiency can also be achieved by keeping the $\frac{R_S}{R_L}$ ratio low. Hence it is important to study and model this source resistance to design an optimal energy harvesting system. Series source resistance include the resistance of connecting leads, armature conductors and the current dependent losses in the machine. Analysis of these losses is done in the following sections.

5.1.3 Source resistance and its relation to losses of the BLDC machine

Basically there are two types of power losses in the stator core of an electrical machine. They are hysteresis loss and eddy current loss [37, 78]. Eddy current loss has two components. One component is dependent on field flux (P_{eF}) and the other component is dependent on armature current (P_{ei}). The losses in any electrical machine can be represented as a set of resistances in the electrical equivalent circuit of machine as shown in Fig. 5.2. The first set of resistances connected in parallel to the voltage source are R_h (due to hysteresis loss), R_{eF} (due to field flux dependent eddy current loss), and extra (anomalous) losses of the machine [37, 78]. The next set of resistance connected in series with the voltage source is R_S. The R_S is the series combination of R_{cu} (due to copper loss) and R_{ei}(current dependent losses of the generator due to armature current). This additional eddy current loss is due to the main flux distortion caused by the current flowing through the armature conductors. These generator losses increase with loading. Sources of these series resistances are determined, and this resistance is expressed using physical parameters of the machine to suggest the technique and guidelines for choosing most appropriate power converter topology for enhancing the harvestable energy from the flywheel in the following sections.

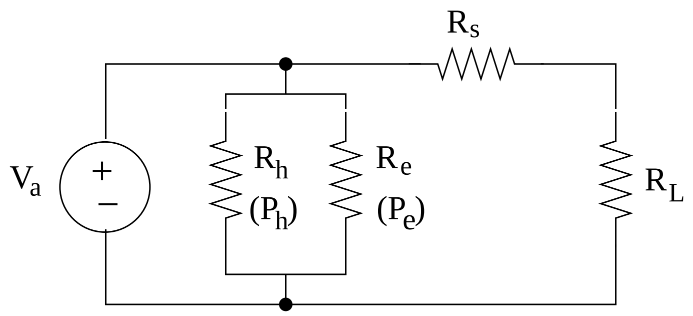

Figure 5.2: Equivalent circuit of losses in the generator

It is necessary to separate the field flux dependent eddy current loss (P_{eF}) and armature current dependent eddy current loss (P_{ei}). This helps in estimating the values of the series resistance which are shown in the Fig. 5.2. Scope of this work is limited to the estimation of only current dependent eddy current loss and its contribution to the series component of source resistance of the generator. This is because they appear as series resistance in the machine equivalent circuit. Various losses of the machine can be computed by using equations given below relations [37, 78].

$$P_h = K_h f B^{\alpha} \tag{5.6}$$

$$P_{eT} = K_e f^2 B^2 \tag{5.7}$$

$$P_a = K_a f^{1.5} B^{1.5} \tag{5.8}$$

where $B = B_F + B_a$

"t"	: Thickness of lamination
"σ"	: Electrical conductivity of lamination
"ρ_v"	: Volumetric mass density

It is well known that the flux produced in the stator core due to armature current (B_a) is directly proportional to armature current and as per the following relation:

$$B_a = K_x I_a \tag{5.9}$$

Total eddy current loss has two components as explained earlier and as per the following relation:

$$P_{eT} = P_{ei} + P_{eF} \tag{5.10}$$

Total current dependent loss (P_s) is as per the following relation:

$$P_s = P_{ei} + P_{cu} \tag{5.11}$$

where

$$P_{ei} = K_e f^2 (B_F B_a + B_a^2) \tag{5.12}$$

$$P_{cu} = I_a^2 R_a \tag{5.13}$$

5.1.4 Computation and Analysis of eddy current loss from first principles

Total flux in the core of the machine is the sum of the flux produced by armature ampere turns and field magnets. Eddy voltages are induced in the stampings of the stator core due to the rate of change of this flux. These eddy voltages make the eddy current to flow in the stampings resulting in the eddy current loss. The eddy current loss has two components as given by (5.10); (P_{eF}) produced by field flux and (P_{ei}) produced by the armature current.

5.1.4.1 Effect of armature current on the flux pattern

The current flowing through the armature coils changes the flux pattern in the air gap. The distortion of the flux takes place due to the armature reaction [75]. Cross sectional view of a typical 4-pole, PM BLDC machine is given in Fig. 5.3 which gives the physical arrangement of stator slots,armature windings, rotor and buried magnets in the machine. The plot of the air gap flux density as a function of mechanical angle ($\theta_{mech} = 0$ to 360^o) is given in Fig. 5.4. The air gap flux density plot without load current is given in Fig. 5.4(a), Fig. 5.4(b) and (c) give the air gap flux density plot with armature current I_a and $2I_a$ respectively. As the armature current changes, the flux pattern also changes as shown in Fig. 5.4. It may be noted from this plot that the peak flux density increases as the armature current increases.
In the generator mode operation, the air gap flux gets affected in the following way [75].

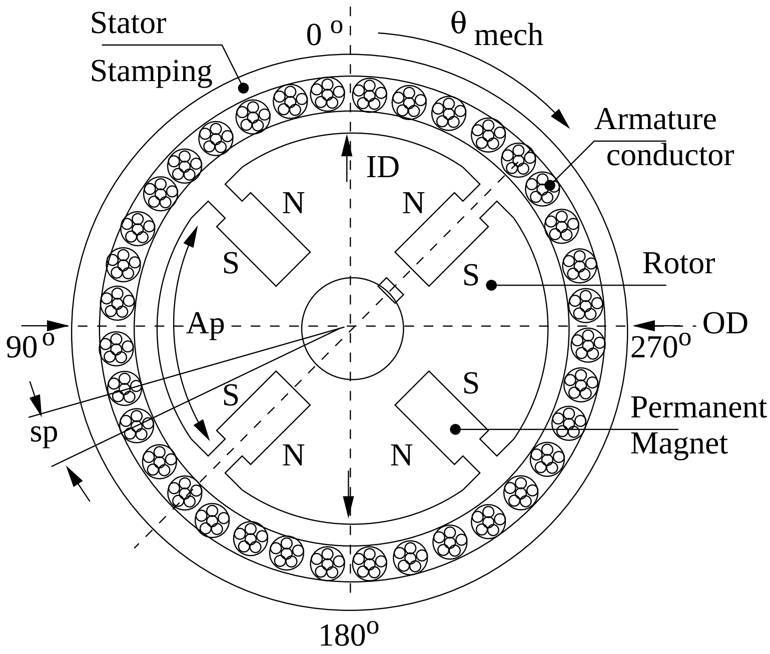

Figure 5.3: Cross sectional view of a typical 4-pole, PM BLDC machine

(i) Trailing pole tips :
The flux produced by armature current and the flux produced by field (i.e. Permanent Magnet in this case) are in the same direction at the trailing tips of the poles of machine and they aid each other. Hence the flux density increases at the trailing tips of the poles.

(ii) Leading pole tips :
The flux produced by armature current and the flux produced by field (i.e. Permanent Magnet in this case) are in the opposite direction at the leading tips of the pole of the machine and they oppose each other. Hence the flux density decreases at these leading tips of poles.

5.1.4.2 Effect of flux pattern on the eddy current loss

(i) Eddy current loss without armature reaction (generator in no load condition $B_{max} = B_F$) :

Substituting $B_{max} = B_F$ in (5.7) we get,

$$P_{eT} = K_e f^2 B_F^2 \tag{5.14}$$

(ii) Eddy current loss with armature reaction (generator in loaded condition;$B_{max} = B_F + B_a$) :
By referring to Fig. 5.4 (b) and (c) we have,

$$B_{max} = B_F + B_a \tag{5.15}$$

$$B_{min} = B_F - B_a \tag{5.16}$$

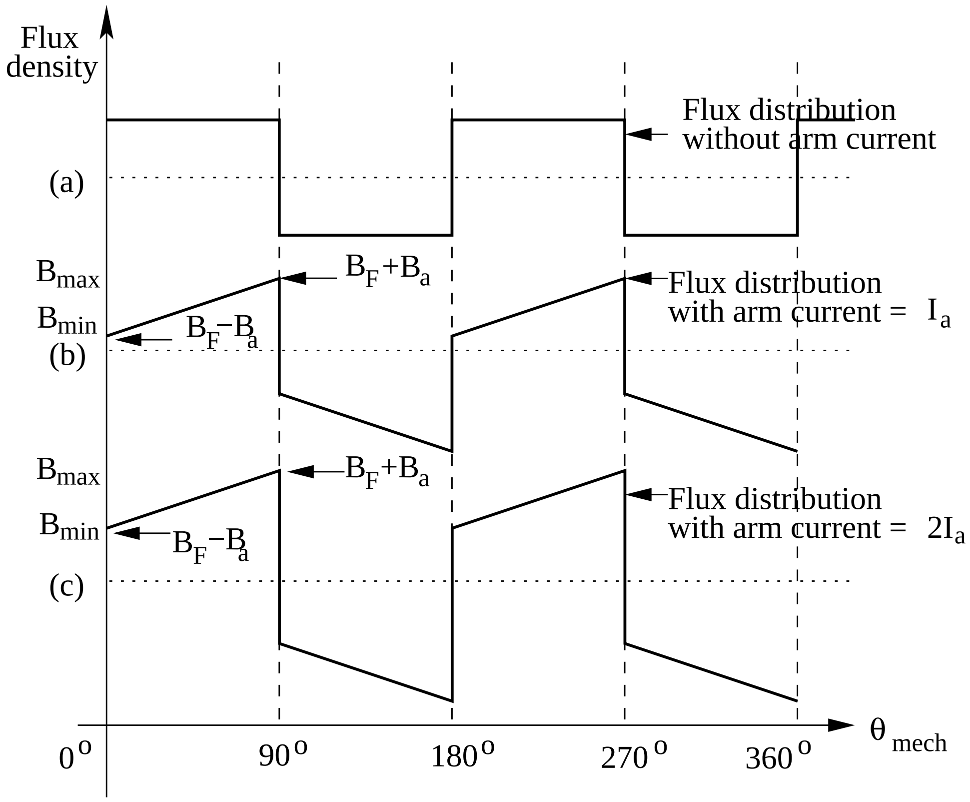

Figure 5.4: Air gap flux as a function of θ_{mech} in generation mode

Substituting $B_{max} = B_F + B_a$ in (5.7) we get,

$$P_{eT} = K_e f^2 (B_F^2 + 2B_F B_a + B_a^2) \tag{5.17}$$

For the machine considered here, the operating point is close to the saturation flux density of the stator core, increase in flux due to current is not proportional and hence the quadratic relationship of P_{eiT} with flux density is lost and (5.18) can be re-written as,

$$P_{eT} = K_e f^2 (B_F^2 + 2B_F B_a) \tag{5.18}$$

Comparing (5.18) with (5.10) we get

$$P_{eF} = K_e f^2 B_F^2 \tag{5.19}$$

$$P_{ei} = 2K_e f^2 B_F B_a \tag{5.20}$$

5.1.4.3 Effect of current waveform distortion on the eddy current loss

Eddy current losses for various harmonics are given below:

$$P_{ei1} = K_e B_F B_a f_1^2 = K_e B_F B_a f^2 \tag{5.21}$$

(At fundamental frequency)

$$P_{ei3} = B_{a3} f_3^2 = 9\frac{B_a}{3} B_F f^2 = 3K_e B_F B_a f^2 \tag{5.22}$$

(At third harmonic frequency)

$$P_{ei5} = B_{a5} f_5^2 = 25 \frac{B_a}{5} B_F f^2 = 5 K_e B_F B_a f^2 \tag{5.23}$$

(At fifth harmonic frequency)

$$P_{ein} = B_{an} f_n^2 = n K_e B_F B_a f^2 \tag{5.24}$$

(At "n" th harmonic frequency)

Total current dependent eddy current loss that takes place in the machine is the sum of individual losses at different harmonic frequencies. Therefore,

$$P_{eiT} = \sum_{j=1,3,5,...}^{n} j P_{ei1} \tag{5.25}$$

It is clear from (5.25) that the loss P_{eiT} increases with increase in the harmonic content of the armature current waveform.

5.1.5 Analysis of eddy current loss using Finite Element Method (FEM)

From the analysis given in previous section, it is found that there are two components in eddy current loss. One is proportional to square of field magnet flux (B_F^2) and the other is proportional to product of B_F and B_a ($B_F \times B_a$). To validate this analysis, it is necessary to find the losses at different armature currents I_a. Hence the FEM analysis of the BLDC generator was carried out using AnSys-Maxwell software and the results are presented here. Flux plots and current waveforms are given in subsection 5.1.5.1 and quantification of losses in subsection 5.1.5.2.

5.1.5.1 Flux density plots

Flux density at various points in the stator core at different armature current were taken and given in the Fig. 5.5(a) and Fig. 5.5(b).

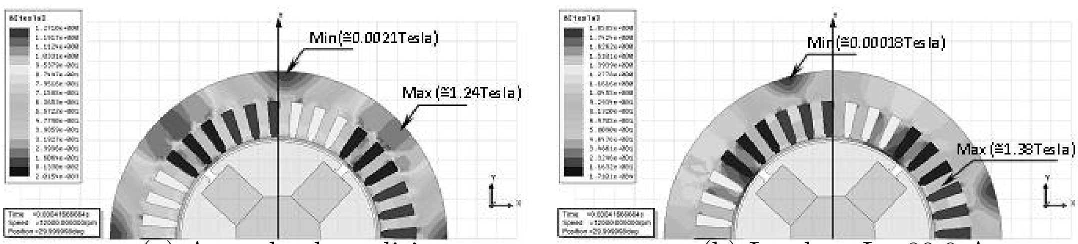

(a) At no load condition (b) Load at I_a=80.0 A,

Figure 5.5: Flux density plot of FEM analysis at various load

It may be noted that under no load condition ($I_a = 0.0A$), the flux is uniformly distributed in the air gap and its peak value is also low under the pole arc. As the machine is loaded, the flux pattern distorts. The peak (B_{max}) flux density is higher at higher armature current and lower at lower armature current. The armature current waveforms (at I_a=8A) and I_a=64.0 A) are given in Fig. 5.6(a) and (b). It may be noted that, if load is increased, the armature current waveform gets distorted and also the armature induced voltage.

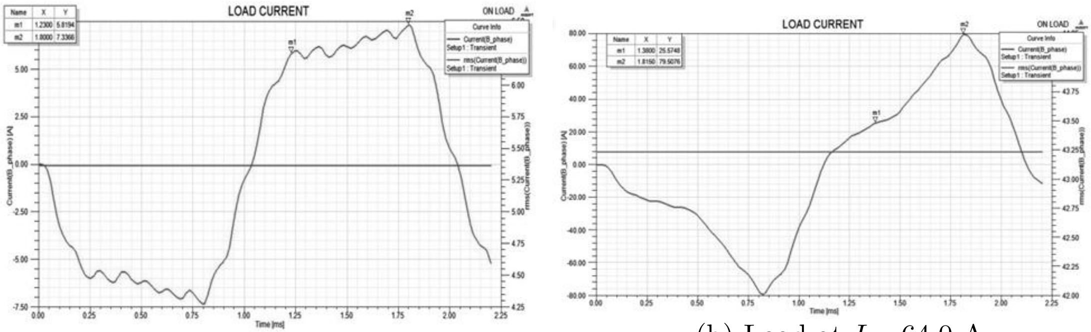

(a) Load at I_a=8.0 A,

(b) Load at I_a=64.0 A

Figure 5.6: Armature current plot obtained from FEM Analysis at various load

5.1.5.2 Quantification and tabulation of various losses

Computation of flux density at various points of stator core, eddy current losses and anomalous losses at various armature current values were carried out using AnSys-Maxwell (FEM analysis software). The eddy current loss is plotted as a function of armature current and air gap flux separately as shown in Fig. 5.7 and Fig. 5.8 respectively.

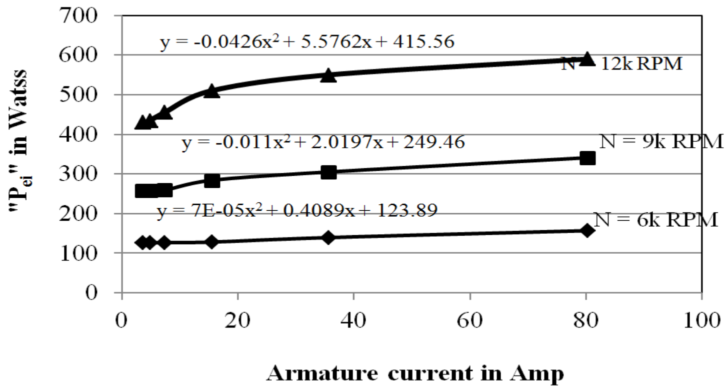

Figure 5.7: Current dependent eddy current loss P_{ei} as a function of armature current with speed as parameter.

From the graphs given in Fig. 5.7 the relation between the armature current and the current dependent losses is found out using the curve fitting method. For the operating range of armature current (considered in this application), the first term is negligible in this expression. Hence this term is ignored. The expression for the current dependent eddy current power loss as a function of armature current at a speed of 12000 RPM is as per the following relation:

$$P_{eT} = 5.5762 I_a + 415.56 \tag{5.26}$$

Different terms of (5.26) are plotted separately as shown in the Fig. 5.9 It may be noted that this equation is identical to (5.10). There are two terms in this equation. One term is dependent on the armature current corresponding to P_{ei} and another term, which is constant, is corresponding to P_{eF}. The first term shows the dependence of P_{ei} on f, B_F and B_a. It may be noted that the relationship

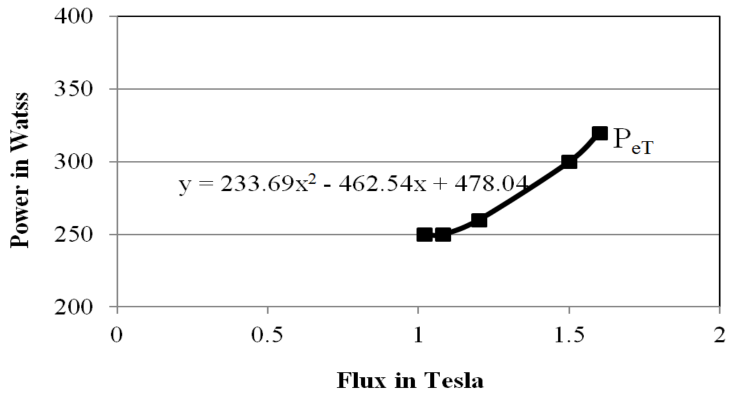

Figure 5.8: Eddy current losses as a function of armature flux at 12000 RPM

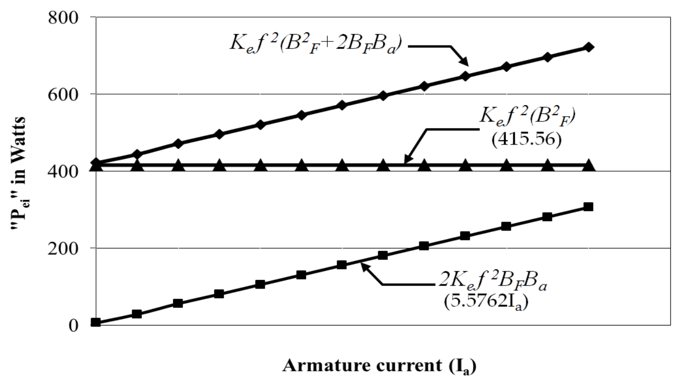

Figure 5.9: P_{ei} versus I_a at 12000 RPM

(5.18) obtained from the theory is identical to relationship (5.26) obtained from FEM analysis.

5.1.5.3 Harmonic analysis of the armature current waveforms

The current dependent eddy current loss obtained from FEM analysis is plotted as a function of armature current for different wave shapes as shown in Fig. 5.10. It may be noted that the P_{ei} loss is higher with armature current of quasi square wave shape (when induced voltage is trapezoidal) as armature current of sinusoidal wave shape for a given RMS value.

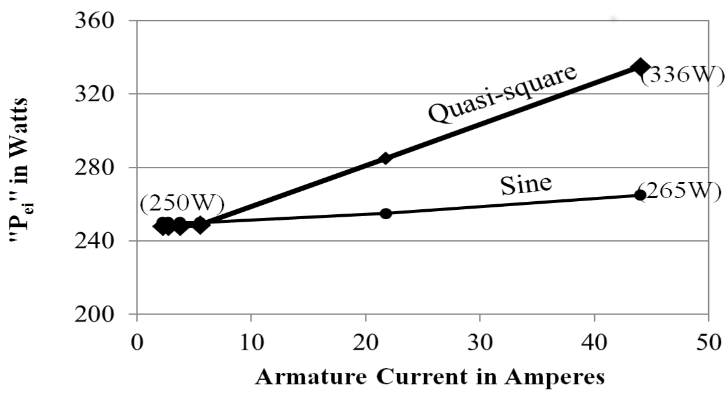

Figure 5.10: P_{ei} versus I_a as a function of harmonics at 12000 RPM

To study the dependency of P_{ei} loss on the total harmonic content, harmonic analysis (using Fast Fourier Transform) of the armature currents obtained from FEM is carried out using MATLAB/Simulink software. Harmonic analysis of armature current waveforms is carried out and THD is plotted as a function of RMS value of armature current as shown in Fig. 5.11

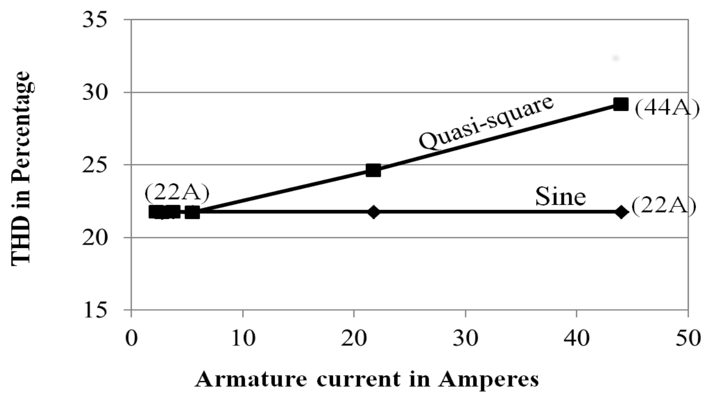

Figure 5.11: THD versus I_a at rotor speed of 12000 RPM

It is clear from this plot that the current harmonics are higher at higher RMS value of load currents. This is due to the fact that the current flowing in the armature conductors cause distortion of air gap flux as explained earlier in this chapter.

5.1.5.4 Observations from FEM and FFT analysis

Observations made from the FEM and FFT analysis are given below:

- When the armature current is quasi-square in shape, the eddy current loss increased from 250 W to 335 W as the armature current is increased from 0–42 A [Fig. 5.10].

- When the armature current is Sinusoidal in shape, the eddy current loss increased from 250 W to 265 W as the armature current is increased from 0–42 A.

- When the current waveform is sinusoidal the variation in P_{ei} is present, but very small (15W) as compared to that of quasi-square wave (85 W)

- It is also observed that the armature current harmonics increase with the load current [Fig. 5.11]. From the above observations it is concluded that the P_{ei} depends on the shape (THD) as well as the peak value of the armature current.

5.1.6 Modeling of the eddy current dependent source resistance

Current dependent eddy loss equivalent circuit of the BLDC generator can be represented as shown in Fig. 5.12. The loss thus represented as series resistance can be mathematically modeled as given below:

$$P_{ei} = \frac{V_d^2}{R_{ei}} \tag{5.27}$$

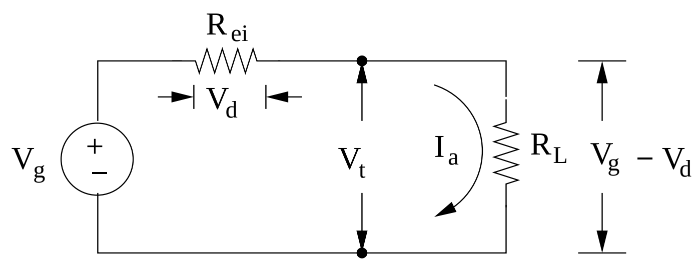

Figure 5.12: Current dependent eddy loss equivalent circuit of BLDC generator

The stator core eddy currents are caused by eddy voltage which is induced in the stator lamination due to the rate of change of flux produced by the armature ampere turns. This eddy current flow through laminations and produces the eddy flux which demagnetizes the main (field) flux. This results in the reduction of induced voltage across the generator armature winding causing the voltage drop V_d shown in Fig. 5.12. The magnitude of eddy current can be computed by knowing the induced eddy voltage in the laminations and its eddy resistances [78, 79].

5.1.7 Performance of boost converters fed by BLDC Generators

From the analysis carried out in the previous section it is found that following parameters of an FES system affects the source resistance as seen by the boost converter:

- Current dependent eddy current loss (depends on the design and selection of machine)
- Peak value and Harmonic content of the armature current of generator (depends on the type of boost converter).
- Magnitude of load current drawn from the generator (Higher the load current, higher is the distortion of the air gap flux and higher the armature current harmonics).

To determine the suitability of a particular boost converter, it is required to know the wave shape and magnitude of the armature current drawn from the generator. Hence the simulation of single stage and two stage boost converter was carried out using MATLAB / Simulink software. The block diagram and the simulation results of single stage boost converter topology is given in Fig. 5.13 and Fig. 5.14 respectively. Same for the two stage boost converter is given in Fig. 5.15 and Fig. 5.16 respectively.

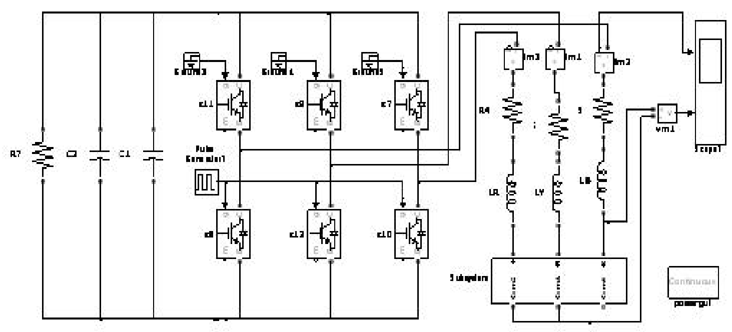

Figure 5.13: Power circuit simulation model of SSBC

From the results obtained from the simulations, it is observed that the peak current in single stage converter (400 A) is much higher as compared to two stage boost converter (70 A) for the same output power (400 V, 5 A). This implies that usage of single stage boost converter leads to an increase in the source resistance and reduction of harvested energy.

5.1.8 Selection criteria of BLDC machine and power converter

For a given output power rating, minimum size and lighter weight (Higher power density) are important factors to be considered during the selection of the machine.

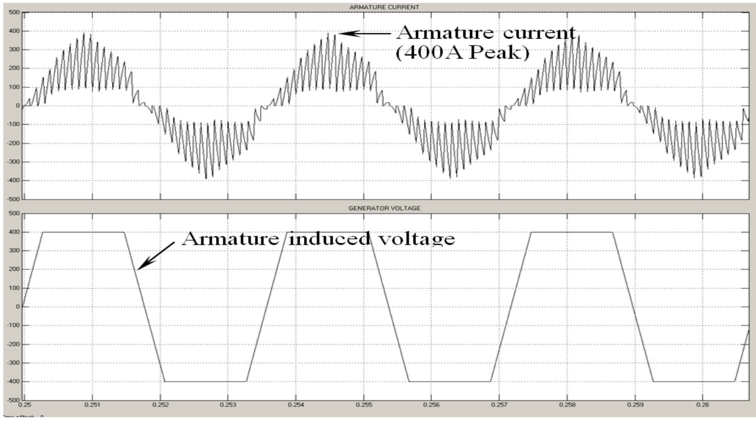

Figure 5.14: Armature current and voltage waveforms of simulated BLDC generator in SSBC mode

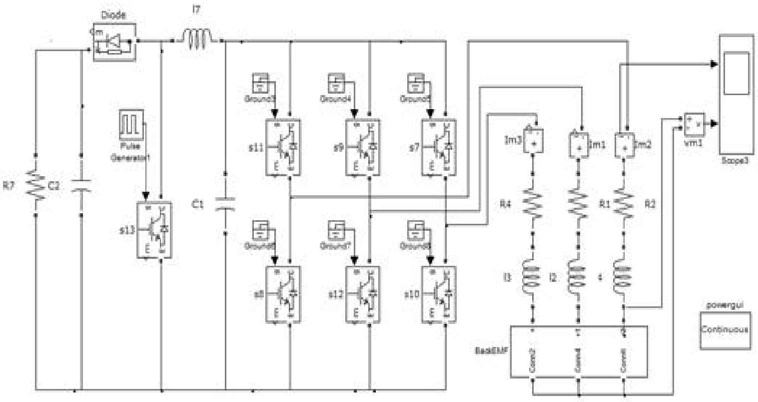

Figure 5.15: Power circuit simulation model of TSBC

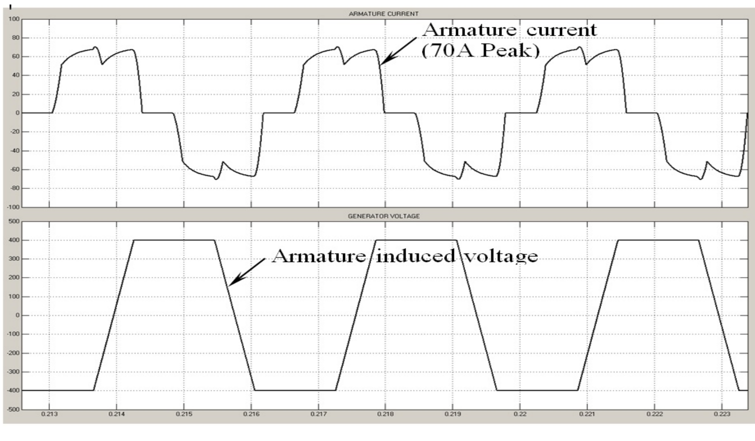

Figure 5.16: Armature current and voltage waveforms of simulated BLDC generator in TSBC mode

For optimum energy harvesting, the selected BLDC machine should offer lowest possible series source resistance to boost converter which is connected at its output. Current dependent eddy current loss and thereby series source resistance can be reduced by selecting the machine with higher air gap, lower stamping thickness, lower width of the tooth, higher no of slots of stator stampings or a combination of all [78, 79]. As seen from the simulation results [Figs.5.14, 5.16,] the peak armature current in two stage boost converter is much less compared to single stage boost converter. Therefore, two-stage boost converter is a better choice as compared to single stage boost converter. It may be noted that the peak value of the armature current in a single stage boost converter can be limited by adding a series inductance at the output of generator terminals. But this will also increase the response time and reduction of output power when the machine is used as a motor [19]

5.1.9 Experimental setup and tabulation of results

Prototype laboratory models of the Single-stage boost converter (SSBC) and Two-stage boost converter (TSBC) for flywheel energy harvesting are built using a PM-BLDC machine. A P+I feedback voltage controller is digitally implemented for maintaining the dc bus voltage constant using the Motorola make, DSP 56F805 processor. TSBC and SSBC are tested with same load conditions for evaluating the schemes and comparing their energy harvesting performances. Tabulation of the experimental results is given in the table 5.1.

Table 5.1: Performance parameters recorded from the experimental set up

V_{dc}=400 V, ω_{max}=1177 rads/s, J=0.681 kgm^2					
Model	R_L (Ω)	Max Gain	T_{bu}(s)	V_{min} (V)	ω_{min}(rad/s)
SSBC	130	2.37	38	169	497
	82	1.65	22	242	713
	40	1.34	17	299	878
TSBC	130	11.43	185	35	103
	82	9.56	130	42	123
	40	5.46	70	73	216

Performance of power converters SSBC and TSBC in terms of harvestable energy and its graphical representation are shown in table 5.2 and Fig. 5.17 respectively.

Table 5.2: Comparison of harvested energy at various loads

V_{dc}=400 V, ω_{max}=1177 rads/s, J=0.681 kgm^2					
	SSBC		TSBC		
I_L (A)	Max Gain	Eh (kJ)	Max Gain	Eh (kJ)	ΔEh (kJ)
3.0	2.37	387.7	11.43	468.1	80.4
4.9	1.65	298.4	9.56	466.5	168.1
10.0	1.34	209.0	5.46	455.9	246.9

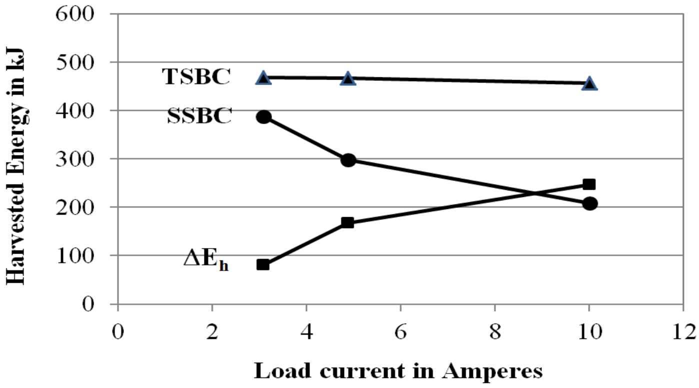

Figure 5.17: Harvested energy versus load current in SSBC and TSBC mode

It is observed that the voltage gain of the boost converter has reduced as the load power is increased [Table 5.1]. This results in the increase of the minimum speed (induced voltage) up to which the boost converter can maintain the output dc voltage. It may be noted that the minimum speed (induced voltage) up to which the boost converter can maintain the output dc voltage is a function of load resistance. This is because the maximum gain of the boost converter is an inverse function of the ratio of $\frac{R_S}{R_L}$

5.2 Analysis of leakage inductance effect on the performance of the BLDC machine

The Permanent Magnet Brushless DC (PM-BLDC)machine has higher power density as compared to others [80]. Non ideal components and imperfection in construction increases the leakage inductance of the machine leading to the reduction of maximum power throughput for a given power rating. Study of the effect of leakage inductance on the performance of the BLDC machine is carried out in the following sections.

5.2.1 Power generation mechanism in a BLDC motor

The BLDC machine can be used as a motor or as a generator. When is being used as a motor, the total power drawn from the dc source and generated mechanical output power reduces when the value of leakage inductance is non zero.

5.2.1.1 Power generation in ideal case

In ideal case $L_a = 0, R_a = 0$. Induced voltage and armature current waveforms in BLDC machine are as shown in the Fig. 5.18. Output power can be obtained by averaging the instantaneous product of armature current and the induced voltage as given below:

$$\mathrm{P}_o = p_R + p_Y + p_B$$

$$P_o = \frac{1}{T}\int e_R i_R dt + \frac{1}{T}\int e_Y i_Y dt + \frac{1}{T}\int e_B i_B dt \tag{5.28}$$

$$P_o = E_{Peak} I_{Peak} \tag{5.29}$$

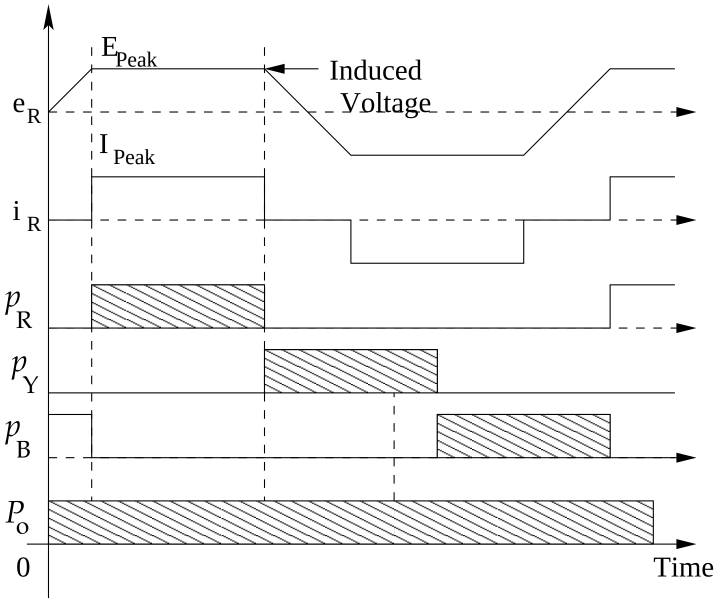

Figure 5.18: Generator voltage,current and power waveforms in ideal case

Instantaneous power output as a function of time is shown in Fig. 5.18. From the Fig. 5.18 and (5.29) it can be concluded that the output power is constant.

5.2.1.2 Power generation non-ideal case

In non-ideal case $L_a > 0, R_a > 0$. the leakage inductance and the resistance of the stator of machine are more than zero. The current waveform no longer remains quasi square but distorted in this case. Induced voltage, armature current and power output waveforms in a non ideal BLDC machine are as shown in the Fig. 5.19.

5.2.1.3 Analysis of the equivalent circuit of the BLDC motor and power converter combination in non ideal case

In the non ideal case $L_a > 0, R_a > 0$. Due to the leakage inductance of the armature winding the current will take finite time to reach the peak value. This results in the reduction in the output power delivered by the machine. The dependency of power delivered by the machine on this inductance can be better understood by analysing the equivalent circuit during the commutation period. The analysis is carried out in the following sections.

(i) Equivalent circuit and computation of neutral voltage(V_n) :
For proper operation of the machine, the current of the commutated phase must reach zero at the end of the commutation process. If the inductance of the stator is

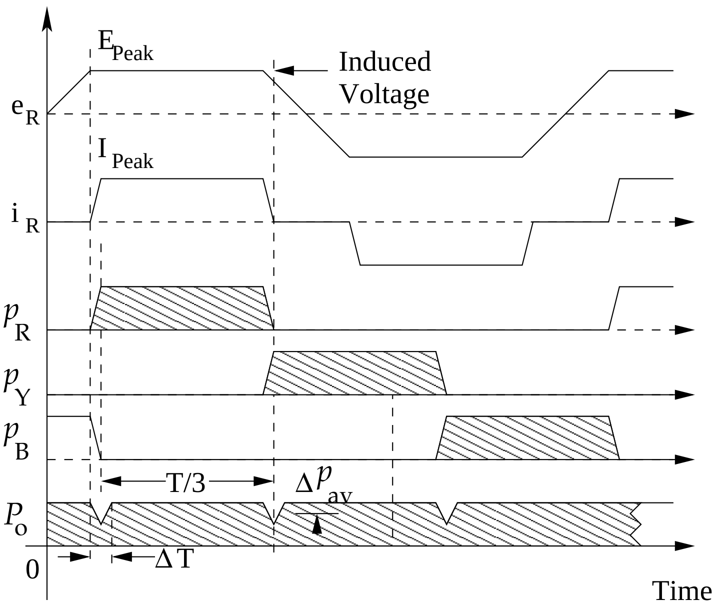

Figure 5.19: Generator voltage,current and power waveforms in non-ideal case

high, armature windings carry current for longer duration affecting the dynamic performance of the machine at higher speeds. The equivalent circuit of BLDC machine along with power converter during this interval is shown in Fig. 5.20. Assume that the commutation is taking place between R-phase and Y-phase. The current is transfering from switch T1 (R-phase) to switch T3 (Y-phase) with B-phase carrying constant current through the switch T2 as shown in Fig. 5.21.

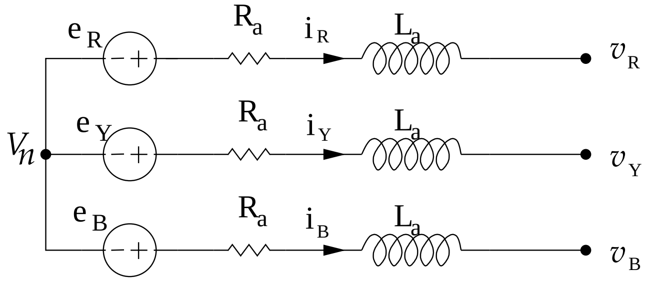

Figure 5.20: Machine equivalent circuit

In the Fig. 5.20 v_R, v_Y, v_B are the phase voltages with respect to negative DC bus voltage. From the equivalent circuit shown in Fig. 5.20, Phase voltages with respect to negative DC bus are written as follows:

$$v_R = i_R R_a + L_a \frac{di_R}{dt} + e_R + V_n \tag{5.30}$$

$$v_Y = i_Y R_a + L_a \frac{di_Y}{dt} + e_Y + V_n \tag{5.31}$$

$$v_B = i_B R_a + L_a \frac{di_B}{dt} + e_B + V_n \tag{5.32}$$

From the above equations, V_n can be computed as given below:

$$V_n = \frac{1}{3}[v_R + v_Y + v_B - \{(e_R + e_Y + e_B) + R_a(i_R + i_Y + i_B) + L_a(\frac{di_R}{dt} + \frac{di_Y}{dt} + \frac{di_B}{dt})\} \tag{5.33}$$

$$(i_R + i_Y + i_B) = 0 \tag{5.34}$$

$$V_n = \frac{1}{3}[(v_R + v_Y + v_B) - (e_R + e_Y + e_B)] \tag{5.35}$$

(ii) Dynamic equations and computation of armature currents :
Neglecting resistive drops and substituting for V_n in (5.30), (5.31), and (5.32) we get,

$$v_R = L_a\frac{di_R}{dt} + e_R + \frac{1}{3}[(v_R + v_Y + v_B) - (e_R + e_Y + e_B)] \tag{5.36}$$

$$v_Y = L_a\frac{di_Y}{dt} + e_Y + \frac{1}{3}[(v_R + v_Y + v_B) - (e_R + e_Y + e_B)] \tag{5.37}$$

$$v_B = L_a\frac{di_B}{dt} + e_B + \frac{1}{3}[(v_R + v_Y + v_B) - (e_R + e_Y + e_B)] \tag{5.38}$$

Thus the dynamic equations and the instantaneous values of three armature currents are given by,

$$\frac{di_R}{dt} = \frac{1}{3L_a}[(2v_R - v_Y - v_B) - (2e_R - e_Y - e_B)] \tag{5.39}$$

$$\frac{di_Y}{dt} = \frac{1}{3L_a}[(2v_Y - v_R - v_B) - (2e_Y - e_R - e_B)] \tag{5.40}$$

$$\frac{di_B}{dt} = \frac{1}{3L_a}[(2v_B - v_R - v_Y) - (2e_B - e_R - e_Y)] \tag{5.41}$$

$$i_R(t) = i_R(0) + \frac{1}{3L_a}\int_0^t [(2v_R - v_Y - v_B) - (2e_R - e_Y - e_B)]dt \tag{5.42}$$

$$i_Y(t) = i_Y(0) + \frac{1}{3L_a}\int_0^t [(2v_Y - v_B - v_R) - (2e_Y - e_R - e_B)]dt \tag{5.43}$$

$$i_B(t) = i_R(0) + \frac{1}{3L_a}\int_0^t [(2v_B - v_R - v_Y) - (2e_B - e_R - e_Y)]dt \tag{5.44}$$

(iii) Equivalent circuit of Drive – BLDC machine combination during commutation interval :
Equivalent circuit of machine along with power converter during commutation interval is shown in Fig. 5.21

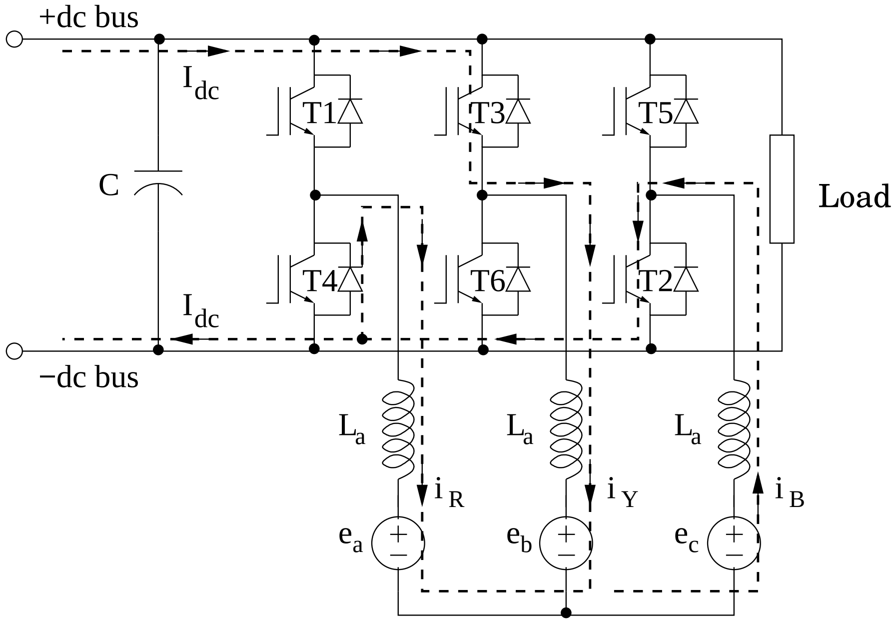

Figure 5.21: Equivalent circuit of machine with the converter during commutation interval

(iv) Initial conditions and armature current equations during commutation process :

At the instant of commutation from R -phase to Y- phase,the initial conditions of various parameters are given below [81]:

$$v_R = 0, v_Y = V_{dc}, v_B = 0 \tag{5.45}$$

$$e_R = E_m, e_Y = E_m, e_B = -E_m, \tag{5.46}$$

$$i_R(0) = I_R = I_{dc}, i_Y(0) = 0, i_B(0) = I_{dc} = -I_R \tag{5.47}$$

Substituting initial conditions in the equations (5.42), (5.43) and (5.44). we get the expressions for all the armature currents during the commutation interval.

$$i_R(t) = \ i_R - \frac{(Vdc + 2E_m)}{3L_s}t \tag{5.48}$$

$$i_Y(t) = \frac{(2Vdc - 2E_m)}{3L_s}t \tag{5.49}$$

$$i_B(t) = \ -i_R + \frac{(4Em - V_{dc})}{3L_s}t \tag{5.50}$$

(v) Overlap time(t_c) and its dependence on leakage inductance :

Expression for overlalp time t_c can be computed as given below:
We know that at $t = t_c, i_R = 0$.

$$0 = i_R(t_c) \tag{5.51}$$

Substituting $i_R(t) = 0$ in the R - phase armature current equation, we get

$$0 = I_{dc} - \frac{(Vdc + 2E_m)}{3L_a} t_c \tag{5.52}$$

$$t_c = \frac{(3I_{dc}L_a)}{V_{dc} + 2E_m} \tag{5.53}$$

(vi) Condition for rate of rise of i_R and rate of fall of i_Y to be equal :
During the rate of rise of i_R there will not be any dip in dc input power to motor. This means,

$$\frac{di_R}{dt} = \frac{di_Y}{dt} \tag{5.54}$$

We know that,

$$I_{dc} = i_Y(t_c) \tag{5.55}$$

$$I_{dc} = \frac{(2Vdc - 2E_m)}{3L_a} t_c \tag{5.56}$$

Now substituting for t_c from 5.53, we get,

$$2Vdc - 2E_m = Vdc + 2E_m \tag{5.57}$$

$$Vdc = 4E_m \tag{5.58}$$

Therefore if the value of dc bus voltage is maintainted four times the peak of the induced voltage in each phase winding, then Y phase current reaches the rated peak current when R phase current reaches zero value.

(vii) Magnitude of dip in output power and its dependence on leakage inductance :

Current drawn by the motor from the dc bus is shown in the Fig. 5.22

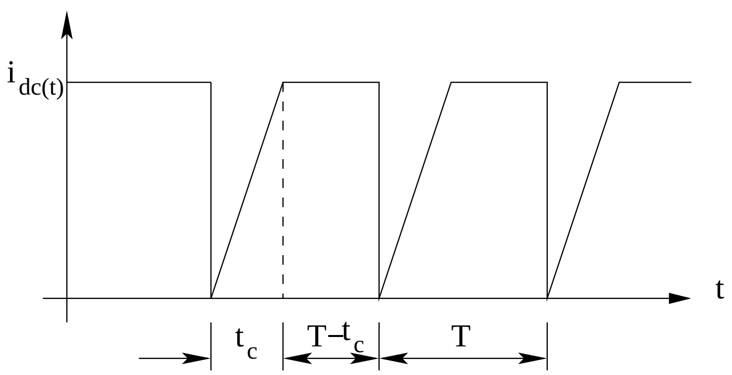

Figure 5.22: DC bus current waveform during motoring mode

Aveage power can be obtained by taking the product of instantaneous dc bus voltage and current. Average power is given by

$$P_{avg} = \frac{1}{T}\int_0^T [(i_{dc}(t).V_{dc}]dt \tag{5.59}$$

$$= \frac{1}{T}\left(\int_{t_c}^T [(I_{dc}.V_{dc}]dt + \int_0^{t_c} [(i_{dc}(t).V_{dc}]dt\right) \tag{5.60}$$

$$= \frac{1}{T}\left(I_{dc}V_{dc}(T-t_c) + \int_0^{t_c} \frac{(2Vdc-2E_m)}{3L_s}V_{dc}tdt\right) \tag{5.61}$$

$$= \frac{1}{T}\left((I_{dc}.V_{dc}(T-t_c) + \frac{(V_{dc}-E_m)}{3L_s}V_{dc}t_c^2\right) \tag{5.62}$$

Substituting the value of t_c from equation (5.53) into (5.62), we get

$$= \frac{1}{T}\left((I_{dc}.V_{dc}(T-t_c) + \frac{(3L_sV_{dc}I_{dc}^2)}{4(V_{dc}-E_m)}\right) \tag{5.63}$$

We know the condition required for keeping the rate of currents in both the phases same is:

$$V_{dc} = 4E_m \tag{5.64}$$

Substituting (5.64) into (5.63) we get,

$$= \frac{1}{T}\left(I_{dc}V_{dc}(T-t_c) + L_sI_{dc}^2\right) \tag{5.65}$$

$$= I_{dc}V_{dc} - \frac{1}{T}\left(V_{dc}I_{dc}t_c - L_sI_{dc}^2\right) \tag{5.66}$$

Substituting the value of t_c this equation becomes,

$$= I_{dc}V_{dc} - \frac{1}{T(2V_{dc}-2E_m)}3V_{dc}I_{dc}^2L_s - \frac{1}{T}L_sI_{dc}^2 \tag{5.67}$$

$$= I_{dc}V_{dc} - \frac{2}{T}L_sI_{dc}^2 + \frac{1}{T}L_sI_{dc}^2 \tag{5.68}$$

$$P_{avg} = I_{dc}V_{dc} - \frac{1}{T}L_sI_{dc}^2 \tag{5.69}$$

Therefore, the reduction in output power due to the leakage inductance is given by,

$$\triangle\ P_o = \frac{1}{T}L_sI_{dc}^2 \tag{5.70}$$

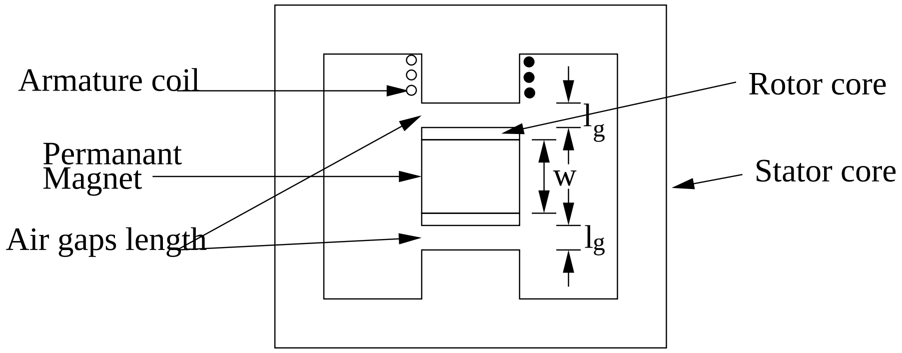

Figure 5.23: Physical layout of a typical BLDC machine

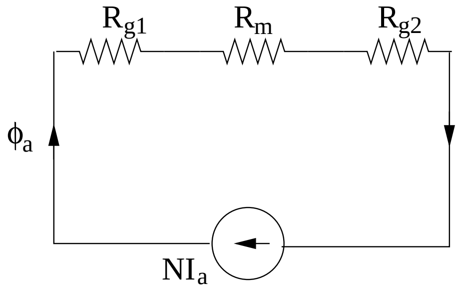

Figure 5.24: Magnetic equivalent circuit of the machine

(viii) Relationship between the leakage inductance and the geometry of the machine :

The leakage inductance can be found out from the geometry and physical dimensions of the motor. Physical layout of a typical PM BLDC machine is shown in the Fig. 5.23 [19]. The flux produced by the permanent magnet experiences three reluctances in series, i.e. reluctance of two air gaps and the permanent magnet. The fluxΦ a produced by the magnet experience a reluctance $\Re$ is the series combination of $\Re_{g1}$ (reluctance of air gap1), $\Re_m$ (reluctance of magnet) and $\Re_{g2}$ (reluctance of air gap2) as shown in Fig. 5.24
Therefore,

$$\Re = \Re_{g1} + \Re_{g2} + \Re_m \tag{5.71}$$

The armature leakage inductance of the BLDC machine can be calculated using following relationship:

$$Ł_a = \left(\frac{N^2 A_P \mu_0}{(2l_g + w)} \right) \tag{5.72}$$

"N"	: Number of armature turn
"l_g"	: Total length of the air gap for field flux
"μ_0"	: Permeability of free space
"A_p"	: Area under pole arc
"w"	: Width of the permanent magnet

It is observed from equation(5.72) that the critical inductance of the machine can be varied by varying either the number of turns of the armature winding, width of the magnet and air gap length.

5.2.1.4 Computation of drop in speed and critical inductance in motoring mode

(i)Drop in Speed :

Output power generated in ideal case is given in (5.29) which is reproduced as below:

$$P_o = E_{peak} I_{peak} \tag{5.73}$$

In non-ideal case generated torque will reduce due to slow rate of rise of armature current. Change in output power due to the leakage inductance is given by (5.70) as,

$$\Delta\omega = \frac{\Delta P_o}{T_L} \tag{5.74}$$

Generated torque in the motor reduces as the output power reduces. Reduction in generated torque makes the motor speed to drop by an amount given by following equations.

$$\Delta\omega = \frac{\frac{1}{T} L_s I_{dc}^2}{T_L} \tag{5.75}$$

It is clear from the above equations that, when a motor with non zero armature leakage inductance will run at a speed lower than the rated speed for a given rated voltage. For a given applied voltage, the motor will run at higher speed with lower armature leakage inductance than with higher armature leakage inductance. Maximum allowable value of machine armature leakage inductance is decided by output power and speed of motor as required by the application. It is usual to assume that the time taken by the armature current to reach maximum value should be less than 10 % of the switching period. Hence the high speed machines shall have high $\frac{di}{dt}$ and the low value of leakage inductance. Fig. 5.25 shows the plot of drop in the motor speed for various rating of the machine as a function of armature leakage inductance.

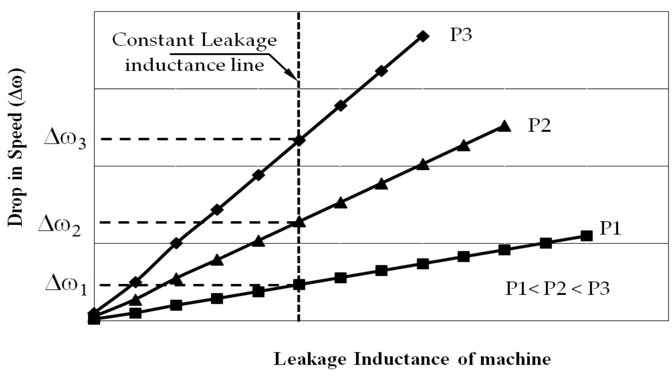

Figure 5.25: Drop in motor speed as a function of leakage inductance

(ii)Critical armature leakeage inductance(L_{crit}) :

Critical inductance of the machine is the maximum permissible value of leakage inductance for which the drop in speed of the motor is within the specified value. The maximum permissible value of inductance depends on how much drop in speed is allowed with respect to the rated speed. Steps to be followed to compute critical inductance are given below:

- Fix the maximum allowable drop in speed ($\Delta\omega$) for the given application.
- By knowing the rated speed of the machine compute the dc bus current drawn by the machine.
- Compute the maximum allowable value of inductance (L_{crit}) using (5.75)

5.2.2 Critical value of armature leakage inductance in generating mode

If a 3-phase boost converter is connected at the output of this generator, the machine leakage inductance appears as a boost inductor. This limits the peak current handled by the power semiconductor device used in the boost converter for a given output power. The generator leakage inductance helps the boost converter to be operated in the Continuous Current Mode (CCM). It is desirable that the leakage inductance is as high as possible for proper boost converter operation in CCM. The minimum value of inductor required for the CCM of the boost converter is computed from (5.76) [33].

$$\text{Ł}_{min} = \frac{R_L D_{min} T_{sw} (1 - D_{min})^2}{2} \tag{5.76}$$

$$\text{Ł}_{min} \geq \frac{V_{dc}}{I_{max}} \frac{1}{f_{av}} \tag{5.77}$$

5.2.3 Simulation and experimental results

The simulation of the operation of the machine in generating mode is carried out with various values of leakage inductances using MatLab/Simulink software and the results are as shown in table 5.3 and Figs. 5.26 and 5.27.

Table 5.3: Peak Armature current as a function of leakage inductance

Output conditions: V_{dc} = 400 V, ω_{max} = 1177 rad/s , J = 0.681 kgm^2		
L_a (mH)	Generator Peak Current (A)	P_o (W)
0.1	80	4000
1.5	40	4000

A BLDC motor was built and tested by connecting different values of series inductance and plot of motor speed as a function of output voltage as shown in Fig. 5.28

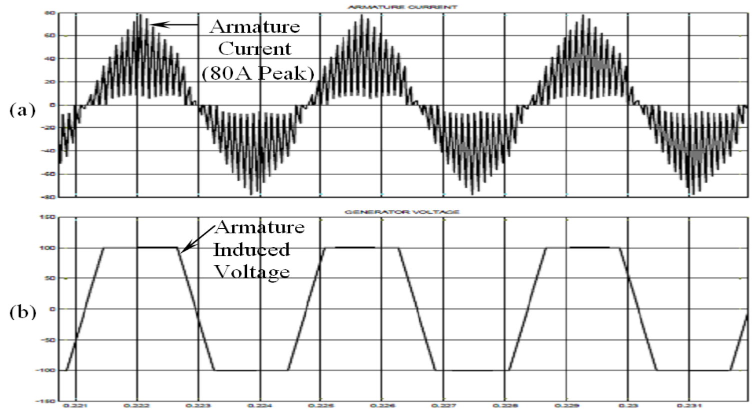

Figure 5.26: Armature current and voltage waveforms of simulated BLDC generator with $L_a = 0.1mH$

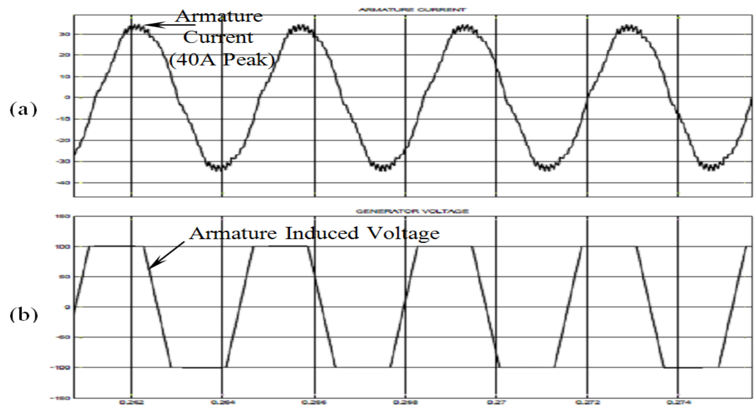

Figure 5.27: Armature current and voltage waveforms of simulated BLDC generator with $L_a = 1.5mH$

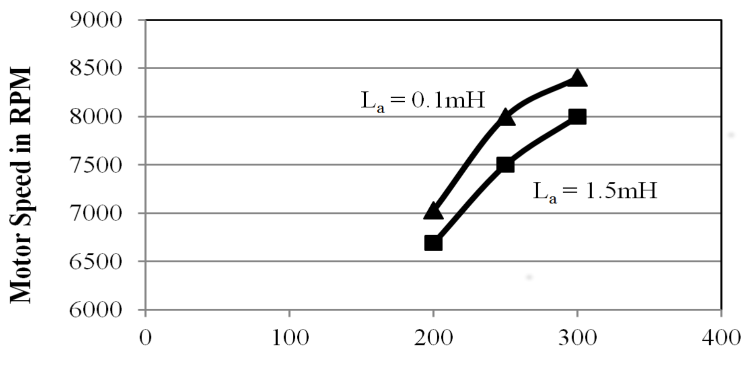

Figure 5.28: Motor speed as a function of induced voltage at constant load torque

5.3 Summary

Armature current dependent eddy current loss in the core appears as a series resistance to boost converter which is connected at the output of the generator. This resistance reduces the maximum voltage gain and the operating range of the duty cycle of the boost converter. This results in the reduction of harvestable energy. This can be avoided by harvested energy can be increased by selecting a PM-BLDC machine with longer air gap, higher tooth width and thinner stator stamping. Usage of Nickel Iron as stator core material will also help in reducing the current dependent eddy current loss thereby increasing the harvested energy from the flywheel. For a given BLDC machine a two-stage boost converter will draw lesser peak current from the generator as compared to that of single-stage for delivering the same output power. This will reduce the current dependent eddy current loss. Hence two-stage boost converter is a better choice as compared to single stage boost converter for FES applications.

From the theoretical studies, simulations, experiments, it is found that the machine inductance should be low enough to allow the rise of armature current to reach rated current to required value within specified time in the motor mode. This inductor should be high enough to maintain the constant current as well as limit the boostconverter device current in generating mode. The same has been validated by the experimentation. Hence for a Flywheel energy storage applications the BLDC machine should be designed with an inductance as low as possible with a provision to connect an external inductor of suitable value to satisfy the condition required for boost converter operation in CCM mode. Due to the inherent problems in the existing converter topologies and BLDC machine configuration which was analysed in this chapter, there is a maximum limit up to which the energy can be harvested from a given flywheel. To overcome these limitations, there is a need to explore the new topology for power converter or configuration for machine which proposed in the chapter 6.

Chapter 6

New topologies for enhancement of harvested energy

This chapter covers new methods for the enhancement of the harvested energy from a flywheel as compared to the existing methods. These methods use a novel unique combination of multiple winding permanent magnet brushless dc machine and buck converters. Analysis of the effect of generator winding configurations and implementation of control strategies adopted for these new methods are carried out and presented in this chapter. Advantages of these methods are highlighted. Simulation of these new schemes are done and the results are given. Experimental results of the prototype system built are presented. The newly proposed theory, simulation and experimental results are in agreement.

6.1 Generator equivalent circuit

As the energy is extracted, speed of the flywheel goes down. The terminal voltage of the generator is a function of armature circuit impedance, rotor speed and induced voltage [75]. The relationship can be established from the machine equivalent circuit diagram as shown in Fig. 6.1. The steady state voltage balance equation is given below:

$$V_{mg} = K_v\omega \pm \left(L_a \frac{di_a}{dt} + i_a R_a \right) \tag{6.1}$$

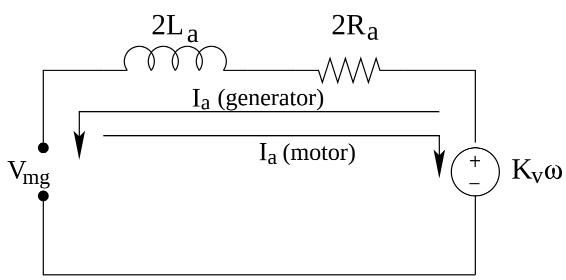

Figure 6.1: Simplified machine equivalent circuit

The drop in the generator voltage due to the reduction in rotor speed depends on the parameters like load current and armature circuit impedance. As discussed in the earlier chapters, there is a requirement of voltage boosting mechanism to maintain the dc bus voltage constant for energy harvesting [19]. Most commonly used voltage boosting topologies are discussed in the following sections.

6.2 Voltage boosting schemes used in FES systems

The available voltage boosting schemes can be classified as single-stage or two-stage and isolated or non-isolated types. Almost all the schemes make use of a PWM dc to dc converter along with a feed forward controller [63] or a feedback controller [64]. Feed forward controller is used for compensating the effect of reducing speed of the flywheel and feedback controller for maintaining the output dc bus voltage constant while energy is being extracted from the flywheel. Some of the representative FES schemes used in conjunction with voltage boosting is briefly discussed in next section.

6.2.1 Single-stage boost converter (SSBC) based FES scheme

Block diagram of a single-stage boost converter based FES scheme is shown in Fig. 6.2. In this scheme, the BDC is operated as a BLDC motor drive in motoring mode and as a boost converter in generating mode. The BDC controls the armature current in the motoring mode and maintains the dc bus voltage constant in generating mode [19].

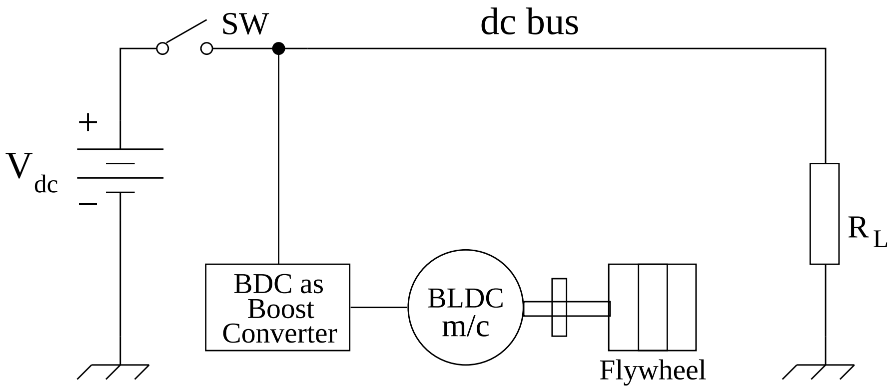

Figure 6.2: SSBC based FES scheme in generating mode

6.2.2 Two-stage boost converter (TSBC) based FES scheme

Block diagram of a two-stage boost converter based FES scheme is shown in Fig. 6.3. In this scheme, BDC is operated as a BLDC motor drive by controlling the armature current in motoring mode similar to SSBC and as a rectifier by converting ac voltage to dc voltage in generating mode. There is an additional boost converter as compared to the "SSBC based FES scheme" which comes into action only during generating mode. This additional boost converter maintains the dc bus at constant voltage during the generating mode of operation.

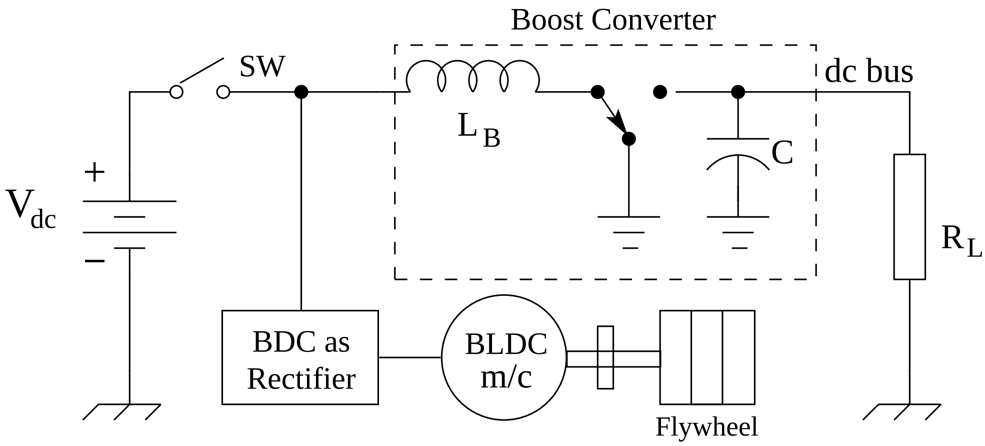

Figure 6.3: TSBC based FES system in generating mode

6.2.3 Resonant converter based FES scheme

Block diagram of Resonant converter based FES scheme scheme is shown in Fig. 6.4

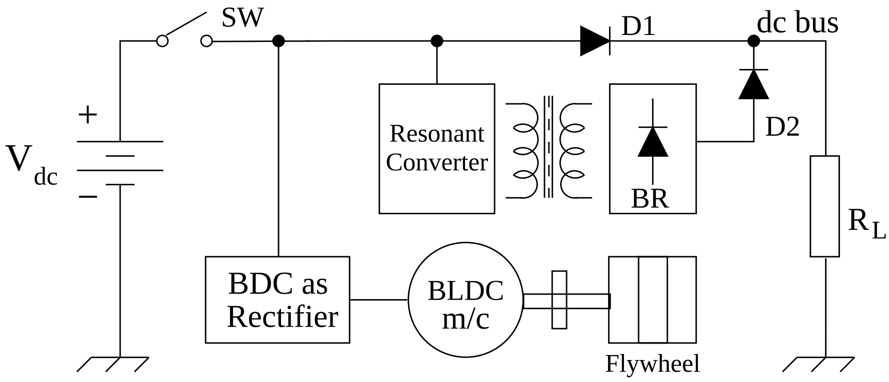

Figure 6.4: Resonant Converter based FES scheme

In this scheme, the BDC is operated as a BLDC motor drive in motoring mode and as a rectifier in generating mode. In other words, it limits the armature current in motoring mode and converts the ac voltage from the generator to a dc voltage in generating mode. This dc voltage is boosted to a higher value by using a resonant converter, a step up transformer and a rectifier as shown in Fig. 6.4. This resonant converter is followed by a step-up transformer and a bridge rectifier(BR) which enables maintaining the dc bus voltage constant during the generating mode. A resonant converter is used as a dc to ac converter with a phase shift method to maintain the output voltage constant. This comes into action only during generating mode.

6.3 Problems of existing voltage boosting schemes

Currently used voltage boosting topologies suffer from the following disadvantages:

- Their efficiency reduces at lower generator speeds due to high input current.

- There is a limitation on the maximum achievable voltage gain of boost converter because of its sensitivity to the ratio of source resistance to load resistance. This limits the harvestable energy from the FES system [34].

- If SSBC is used, the inductance of the machine should be high enough to limit the armature current. If low inductance machine is used, additional inductance needs to be added which adversely affects the performance during motoring mode of operation [19].

The above limitations lead to a reduction in the harvestable energy from the FES system. Hence there is a need to design a new power converter whose gain is insensitive to the ratio of source resistance to load resistance to overcome these limitations.

6.4 Novel scheme of Dual winding BLDC generator and Buck converter combination

The proposed new scheme is shown in Fig. 6.5

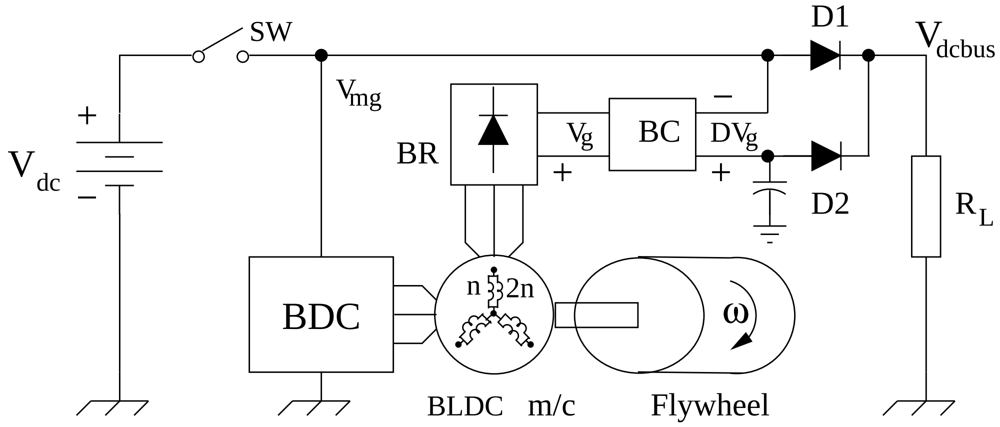

Figure 6.5: Proposed scheme for voltage boosting in generating mode

This scheme consists of a Dual Winding armature BLDC machine, Bridge rectifier (BR), BDC and a Buck converter (BC). The Dual Winding armature BLDC machine has two sets of independent (isolated) armature windings. One of these windings carries current during both motoring and generating modes of operation and is called as “M/G winding” (main winding). The other winding carry current only during the generating mode and is called as “G-winding”. The G-winding has 2- times the number of turns as compared to the M/G winding. Input terminals of BDC and BR are connected to the output terminals of M/G winding and G-windings respectively. BDC acts as a rectifier in the generating mode with an output voltage of “V_{mg}”. The BC is connected at the output of BR to give an output voltage of “DV_g”. This arrangement results in the creation of two independent dc voltage sources V_{mg} and DV_g in the generating mode. These two independent dc voltage sources are connected to the load R_L through coupling diodes D_1 and D_2 as shown in Fig. 6.5

In the motoring mode, the BDC works as a BLDC motor drive, pumping controlled current into the M/G winding. In this mode, by disabling the buck converter pulses, the output of G-winding gets disconnected from the load R_L. In the generating mode the pulses to the BC are enabled and corresponding gate pulses to BDC are disabled to make BDC work as a rectifier and the BC as a buck converter. This circuit configuration results in output voltage of BDC comes in series with output voltage of BC. Hence the dc bus voltage will become equal to the sum of the voltage outputs of these two [Fig. 6.5].

6.4.1 Working principle of the new scheme

The proposed system has two operating modes which are described as below:

i) Motoring mode (Switch "SW" is CLOSED) [Fig. 6.5]:
In this mode, pulses to BC are disabled (D=0). Main dc source V_{dc} supplies power to the load R_L directly and to the BLDC machine through BDC. Therefore, $V_{dcbus} = V_{mg} = V_{dc}$.

ii) Generating mode (Switch "SW" is OPEN) [Fig. 6.5]:
Flywheel continues to run due to its inertia and drives the generator. The terminal voltage of the machine drops as the flywheel decelerates with the time. In this mode, pulses to BC are enabled ($D = 0 - 1$). As explained earlier dc bus voltage (V_{dcbus}) is the sum of the output voltages of BDC and BC in this mode and can be computed by the following relation:

$$V_{dcbus} = V_{mg}(t) + V_g(t)D(t) \tag{6.2}$$

Let us define $\frac{V_g}{V_{mg}} = K$ which implies (6.2) can be re-written as;

$$\frac{V_{dcbus}}{V_{mg}} = (1 + KD(t)) \tag{6.3}$$

6.4.2 Importance of $K - factor$ and its relationship with dc bus voltage

As defined earlier K is the ratio of induced voltage of "G-winding" to "M/G winding". K more than one implies that there is more than one set of armature winding exists in the machine. It may be noted here that the magnitude of K (hereafter called as "$K-factor$") decides the quantity of energy harvested from the flywheel. Increase in the $K - factor$ results in the enhancement of the harvestable energy, increase in cost /size of machine, increased voltage stress across the buck converter device. Graphical representation of this relation with $K = 2$ is shown in Fig. 6.6 . For the sake of simplicity it is assumed that speed of the flywheel reduces linearly with time; the induced voltages V_g and V_{mg} will also follow. Variation of generator voltage and generator current as a function of time (during energy extraction at contant power from flywheel) and computation of average values of dc voltage and dc current during power backup period are carried out and given in Appendix-A.

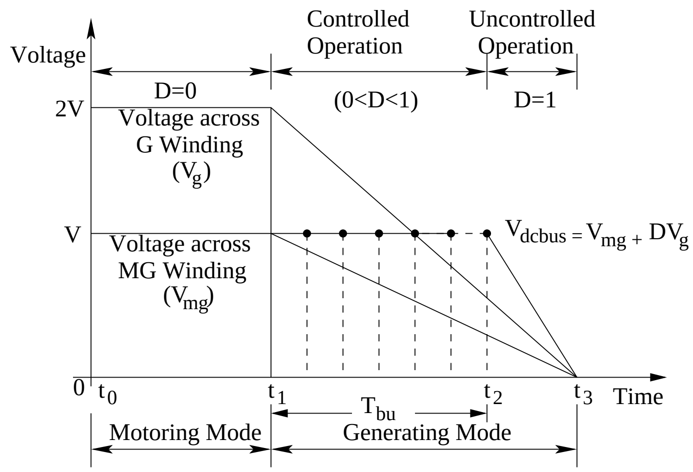

Figure 6.6: Voltage-time characteristic of the new DWBC scheme

Referring to graph shown in Fig. 6.6 motoring mode and generating mode mentioned in section 6.4.1(i) and (ii) shown in the time zone t_0 - t_1 and $t_1 - t_3$ respectively. As the buck converter pulses are disabled in motoring mode it is shown as $D = 0$. In generating mode pulses are enabled and its duty cycle varied from $(0 < D < 1)$ during the interval $t_1 - t_2$ is called as controlled operation in which the controller is able to maintain the dc bus voltage constant as per (6.3). At time instant t_2 the duty cycle D reaches its maximum value of unity. At this instant the dc bus voltage starts decreasing and reaches zero at t = t_3. As the induced voltages become too low, the controller is not be able to maintain the dc bus voltage during the interval $t_2 - t_3$, this region of graph is called as uncontrolled operation. The voltages V_g and V_{mg} change with time and the magnitude of the output voltage can be maintained constant by suitably adjusting duty cycle "D" (D = 0% to 100%) as per (6.3). Following are the advantages of the proposed scheme:-

- Harvestable energy can be increased to 90% of the stored energy as compared to existing systems which typically yields 75%-80%.

- Regulation of dc bus voltage is achieved by using a buck converter instead of the boost converter. This results in much lower input current as compared to that of boost converter thus improving the overall efficiency.

- Machine can be built with lower inductance resulting in improvement in response time in motoring mode, higher efficiency and improved load regulation of the machine.

- Converter gain is independent of the source resistance or load resistance. Considering the definite advantages of the proposed scheme over the existing ones, the detailed analysis of the proposed scheme and $K - factor$ is carried out in the next section.

6.5 Analysis of the effect of $K - factor$ on harvestable energy

A part of the generated mechanical power from the flywheel is dissipiated as losses before its transfer to the load. Power balance equation of the FESS in generating mode obtained from first priciples as given in Appendix - A is given below:

$$J\omega\frac{d\omega}{dt} = P_o + C_1\omega + C_2\omega^2 \tag{6.4}$$

Solving this differential equation for $'\omega'$ we get

$$\omega(t) = C1\frac{1 + e^{-(\frac{t}{J}+\frac{C_2}{J})}}{1 - e^{-(\frac{t}{J}+\frac{C_2}{J})}} \tag{6.5}$$

Where ω, C_1 and C_2 are constants.

It is evident from the above equation that the speed drops exponentially with time as the energy is extracted from the flywheel. Therefore, the voltages across the armature windings also droop with time as per the following equations:

$$V_g = KVe^{-\frac{t}{T}} \tag{6.6}$$

$$V_{mg} = Ve^{-\frac{t}{T}} \tag{6.7}$$

where "V" is the rated voltage of the motor. Equations (6.6) and (6.7) can be graphically represented (for $T = 80$ seconds) as shown in Fig. 6.7

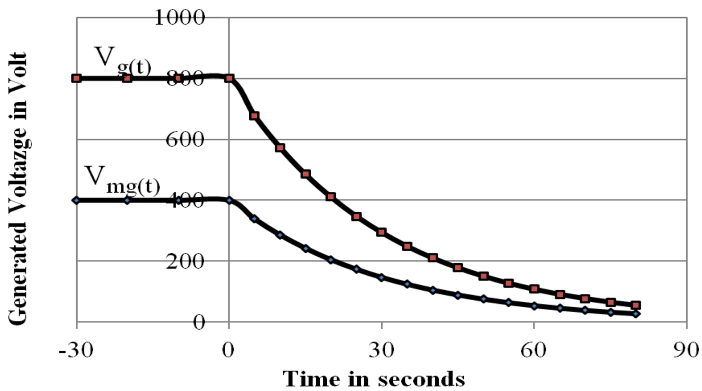

Figure 6.7: Voltage-time characteristics of the BLDC generator

From (6.3), (6.6) and (6.7) we have,

$$V_{dcbus} = V\left(1 + KD(t)e^{-\frac{t}{T}}\right) \tag{6.8}$$

During energy harvesting time (t$\leq T_{bu}$), the dc bus voltage should be maintained constant by adjusting the duty cycle. Assume that the maximum value of D(t) = 0.9 which occurs at $t = T_{bu}$. From (6.6) we have,

$$V_{mg(min)} = Ve^{-\frac{T_{bu}}{T}} \tag{6.9}$$

$$\frac{V_{dcbus}}{V_{mg(min)}} = (1 + 0.9K) \tag{6.10}$$

Therefore

$$V_{mg(min)} = \frac{V_{dcbus}}{(1 + 0.9K)} \tag{6.11}$$

Similarly

$$\omega_{mg(min)} = \frac{\omega_{max}}{(1 + 0.9K)} \tag{6.12}$$

The minimum required armature induced voltage V_{mg} is computed from (6.10) such that $V_{mg(min)}\,(1 + 0.9K) > V_{dcbus}$

6.5.1 Variation of $V_{mg(min)}$ with $K - factor$

The $V_{mg(min)}$ can be computed for various values of K and plotted as shown in Fig. 6.8

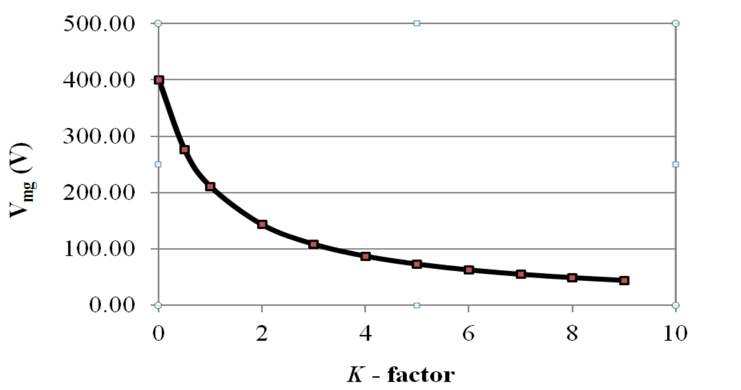

Figure 6.8: Lowest required induced voltage as a function of $K - factor$

This figure indicates that with $K = 2$ the lowest required induced voltage goes down to 35% of the rated value which enables the energy harvesting down to a flywheel speed of 35% of rated speed.With this, 88% of the stored energy from the flywheel is harvested. It is observed that if K is higher, higher power can be drawn for the same backup time (higher harvested energy) or if the power drawn is constant, higher back up time (higher harvested energy) is achieved.

6.5.2 Variation of percentage of energy harvested with $K-factor$

The energy harvested from flywheel is given by,

$$E_h = \frac{1}{2} J(\omega_{max}^2 - \omega_{min}^2) \tag{6.13}$$

As shown in Fig. 6.7, the flywheel decelerates exponentially with time, and the flywheel speed at time t = T_{bu} can be computed as

$$\omega_{min} = \omega_{max} \times e^{-\frac{T_{bu}}{T}} \tag{6.14}$$

Percentage of energy harvested can be obtained from the following equation,

$$\%E_h = \left(1 - \frac{\omega_{min}^2}{\omega_{max}^2}\right) \times 100 \tag{6.15}$$

Combining (6.12) and (6.15) we get,

$$\%E_h = \left(1 - \frac{1}{(1+0.9K)^2}\right) \times 100 \tag{6.16}$$

Plot of the percentage of energy harvested as a function of $K - factor$ is given in Fig. 6.9, which clearly indicates that, with $K = 2$, more than 88% of the maximum stored energy in the flywheel can be harvested.

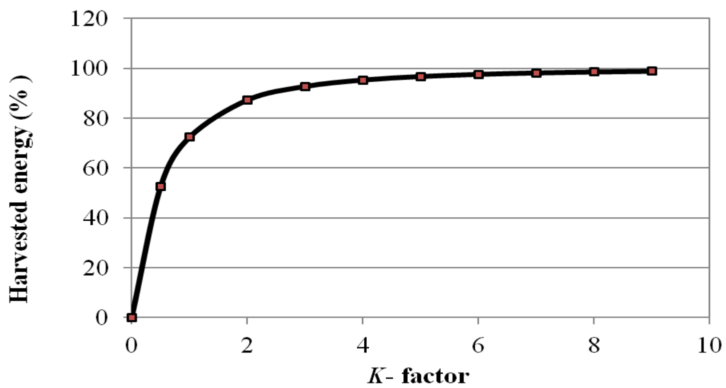

Figure 6.9: Percentage energy harvested as a function of $K - factor$.

6.6 Voltage control strategy

The dc bus voltage is required to be maintained constant in spite of reduction in the speed of generator. This voltage can be maintained using a simple feed forward controller or a feedback controller. Control methodology is explained in the following sections.

6.6.1 Feed forward controller

Feed forward controller is used for compensating the effect of reduction of the flywheel speed. It is well known that reduction of the speed of flywheel causes the dc bus voltage to reduce. In feed forward controller, the speed reduction information is fed to the controller in advance to increase the width of gate pulses to the chopper device. Increase of the pulse width of buck converter is synchronized with the reduction of flywheel speed by feeding the speed signal (or generator voltage V_{mg}) to the controller to maintain the dc bus voltage constant.

From (6.3) we have,

$$D(t) = \left(\frac{V_{dcbus}}{V_{mg}(t)} - 1 \right) \times \frac{1}{K} \tag{6.17}$$

In this method the duty cycle of the chopper gate control pulses is adjusted such that the output voltage is maintained constant which is inversely proportional to the generator induced voltage (speed of the flywheel). The generator induced voltage is sensed and used for implementing the feed forward controller. A representative graph of the generator votlage, dc bus voltage and the duty cycle of chopper control pulses is shown in Fig. 6.10

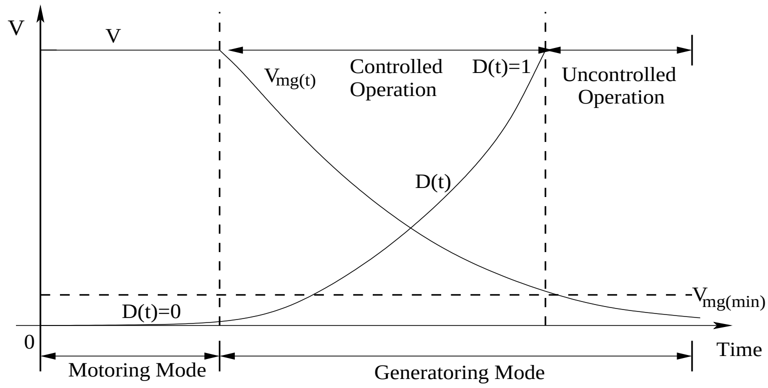

Figure 6.10: Plot of $V_{mg}(t)$ and $D(t)$ as a function of time

The controller implementation is given in the Fig. 6.11

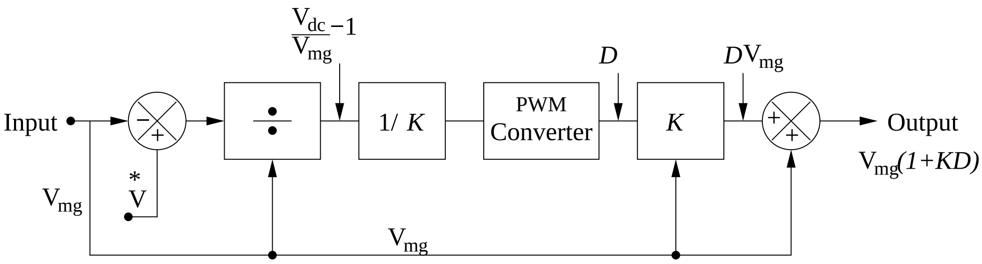

Figure 6.11: Block diagram of feed forward Controller

6.6.2 Closed loop feedback PI controller

In this apporach a Proportional plus Integral voltage feedback controller [9] is implemented by sensing the dc bus voltage and comparing with the required set voltage. Output of this controller determines the width of the control pulses (duty cycle) which is given to the chopper gate to maintain the dc bus voltage. Block diagram of the feedback controller is shown in the Fig. 6.12

6.7 Simulation of the DWBC scheme

The simulation of the proposed scheme was carried out using MATLAB/Simulink software and the results were recorded. Simulation parameters used are given in table 6.1

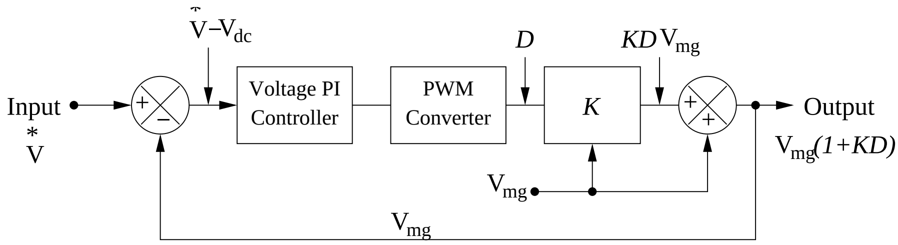

Figure 6.12: Block diagram of feedback Controller

Table 6.1: Simulation parameters for DWBC, MWSC and MWMC schemes

V_{dc} = 400 V, ω_{max} = 1177 rads/s	
Parameter	Value
Moment of inertia of flywheel	0.681 kgm^2
Maximum flywheel speed	8000 RPM
Rated voltage of the dc machine	400V DC
Rated speed of the dc machine	10000 RPM
Simulation sample time	5 μs.

The block diagram of the Simulink model is given Fig. 6.13, the results (waveforms) obtained from the simulations are given in Fig. 6.14. It is clear from Fig. 6.14 that the results obtained from simulations are completely in line with the predicted results.

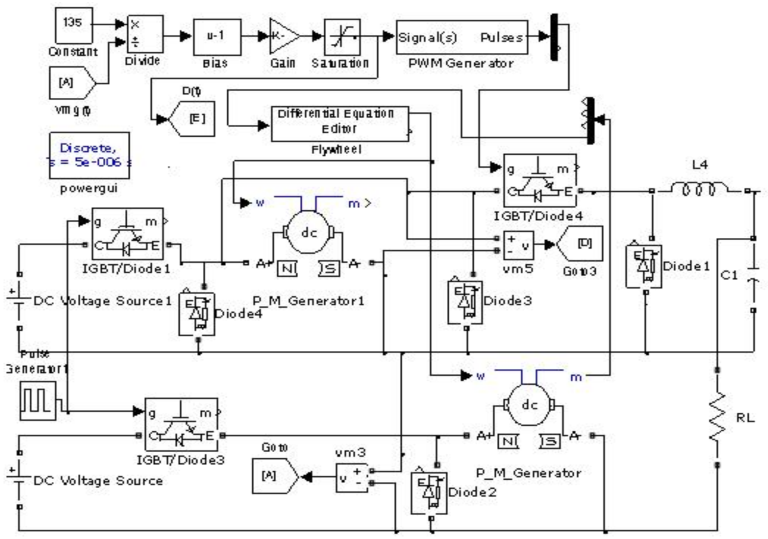

Figure 6.13: Simulink model of the proposed DWBC scheme

6.8 Experimental setup and discussion of the results

Prototype laboratory models of the conventional (SSBC) and newly proposed scheme (DWBC) for flywheel energy harvesting are built using a PM-BLDC machine. A P+I feedback voltage controller is implemented using a Digital Signal

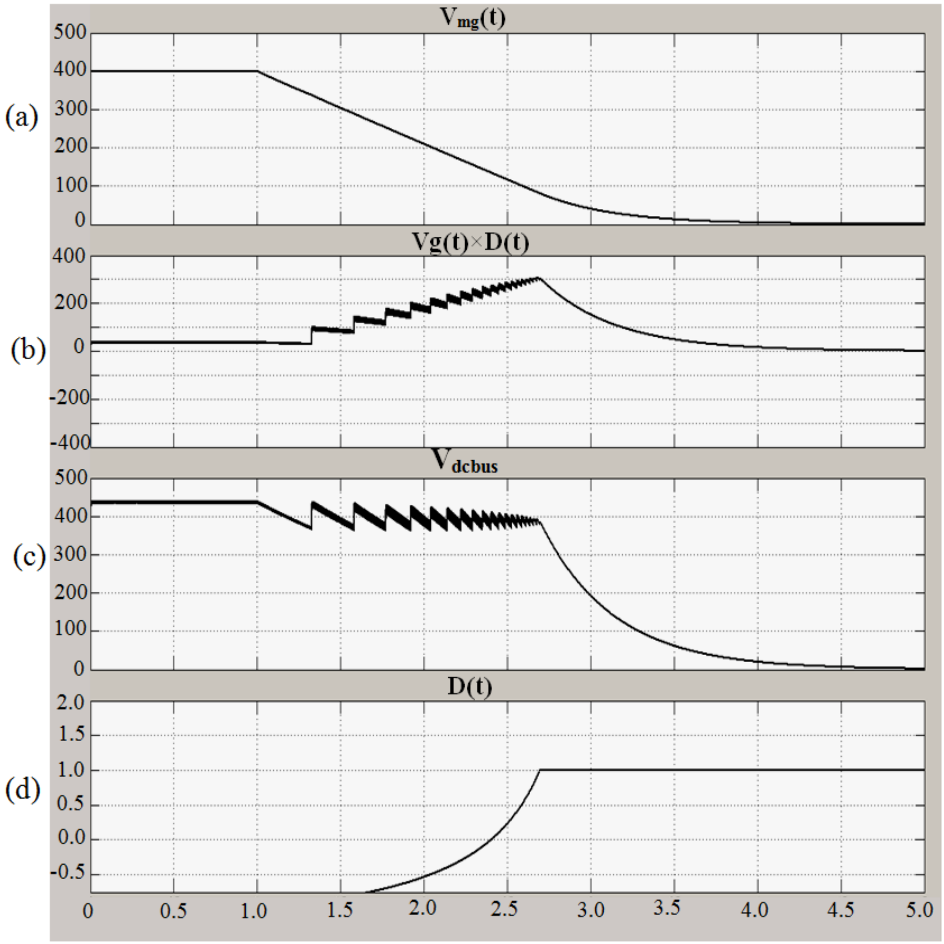

Figure 6.14: Results from the MatLab simulation of DWBC

Processor of Motorola make, model: DSP 56F805. DWBC and SSBC are tested under same loading conditions for evaluating the proposed schemes and comparing their performances. The dc bus voltage versus time plots of SSBC and DWBC are recorded using a digital storage oscilloscope (DSO) are shown in Fig. 6.15(a) and (b) and in Fig. 6.16(a) and (b) respectively for various similar load currents. It is observed that the backup time as well as maximum achievable boost gain of the SSBC is reduced with increase in load whereas when DWBC is used the gain of the converter remains constant under all loading conditions

It may also be observed in these plots that the power back up time is higher in DWBC as compared to SSBC. It may be noted that the results obtained from the experiments are in line with those of the theoretically predicted ones. It can be seen from Fig. 6.16 that the controller is able to maintain the output voltage constant up to an input voltage (minimum flywheel speed), which is 33% of the rated voltage (maximum flywheel speed). It clear from the experiments that around 90% of the energy, which is stored in the flywheel is extracted. Various parameters of both these converters measured at different load conditions are given in table 6.2. Fig. 6.17 shows the variation of various parameters of SSBC with load conditions. It is clear from this figure that the gain of converter and the backup time reduce at higher loads.

Table 6.2: Measured parameter of SSBC and DWSC schemes

Test conditions: Vdc = 200 V, ω_{max} = 544 rads/s (5200 RPM)						
Model Type	R_L (Ω)	Max Gain	T_{bu} (s)	V_{min} (V)	ω_{min} (rad/s)	E_h (Joules)
SSBC	240	2.37	27.2	67	182	4533
	120	1.65	13.9	121	238	4633
	90	1.34	11.2	147	361	4977
DWBC	240	3.0	27.2	66	179	4533
	120	3.0	16.0	66	179	5333
	90	3.0	13.6	66	179	6044

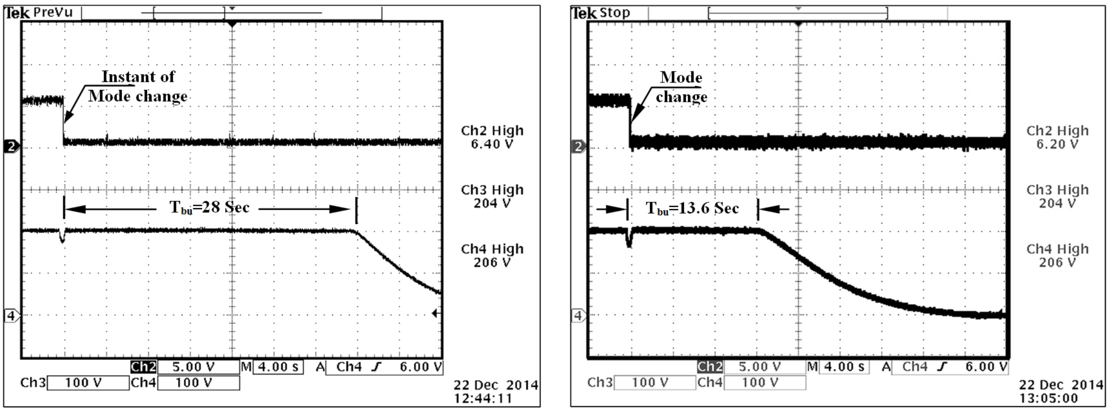

(a) (b)

(a). V_{dcbus} = 200 V, R_L = 240 Ω, N_{min} = 182 rads/s,D_{max} = 86%, T_{bu} = 28.0 s.
(b). V_{dcbus} = 200 V, R_L = 120 Ω, N_{min} = 238 rads/s, D_{max} = 80% , T_{bu} = 13.6 s.

Figure 6.15: Voltage-time plots of SSBC scheme recorded in DSO

Table 6.2 and Fig. 6.18 show the comparison of performance of DWBC and SSBC schemes. Plot of harvested energy as a function of output power is given in Fig. 6.18. This plot shows that the usage of DWBC has resulted in enhancing the harvested energy from 70% to 88% as compared to that of SSBC.

6.9 Effect of $K - factor$ on the converter performance

As explained earlier sections larger $K - factor$ results in the enhancement of the harvestable energy [Fig.6.9] but also increases the cost /size of the machine and higher voltage stress on the buck converter device. This results in following disadvantages:

- Increased voltage stress on the power device
- Requirement of higher votlage rating of the devices for buck converter
- Large voltage trasient and $\frac{dv}{dt}$ during changeover to other mode
  Therefore in order to over come the above mentioned disadvantages a new

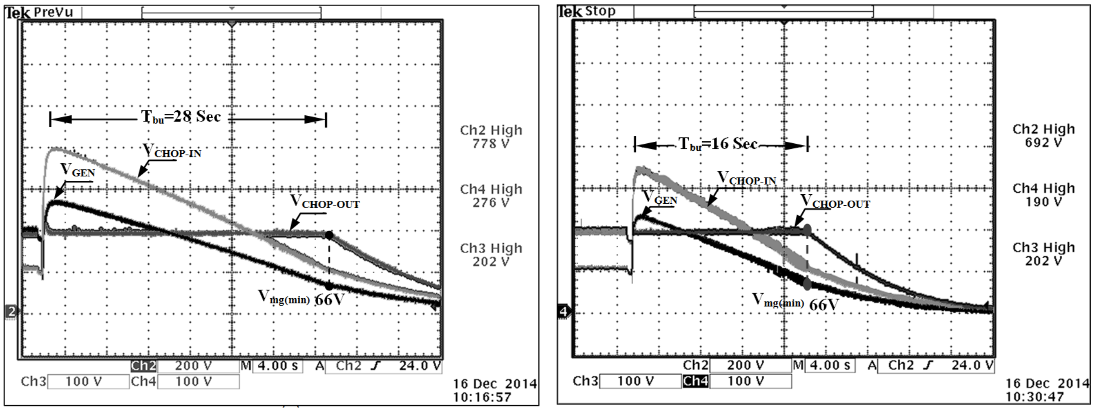

(a) (b)

(a).V_{dcbus} = 200 V (Ch4 = 100 V/div), R_L = 240 Ω, T_{bu} = 28 s, $V_{g(t)}$ (Ch2 = 100 V/ div, $V_{CHOP-INmax}$ = 800 V), $V_{mg(t)}$ (Ch3 = 100 V/ div, $V_{GENmax} = 270V$)., (b)V_{dcbus} = 200 V (Ch4 = 100 V/ div), R_L = 120 Ω, T_{bu} = 16 s, $V_{g(t)}$(Ch2 = 200 V/ div,$V_{CHOP-INmax}$ = 692 V), $V_{mg(t)}$ (Ch3 = 100 V/ div, V_{GENmax} = 230 V)

Figure 6.16: Voltage-time plots of DWBC scheme recorded in DSO

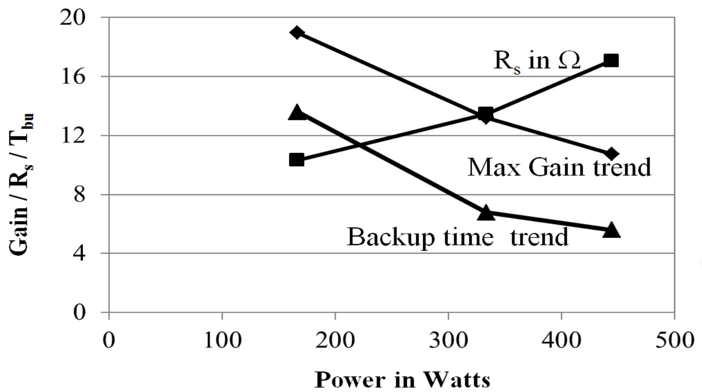

Figure 6.17: Variation of SSBC parameters as a function of output power

scheme using a Multi-Winding BLDC machine (MW-BLDC) is proposed in the next section.

6.10 New scheme for FES system using multi-armature BLDC machine

The new scheme uses Multi Winding BLDC (MW-BLDC) machine. This BLDC machine consists of multiple G-winding instead of single G-winding as in the case of DW-BLDC machine. The number of turns of G-winding of DW-BLDC and MW-BLDC machine has two and half the number of times respectively as compared to the M-winding of respective machine. There are "m" number of G-windings in MW-BLDC machine. Output of each of these windings are rectified separately and connected in series to get a higher dc bus voltage. New topology has been devised using matrix of switches consisting of unique combination of IGBTs and power

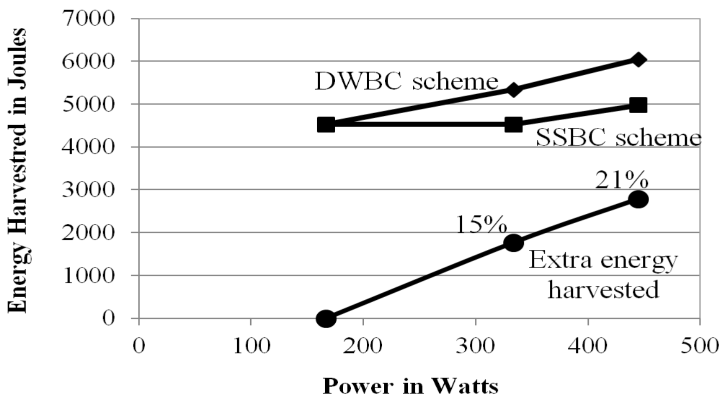

Figure 6.18: Comparison of energy harvested in SSBC and DWBC schemes

diodes for connecting the multiple auxiliary armature winding voltages in series depending on the value of armature induced voltage at that particular instant which is explained in detail here.
The new scheme is shown in the Fig.6.19. In this scheme, the BLDC machine will have "m" number of auxiliary armature windings (G-Windings) each having "α" times the number of turns as compared to that of main armature winding (M-Winding). Out put of each one of these windings is fed to separate rectifiers to get "m" number of dc voltage sources (V_{dc1} , V_{dc2},.... V_{dc-m}). It is required to maintain dc bus voltage constant in spite of reduction in the speed of generator. This voltage can be maintained using a single chopper or multiple-chopper configuration along either with feed forward controller or with a feedback controller. Control methodology is explained in detail in the following sections.

6.10.1 Switching topology and voltage control using multi winding single chopper configuration(MWSC)

DC voltage sources obtained from MW-BLDC machine windings are connected in series and given as the input to a bucking dc-dc converter (chopper) which maintains the dc bus voltage constant. Guiding equations in this configurations are given below:

$$\text{Assume } \alpha = \tfrac{V_g}{V_m}$$

$$K - factor = \alpha \times m \tag{6.18}$$

$$V_{Chop-in} = (1 + i\alpha) \times V_m \tag{6.19}$$

$$\text{where i = 0,1,2,3,....m}$$

$$V_{dcbus} = D \times V_{Chop-in} \tag{6.20}$$

"i" is the no of auxiliary winding connected in series at any instant; "m" is the total no of auxiliary windings; "D" is the duty cycle of the chopper pulses.

As the generator speed drops, one or more dc sources which are derived through auxiliary windings (V_{g1} , V_{g2},.... V_{g-m}) are connected in series to compensate the fall in induced votage. A new topology is designed for connecting these sources in series as shown in Fig. 6.19.

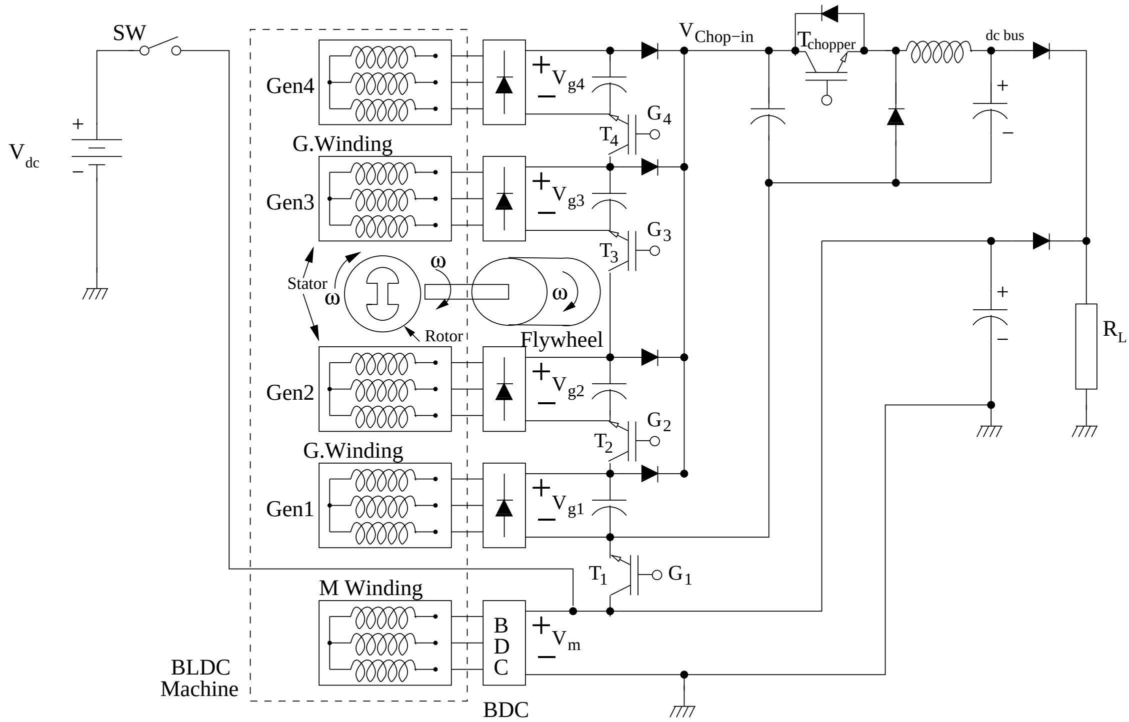

Figure 6.19: Block diagram of the new scheme using MWSC, with $m = 4, K = 2$

When the generator speed is falling, the reduction in induced voltage is compensated in a piecewise manner by connecting one or more DC voltage sources in series. These DC voltage sources are derived from induced voltages in G-windings (V_{g1}, V_{g2},.... V_{gm}) followed by separate rectifiers and filters. One or more of these voltage sources are connected in series with the DC source derived from M-winding by turning ON of an appropriate switch (i.e. T_1 to T_4). A logic is implemented using the generator voltage as feedback for turning ON the switches T_1, T_2, T_3, T_4. This voltage is fed as an input to a chopper which maintains the dc bus voltage constant by adjusting the duty cycle of its gate drive pulses.

6.10.1.1 Salient features

Following are the salient features of MWSC configuration.

- Simple Control
- All devices including chopper experiences almost same level of voltage stress
- Reduced reliability due to series connection

6.10.1.2 Working principle

As the induced voltage drops with speed, the chopper input voltage is maintained within the specified range by switching ON the appropriate switch out of T_1 to T_m. Mathematically it can be expressed as follows:

In a dual winding configuration the chopper input voltage can be computed as:

$$V_{Chop-in} = (V_{m-max} + V_{g-max}) \times \frac{N}{N_{max}} \tag{6.21}$$

In a multiwinding configuration, this can be re-written as,

$$V_{Chop-in} = (V_{m-max} + V_{g-max} \times i) \times \frac{N}{N_{max}} \tag{6.22}$$

Where i=0,1,2,3 ..... m,

Expressing in terms of *"K"*

$$V_{Chop-in} = V_{m-max}(1 + K) \times \frac{N}{N_{max}} \tag{6.23}$$

From the above equations it is seen that, the chopper input voltages can be maintained in the desired range by making one or more switches "ON" out of T_1, T_2....... T_m. e.g.
(i) Speed range: 100% - 80% :V$_{chop-in} = V_m, i = 0$(T$_1$, T_2....... T_m = OFF)

(ii)Speed range:79% -60%:V$_{chop-in} = V_m + V_g, i = 1$(T$_1$ = ON and T_2 ..... $T_m = OFF$)

(iii)Speed range:59%-40%:V$_{chop-in} = V_m + 2V_g, i = 2$(T$_1$ =ON,T_2 =ON and T_3 ... T_m = OFF);and so on.
With this logic implementation, chopper input voltage of a function of normalized speed is shown in Fig. 6.20

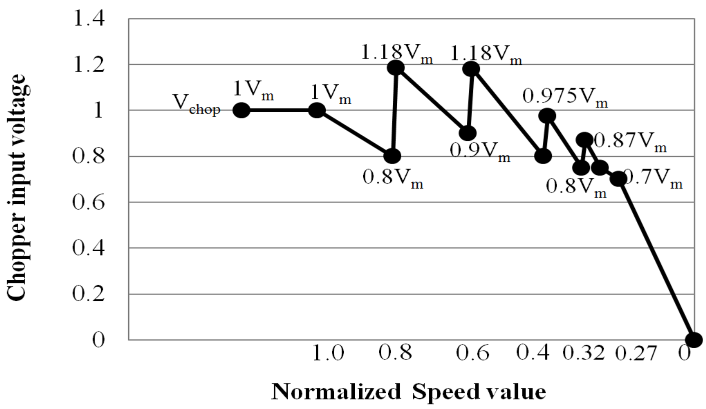

Figure 6.20: Chopper input voltage as a function of normalized speed value

For a MWSC system with V_{m-max} = 500 V, K=2, m=4, $\alpha = 0.5$, representative values of various parameters are given in the table 6.3

6.10.1.3 Duty cycle variation of chopper gate pulses

The duty cycle variation of chopper gate pulses as a function of normalized Generator voltage is as shown in the Fig. 6.21

Table 6.3: Representative operating range of various parameters

Chopper Output V_0 retained at 400 Volts									
Normalised Speed range		Generator voltage rang(V)		chopper input voltage (V)		No of Devices ON	chopper Duty cycle	
		Max	Min	Max	Min		Max	Min
1	0.8	500	400	500	400	None	0.80	1.00
0.79	0.6	399	300	598	450	1 (T1)	0.67	0.89
0.59	0.4	299	200	598	400	2 (T1, T2)	0.67	1.00
0.39	0.32	199	160	497	400	3 (T1, T2, T3)	0.80	1.00
0.31	0.27	159	134	477	402	4 (T1, T2, T3, T4)	0.84	1.00

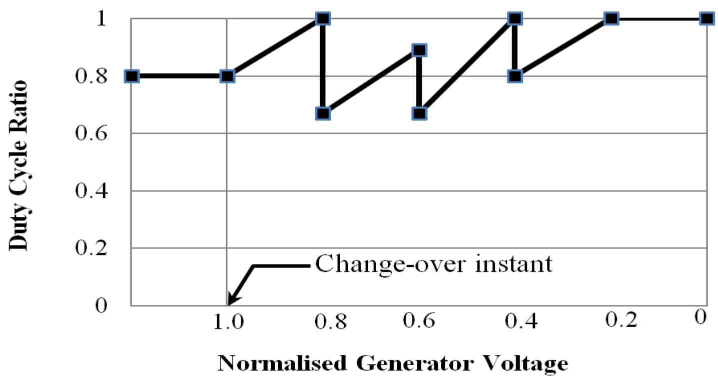

Figure 6.21: Duty cycle variation as a function of normalized generator voltage

6.10.2 Switching topology and voltage control using multi winding multi- chopper configuration(MWMC)

Multi winding multi chopper (MWMC) configuration is shown in the Fig. 6.22 In this configuration, output of each of the G-windings are rectified and filtered before it is given to a buck converter. There are as many independent set of rectifiers and buck converters as G-windings. This make them independent variable dc voltage sources. When the generator speed is falling, the reduction in induced voltage is compensated on continuos basis by connecting number of variable dc voltage sources (choppers) in series.These dc sources are derived from induced voltages in the isolated G-windings (V_{dc1}, V_{dc2},.... V_{dc-m})followed by separate rectifiers, filters and choppers. One or more of these chopper outputs are connected in series with the dc source derived from M- winding. This configuration of choppers maintains the dc bus voltage constant by adjusting the duty cycle of their gate pulses.

6.10.2.1 Salient features

- Increased reliability
- Controller complexity
- Control strategy: Control choppers one by one

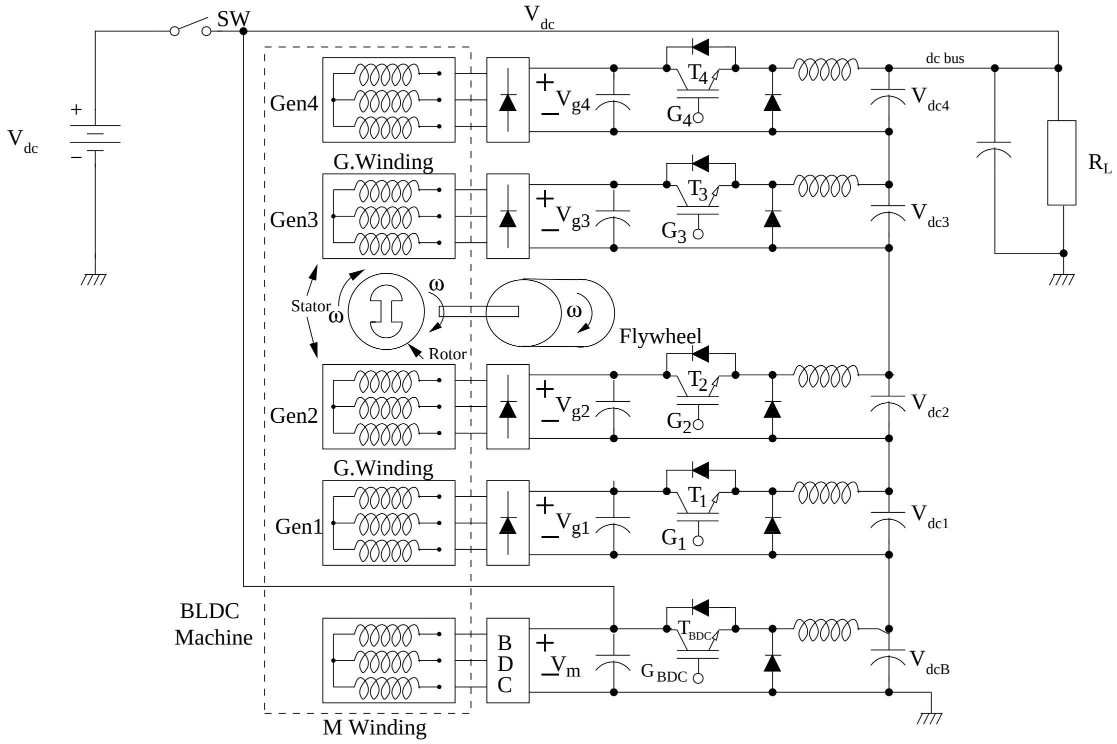

Figure 6.22: Block diagram of the new scheme using MWMC, with $m = 4, K = 2$

6.10.2.2 Working principle

It can be seen from the Fig. 6.22 that the dc bus voltage is the sum of all the voltage output of individual chopper (buck converter) and it can be computed as follows:

$$V_{dcbus} = (D_0V_{m-max} + D_1V_{g1} + D_2V_{g2} + D_3V_{g3} + ... + D_mV_{gm}) \times \frac{N}{N_{max}} \quad (6.24)$$

$$V_{dcbus} = (V_{m-max} \times D_0 + V_g \times (D_1 + D_2 + D_3..... + D_m)) \times \frac{N}{N_{max}} \quad (6.25)$$

$$V_{dcbus} = (V_{m-max}(D_0 + K(D_1 + D_2 + D_3..... + D_m)) \times \frac{N}{N_{max}} \quad (6.26)$$

Hence,

$$V_{dcbus} = \left[(V_{m-max}(D_0 + K \sum_{i=1}^{m} D_i \right] \times \frac{N}{N_{max}} \quad (6.27)$$

Therefore, the dc bus voltage can be maintained constant by adjusting the value of $D_i(i = 1, 2....m)$. Depending on the running speed of the machine, the duty cycle of gate control pulses of these choppers are adjusted to maintain the output DC bus voltage as required. At any point of time the duty cycle of only one chopper is adjusted and the remaining choppers are kept either fully OFF or fully ON depending on the range of speed. Generator speed is divided into different ranges like,

(i) 100% to 80% (range indicator R = 0),
(ii)80% to 60% (range indicator R = 1),
(iii) 60% to 40% (range indicator R = 2) and so on

Depending on the value of the range indicator, the value of the duty cycle is adjusted in the equation (6.27) as given below:
$R = 0, D_0 = 0$–1.0(BDC chopper device duty cycle is varied from 0 to 100%).
$i \leqslant R, Di = 1$ (i^{th} chopper device permanently ON).
$i = R, Di = 0$–1.0 (i^{th} chopper device duty cycle is varied from 0 to 100%).
$i \geqslant R, Di = 0$ (i^{th} chopper device permanently OFF).

For a MWMC system with $V_{m-max} = 500V, K = 2, m = 4, \alpha = 0.5$ representative values of various parameters are in table 6.4.

Table 6.4: Control logic of MWMC configuration

DC bus voltage maintained at 400 Volts							
Normalised Speed range		Generator voltage range(V)		Controlling device		Chopper device Fully ON	Chopper device Fully OFF
		Max	Min	R	Devive		
1	0.8	500	400	0	BDC	None	T_1, T_2, T_3, T_4
0.79	0.6	399	300	1	T_1	T_{BDC}	T_2, T_3, T_4
0.59	0.4	299	200	2	T_2	T_{BDC}, T_1	T_3, T_4
0.39	0.32	199	160	3	T_3	T_{BDC}, T_1, T_2	T_4
0.31	0.27	159	134	4	T_4	T_{BDC}, T_1, T_2, T_3	None

6.10.2.3 Duty cycle variation of choppers gate pulses

The duty cycle (D_i) variation of various choppers and sigma sum (ΣDi) of gate pulses as a function of normalized generator voltage is as shown in the Fig. 6.23 and Fig. 6.24 respectively.

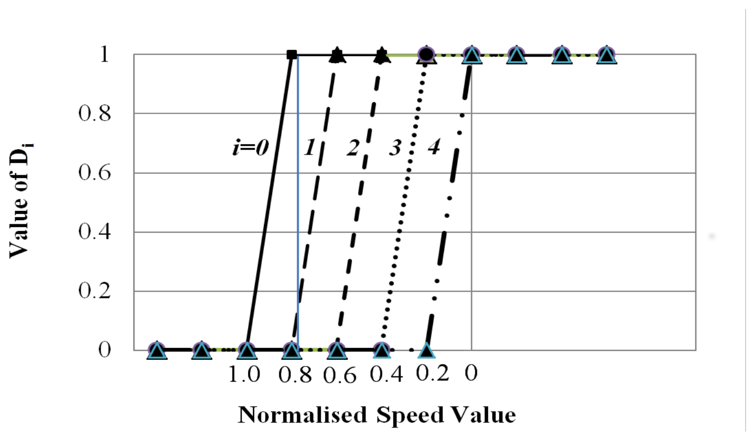

Figure 6.23: Duty cycle variation of choppers as a function of normalized generator voltage

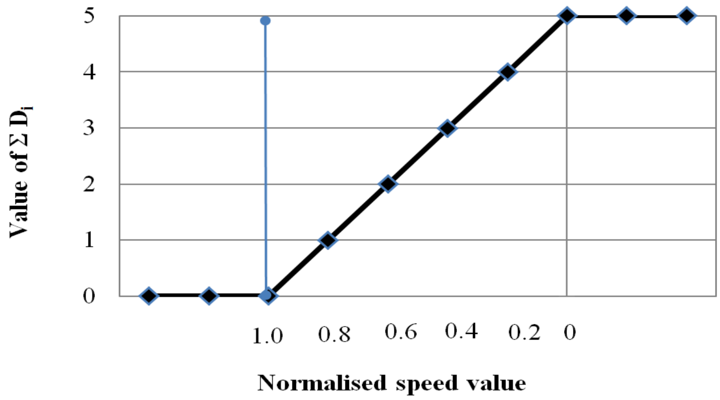

Figure 6.24: Cumulative duty cycle variation of choppers as a function of normalized generator voltage

6.11 Simulation of the MSSC scheme

6.11.1 Multi Winding Single Chopper Scheme

The simulation of this proposed scheme was carried out using MATLAB/Simulink software and the results obtained are presented. Simulation parameters are as given in the table 6.1. The block diagram of the simulation model is given Fig. 6.25 The results (waveforms) obtained from the simulations are given in the Fig. 6.26.

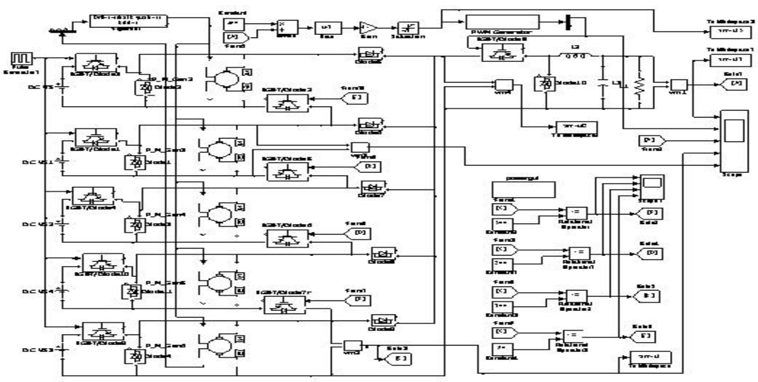

Figure 6.25: Simulink model of the topology for MWSC scheme

Fig. 6.26(a) and (b) show the voltage v/s time plots of generator and load respectively. It may be noted that the load voltage is maintained constant in spite of the drop in generator voltage during backup time. Plot of Fig. 6.26 (c) show that the chopper input voltage is limited to within 118% of V mg . This means the chopper device is subjected to lower voltage stress as compared to DWBC. It is clear from Fig. 6.26 that the simulation results are comparable with the predicted results.

6.11.2 Multi Winding Multi Chopper Scheme

The simulation of this proposed scheme was carried out using MATLAB/Simulink software and the results obtained are presented. Simulation parameters are as

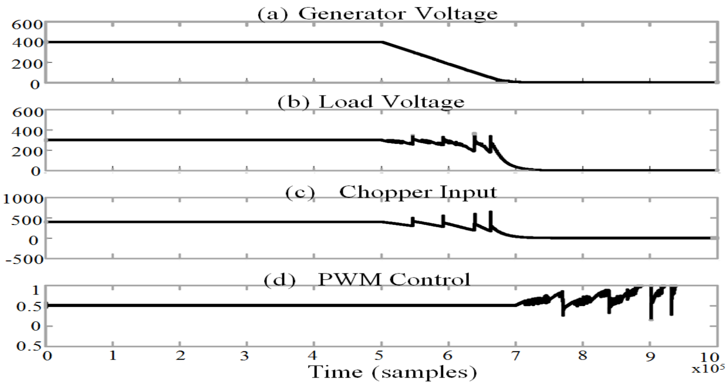

Figure 6.26: Simulation results of MWSC scheme

given in the table 6.1. The block diagram of the simulation model is given Fig. 6.27.

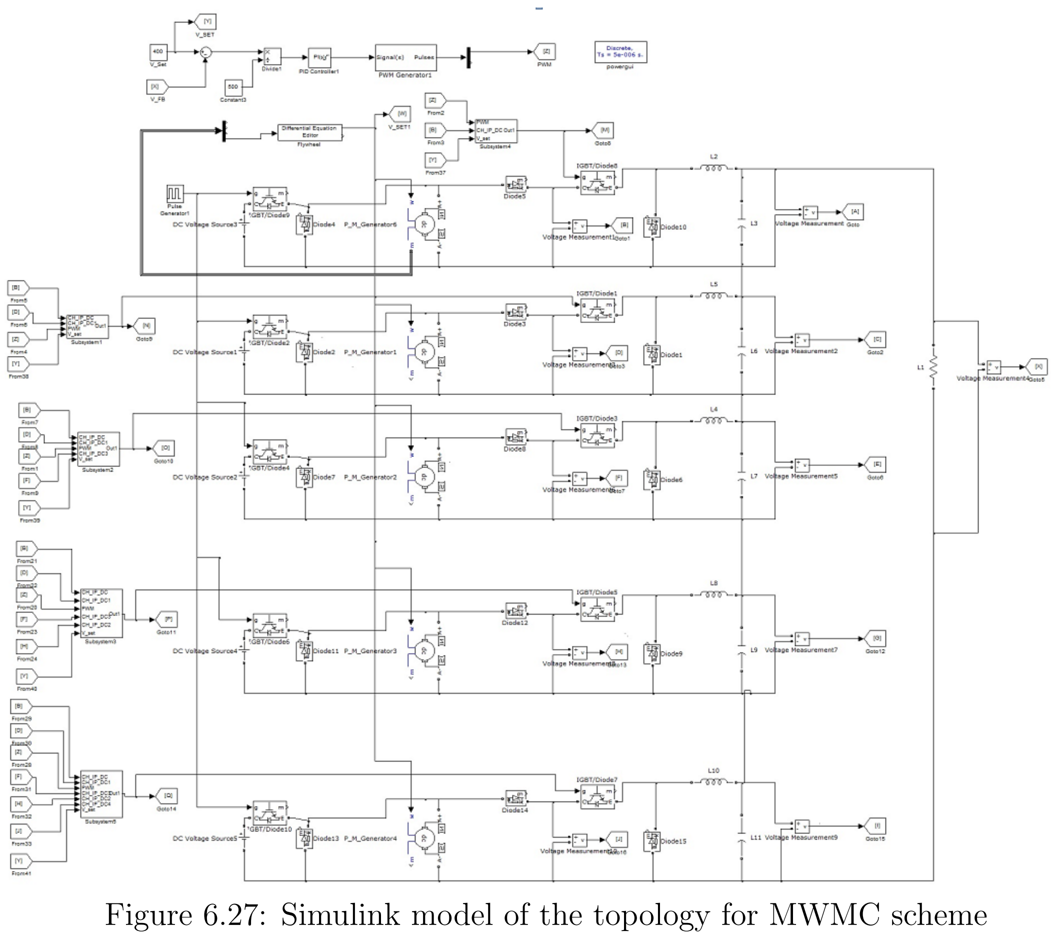

Figure 6.27: Simulink model of the topology for MWMC scheme

The results (waveforms) obtained from the simulations are given in the Fig. 6.28 Fig. 6.28(b) and (c) show the input voltage experienced by the individual choppers. It is clear that the voltage stress on all these chopper devices in MWMC scheme is much less as compared to DWBC scheme for maintaining the same dc bus voltage [Fig. 6.28(d)]. Moreover, the chopper devices don't experience voltage transients (which might lead to high dv/dt) at changeover instants in contrast to the DWBC scheme. It may be noted that the voltage transients across an IGBT device may cause the current to flow through the collector-gate and gate-emitter capacitances, resulting in increased gate-emitter voltage, which can drive the IGBT into conduction. Therefore it is desirable to maintain the voltage transients low across the device. Again, from Fig. 6.28, it can be concluded that the simulation results compare well with the predicted results.

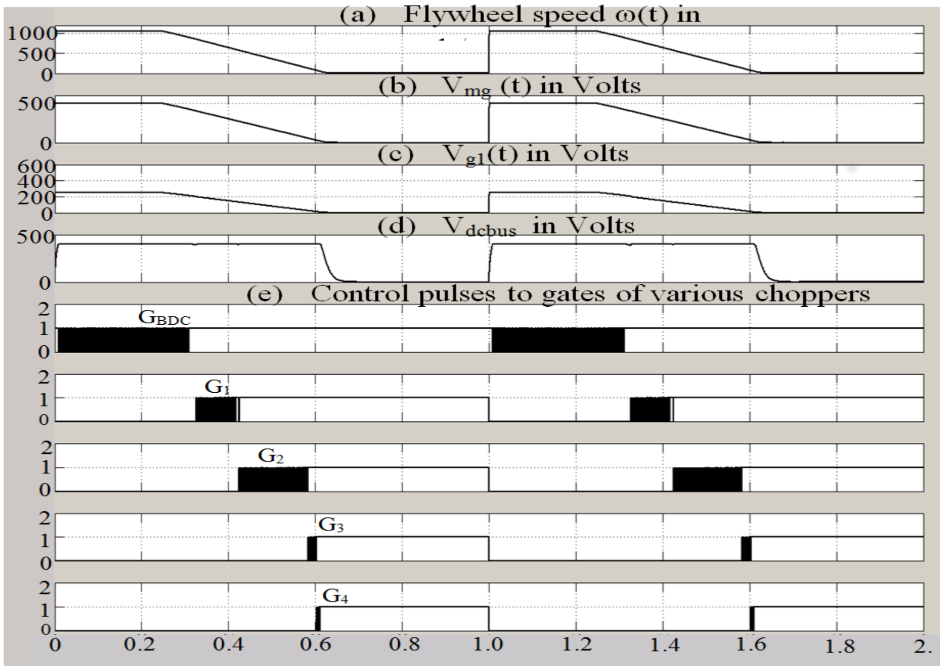

Figure 6.28: Simulation results of MWMC

6.12 Experimental setup and discussion of the results of multiwinding schemes

Prototype laboratory models of the newly proposed MWSC and MWMC topologies/schemes for flywheel energy harvesting are built using a PM-BLDC machine. Proposed control methods are implemented using a Digital Signal Processor of Motorola make, Model: DSP 56F805. A logic for controlling the switches (T_1, T_2,T_3, T_4), closed loop feedback PI controller and overall control algorithm is implemented and evaluated. MWSC and MWMC are tested with same load conditions for the evaluation and comparison their performances. The dc bus Voltage-Time plots of the above mentioned schemes are recorded using a digital storage oscilloscope (DSO) are shown in Fig. 6.29(a) and (b) and in Figs. 6.30(a) and (b) respectively for various similar load currents. It may also be observed in these plots that the power back up time is about 20% higher as compared to single armature winding machine. It may be noted that the results obtained from the experiments are in line with those of the theoretically predicted ones.

6.12.1 Voltage-time plots of MWSC scheme

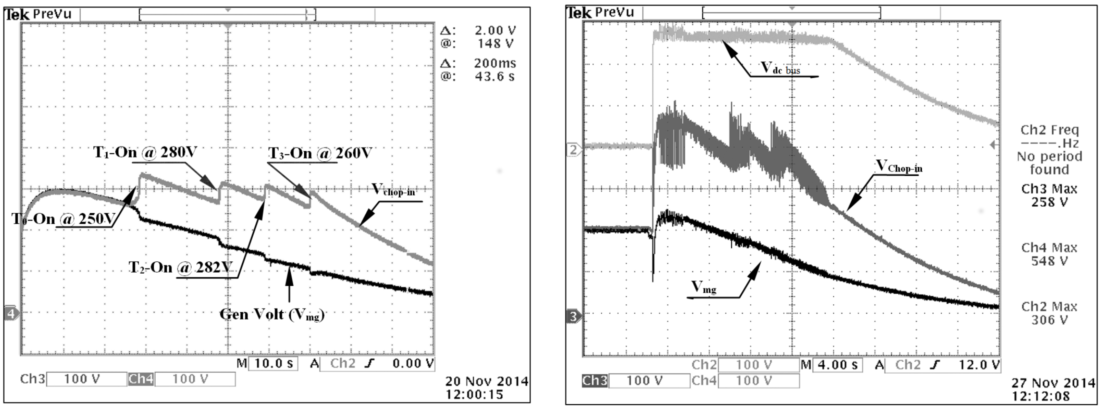

(a) (b)

(a). At V_{dc} = 300 V, Speed = 5000 RPM, R_L = 3.3 KΩ
(b). At V_{dc} = 300 V, Speed = 5000 RPM, R_L = 240 Ω

Figure 6.29: Voltage-time plots of MWSC scheme recorded in DSO

6.12.2 Voltage-time plots of MWMC scheme

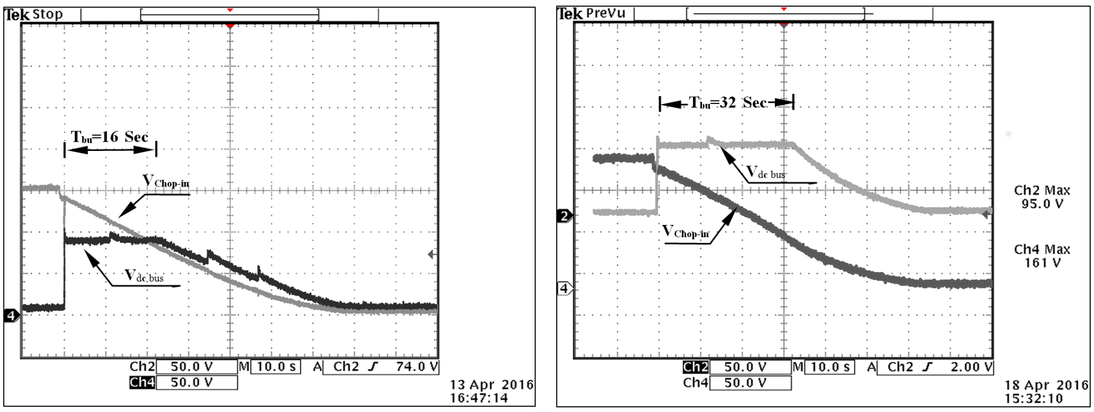

(a) At V_{out} = 200 V, T_{bu} = 22 seconds (b) At V_{out} = 200 V, T_{bu} = 38 seconds

Figure 6.30: Voltage and Input current-time plots of MWMC scheme recorded in DSO

6.13 Summary

Design of a new topology has been carried out whose voltage gain and efficiency are independent of its source resistance or load resistance using a novel unique combination of dual armature winding permanent magnet brushless dc machine and a buck converter. This has also helped in overcoming the limitations of the boost converters completely. From the theoritical analysis and simulation results, it is found that the newly proposed DWBC scheme is found to be an attractive proposition for increasing the harvestable energy and impoving the energy efficiency. It is concluded from the analysis of experimental results that the harvestable energy has been increased by about 20% as compared to existing schemes by adopting the proposed topology/scheme. It can be further improved by increasing $K - factor$. But increasing the $K - factor$ also increases the voltage stress on the buck converter chopper device. This also results in increase in overall size of generator/machine, voltage rating of the buck converter device. Novel MWSC and MWMC schemes are adopted to reduce the voltage stresses on the buck converter power device. Prototype models of both schemes mentioned above are built and tested. The results obtained from these tests/experiments conducted are in line with those of the theoretically predicted ones.

The FESS has the potential of using for wide range of applications and one of them is described in the Chapter 7.

Chapter 7

Design and Analysis of Capacitor Charging Power Supply

Usually charged capacitors are used as the power source where pulse power is required. Hence there is a need for the Capacitor Charging Power Supply (CCPS). This chapter covers the application of FESS in a CCPS. These CCPS draw high peak current from the input supply to meet the charging current requirement of Capacitors even though the average current requirement is low. It requires high rated switchgears and power semiconductors devices at the input circuitry. This can be avoided by using an Intermediate Energy Storage (IES) device which stores energy for a longer duration (drawing low power from the mains) and deliver the same to charge the Capacitor for a shorter duration (delivering higher power). One such CCPS has been designed, simulated and built using a flywheel as an IES device. Design procedure is given in this chapter. Results obtained from simulation and experiments conducted are presented.

7.1 Typical pulse power source

A typical pulse power supply system is shown in a block diagram in Fig. 7.1. It consists of a rectifier, an intermediate energy storage device (IES), capacitor charging circuit (CC) and an output capacitor (C_o). The voltage modulator stores the energy in the IES device slowly over a longer period for the IES device to discharge the same later into C_o through the CC in a shorter period. Capacitor C_o is used as an energy source and made to deliver this energy to the pulse load for a short period of time.

The amount of energy stored in a capacitor is given by the following equation:

$$E_c = \frac{1}{2} C_o V_o^2 \tag{7.1}$$

Therefore a compact CCPS can be built by designing a higher voltage (low value capacitor) rather than a lower voltage (high value capcitor) system. Capacitor charging circuits are basically a high voltage source capable of supplying charging current to the capacitor at the rated voltage. The high voltage can be generated by employing either a dc-dc boost converter or dc-ac high frequency inverter followed by a step up transformer or voltage multiplier circuits and is used for charging

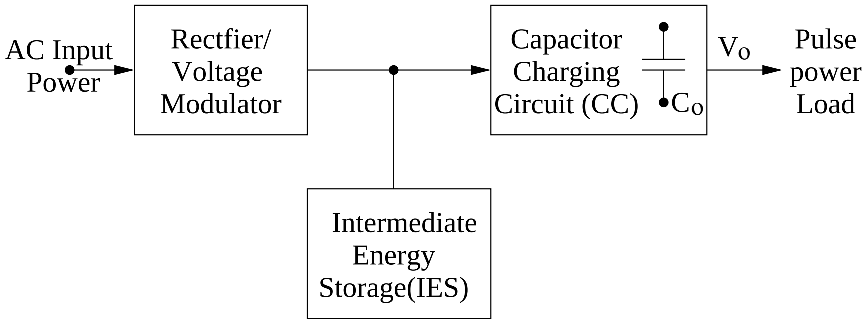

Figure 7.1: Typical capacitor charging power supply

the output capacitor (C_o). In a typical CCPS, the bulk energy from mains is first stored in an IES device, then it is transferred to the output capacitor C_o as and when it is required. This energy is delivered to the load in a short time using a fast acting semiconductor switches (High pulse power). The characteristics of an ideal CCPS are, low charging time, high efficiency, high discharging rate, compact in size, good reliability, long life, lowest input power for a given pulse output power etc.

7.2 Intermediate Energy Storage devices

Pulsed power supplies (PPS) will deliver very high power to the load in short time. Even though the average power drawn is very less (duty cycle is very low), the input circuitry should be rated to handle large power. This makes unnecessary over sizing of the input power section. Over sizing the input power section can be avoided by storing the energy from ac mains in an intermediate energy storage (IES) device for a longer period (at low power) and releasing the same to the output capacitor in a short time as required (at high power).

7.3 CCPS with flywheel as an IES device

A flywheel is used as an IES device in the new scheme of CCPS as it is ideally suited with their features of very high rate of charging and discharging.

7.3.1 Working Principle

Capacitor charging power supply with flywheel as the energy storage device is as shown in Fig. 7.2. Input voltage from ac mains is converted to dc voltage using a rectifier. This dc voltage is applied across the terminals of an electrical machine through a 3-phase Bidirectional converter by connecting P1 to NC1 as shown in the Fig. 7.2. The BDC acts as a motor drive to make the machine to run as a motor. This motor accelerates the flywheel coupled to it and the flywheel stores the energy in the form of angular velocity. When this stored energy is required to be transferred to the output capacitor C_o, P1 is connected to NO1 (of S1) and P2 connected to NC2 (of S2). In this condition, the flywheel continues to run due to its inertia driving the machine (which starts working as generator) inducing the voltage across its terminals. Now the BDC acts as a rectifier charging the output capacitor (C_o) through a capacitor charging circuit. This makes the capacitor to get charged to the required voltage.

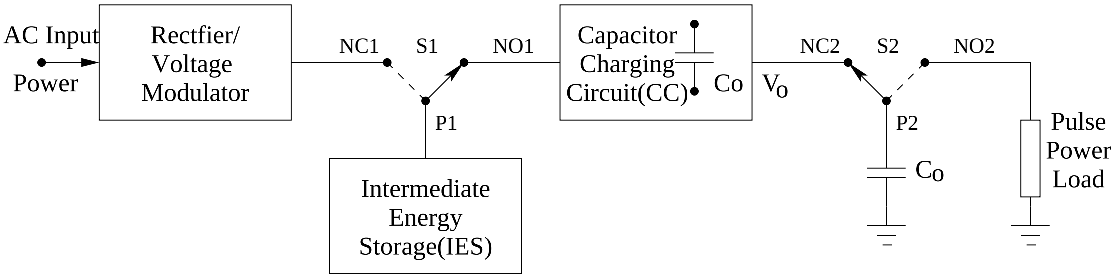

Figure 7.2: Capacitor charging system with flywheel as intermediate energy storage

When the output capacitor (C_o) is fully charged, it is ready to supply energy to the load. Whenever this energy required to be transferred to the load, the P2 is connected to NO2 (of S2) and the capacitor C_o discharges to the load. When C_o is fully discharged, P2 is connected to NC2 (of S2) to charge the capacitor C_o again. This way of charging and discharging of capacitor will continue till the flywheel speed reduces to so low that it is not sufficient to charge C_o to the required voltage. Speed of the flywheel becomes zero when all the energy stored is used in charging the output capacitor and consumed in meeting the system losses. Once speed becomes zero, P1 is connected to NC1 (of S1) again and BDC is made to act as motor drive accelerating the flywheel to store the energy. This charging/discharging cycle repeats.

7.3.2 Modes of Operation

There are four modes of operations in a CCPS where flywheel is used as an IES device. They are, energy storing in the flywheel, energy transfer from flywheel to capacitor, energy storing in flywheel / capacitor discharge to the load and capacitor discharge to the load. The system can be taken to any of those operating modes by changing the position of switch S1 and S2. Details of these operating modes are given in table 7.1

7.3.3 Methods of using flywheel as IES

Energy stored in the flywheel can be transferred to output capacitor two methods. In the first method, all the stored energy in the flywheel is transfered to the capacitor before the flywheel is charged again ("Full discharge method"). In the second method, part of the stored energy is transfered to the flywheel to the capacitor before the flywheel is charged again ("Partial discharge method").

7.3.3.1 Full discharge method

The charging/discharging cycles of the flywheel/capacitors in this method is represented graphically as shown in Fig. 7.3 and the flow chart of their operation is shown in Fig. 7.4.

Table 7.1: Operating modes

Mode	Switch Posistion		Mode	
	S1	S2	Description	Operation
Mode1	P1→NC1	P2→NC2	Energy Storing	Input energy is being stored in the flywheel
Mode2	P1→NO1	P2→NC2	Capacitor charging	Energy from the flywheel is transferred to output capacitor
Mode3	P1→NC1	P2→NO2	Energy storing and capacitor discharging	Input energy is being stored in flywheel; Energy from output capacitor discharged to load
Mode4	P1→NO1	P2→NO2	Capacitor discharging	Energy from the output capacitor is discharged to the load and flywheel idles

In "Full discharge method" the flywheel is accelerated to full speed using input power to store the energy (Mode1). Once it reaches the full speed, a part of stored energy transferred to output capacitor C_o(Mode2). Whenever load demands the energy, C_o supplies the same to load (Mode4). This cycle (switching between Mode2 and Mode4) is repeated as many number of times till the flywheel speed reduces to a level which is just sufficient to charge C_o to the required voltage. Amount of energy transferred each time and number of times of it is transferred depends on the value of the capacitor to be charged and its charging voltage. Once the flywheel is fully is discharged (speed/stored energy becomes to zero), the system is switched to Mode1 and the cycle is repeated. When system is in Mode1 (flywheel is accelerating), the capacitor will be idling (zero voltage condition)

7.3.3.2 Partial Discharge method

The charging/discharging cycles of the flywheel/capacitors in this method is represented graphically as shown in Fig. 7.3 and the flow chart of their operation is shown in Fig. 7.4. The flywheel is accelerated to full speed using input power to store the energy (Mode1). When the flywheel reaches the full speed, a part of stored energy transferred to output capacitor C_o(Mode2). Whenever load demands the energy C_o supplies the same to the load (Mode4). This cycle (switching between Mode2 and Mode4) is repeated as many number of times until the stored energy (speed) in the flywheel is reduced below predefined non zero level. Amount of energy transferred each time and number of times of it is transferred depends on the value of the capacitor to be charged and its charging voltage. Once the speed of the flywheel reached the predefined level, the system is switched to Mode1 to charge again and the cycle is repeated. When system is in Mode1 (flywheel is accelerating) and the capacitor will be idling (zero voltage condition).

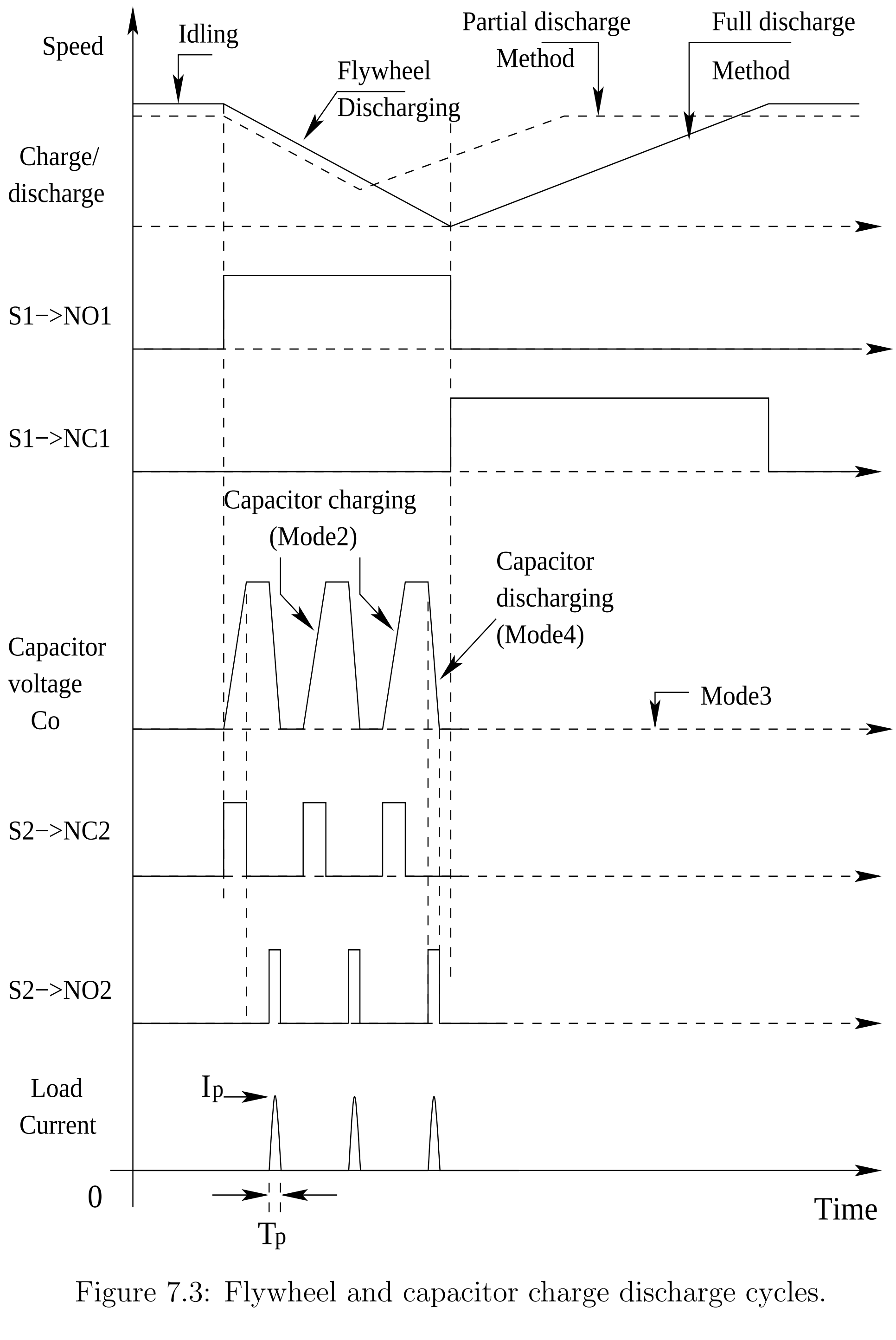

Figure 7.3: Flywheel and capacitor charge discharge cycles.

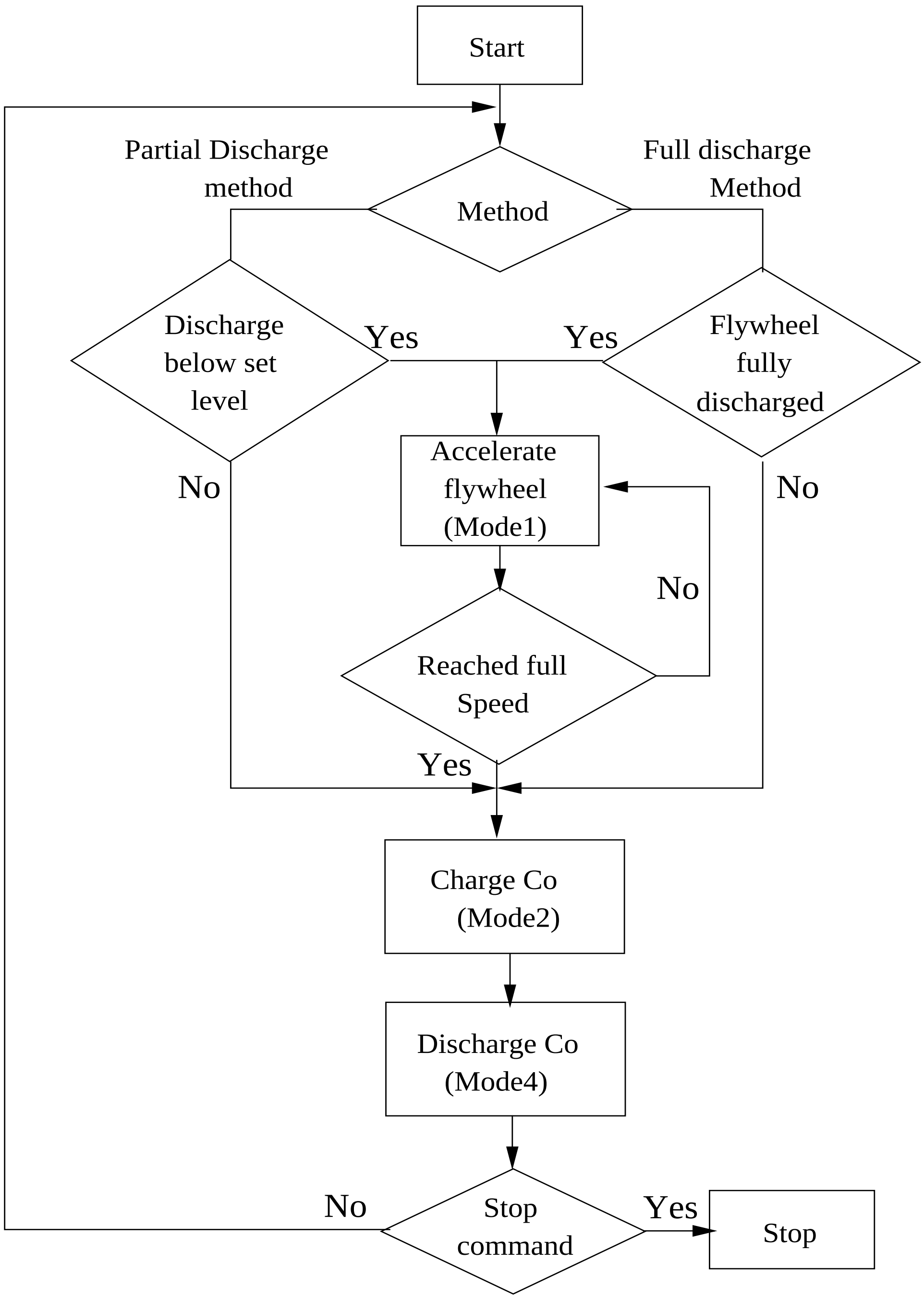

Figure 7.4: Flow chart of Flywheel based CCPS operation

7.4 Computation of various parameters related to flywheel

The energy is transferred from IES device i.e. flywheel to the output capacitor through the charging circuit. By using energy balance equations, one can compute the number of times (N_c) a capacitor can be charged for the given energy stored in a flywheel. This can be expressed as follows:

No of capacitor charging cycles

$$N_c = \frac{E_h}{E_c} \tag{7.2}$$

Total flywheel discharge time per cycle

$$T_c = \frac{1}{f_c} \tag{7.3}$$

Coasting down time of the flywheel

$$T = (1 - D_m)T_{acc} = N_c \times T_c \tag{7.4}$$

7.5 Design methodology of a CCPS with FESS

This section explains the step by step procedure of computation of various parameters, values of individual components and sizing of subsystems from the design specifications followed by a design example.

7.5.1 Selection of output voltage and value of output capacitor

By knowing the value of required peak power and its duration, one can decide the value of capacitor. Energy required to be stored in the capacitor is given by the following equation.

$$E_c = P_p \times T_p \tag{7.5}$$

Assuming the ideal condition of stray inductance and path resistance equal to zero, the voltage to be applied and value of the capacitor can be computed as follows:

$$V_c = \sqrt{P_p \times \ R_L} \tag{7.6}$$

$$C_o = \frac{2 \times E_c}{P_p \times R_L} \tag{7.7}$$

7.5.2 Sizing of FES system

The required harvestable energy and moment of inertia "J" can be computed using following equations:

$$E_h = \frac{E_c \times N_c}{\eta} \tag{7.8}$$

$$J = \frac{2 \times \; E_h}{(\omega_{max}^2 - \omega_{min}^2)} \tag{7.9}$$

Physical dimensions of the flywheel can be computed using the following relation:

$$J = \frac{1}{2} m r^2 \tag{7.10}$$

7.5.3 Capacitor charging time and frequency

We can compute the charging time available for the capacitor if the pulse repetition frequency is known.

Discharging Time

$$T_p = \frac{E_c}{P_p} \tag{7.11}$$

Interval between two charging cycle (T_c)

Voltage waveform across the output capacitor as a function of time is shown in Fig. 7.5.

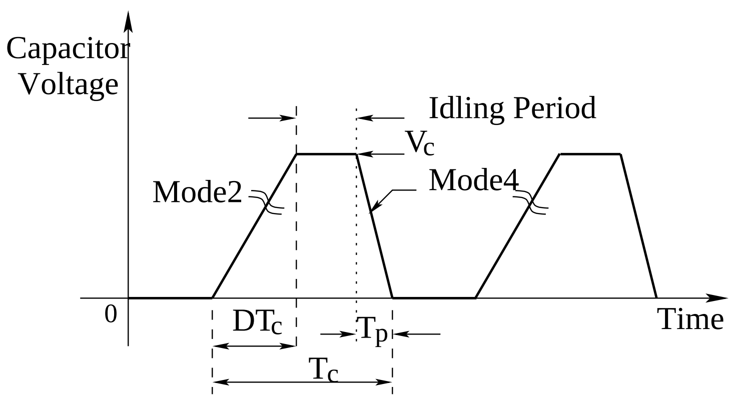

Figure 7.5: Capacitor charging and discharging process.

It is in from Fig. 7.5 that the maximum time available for the charging the capacitor C_0 is (T_c-T_p). Therefore, the response time of the boost converter should be less than this time.

$$\pi\sqrt{L_B C_o} \leqslant (T_c - T_p) \tag{7.12}$$

7.5.4 Selection of the rating of BLDC machine and power converter

The instantaneous current drawn from the source (i.e. IES device) in one charging cycle is shown in Fig. 7.6.

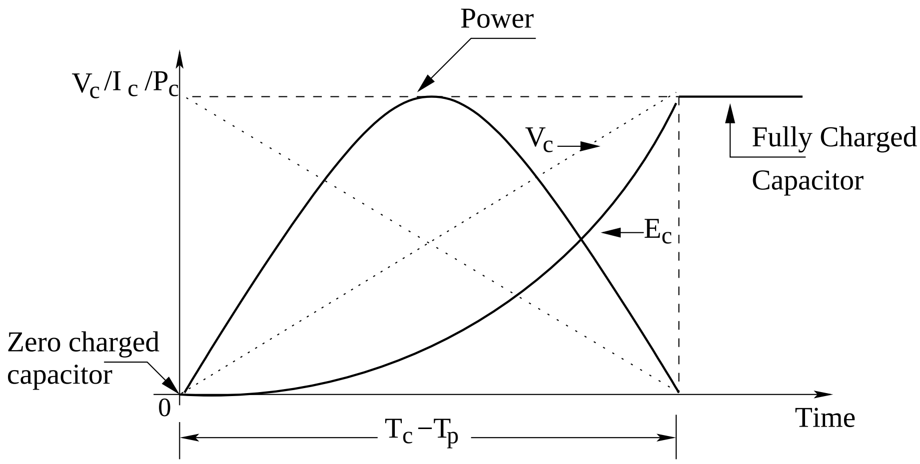

Figure 7.6: Current voltage waveforms during charging of the capacitor

7.6 Average current, voltage and power of the machine

FESS is characterised by slow acceleration (storing energy) and fast deceleration (releasing energy), the subsystem should handle high power for a shorter duration though the average power drawn is less. For selecting the rating of the machine, power semi conductor devices and other switch gears, it is necessary to compute the average and RMS value of voltage and current handled by these devices.

7.6.1 Generating mode (during discharging of flywheel)

It is assumed that, the rated voltage of machine is V_{dc}, Energy harvested is E_h, Capacitor voltage is Vc and the energy is harvested is down to the speed of 10% of top speed (N_{max}). We can compute various parameters of the system as given below:

(i) Boost converter gain:

$$G = \frac{V_c}{V_{dcmax}}(\omega_{max}) \tag{7.13}$$

$$G = \frac{V_c}{V_{dcmin}}(\omega_{min}) \tag{7.14}$$

(ii) Average power per cycle:

$$P_{m(av)} = \frac{G}{6} V_{dc}^2 \sqrt{\frac{C_o}{L_B}} \tag{7.15}$$

(iii)Peak current through the capacitor:

$$I_P = \frac{V_{dc}}{\sqrt{\frac{L_B}{C_o}}} \tag{7.16}$$

(iv) Worst case peak current through device of boost converter:
Assuming maximum available dc voltage and maximum duty cycle, we can compute the peak current as follows:

$$I_P = \frac{1}{L_B}\frac{V_{dcmax}}{f_{sw}} \tag{7.17}$$

(v) Worst case average generator current (Instantaneous; during charginoutput capacitor):

$$I_g = \frac{1}{2L_B}\frac{V_{dcmin}}{f_{sw}} \tag{7.18}$$

7.6.2 Motoring mode (during charging the flywheel)

BLDC machine operation can be represented graphically as given in Fig. 7.7

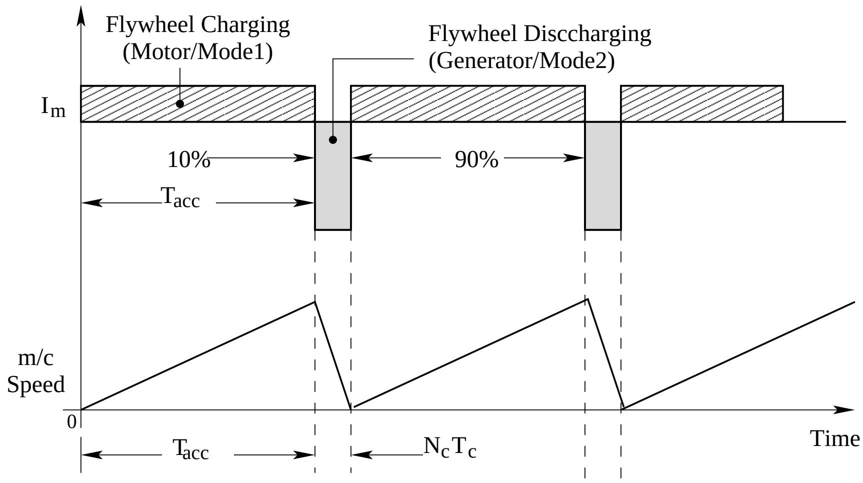

Figure 7.7: Flywheel charging and discharging cycles

Considering an ideal system (Power loss = 0). Power drawn from the source is only the accelerating power of the flywheel. The current drawn from the source is given by,
(i) Machine current in motor mode:

$$I_m = \frac{J}{V_{dc}}\omega\frac{d\omega}{dt} \tag{7.19}$$

(ii) Average machine current (both Generating mode motoring mode together):

$$I_{m(av)} = (I_m \times D_m + I_g \times (1 - D_m) \tag{7.20}$$

Machine is selected based on above parameter values with proper de-rating (as the duty cycle is very less). Devices used in the Boost converter shall be selected based on $I_c = I_{max}$, $V_{ce(off)} = V_c$ with proper de-rating factor.

7.7 Design Example

Design specifications are given in table 7.2

Table 7.2: Design specifications

Parameter	Value
Load resistance (R_L)	0.27 Ω
Load peak current (I_p)	2300 A
Current pulse width	4.0 ms
Pulse repetation rate	0.2 Hz
No of current pulses in a cycle	10

Values of various components and sub systems were computed using the design equations derived in the sections 7.5 and 7.6 and given in table 7.3

Table 7.3: Computed values of various parameters

Parameter	Value
Output capacitor(C_o)	29300 μF
Energy to be stored in Co per cycle (Ec)	2344 J
Harvestable energy in flywheel(Eh)	23440 J
Maximum available time for charging	4.996 s
Critical(Max)value of inductance LB	86.38 H
Required moment of inertia	0.075 kg-m
Mass of flywheel and diameter	15 kg, 200 mm
Required gain range of boost converter	3.0 to 9.32
Peak current in motor mode	2.24 A
Peak current in generator mode	6.50 A
Machine average current ($I_{m(av)}$)	3.20 A
Boost converter device rating	300 V, 13 A
BLDC Machine rating	960 W
Output capacitor charging switch (S2,P2$\rightarrow$NC2)	600 V, 700 A
Output capacitor discharging switch (S2,P2$\rightarrow$NC2)	600 V, 2300 A

7.8 Simulation of the system and tabulation of the results

The simulation of this new scheme with flywheel as an IES along with control methodology is carried out using MATLAB/Simulink software. Simulation parameters are as given in the table 7.4
The block diagram of the simulation is given Fig. 7.8.
The results (waveforms) obtained from the simulations are given in the Fig. 7.9.
It may be noted from the waveforms (obtained from simulations) that the flywheel accelerates when the supply from mains is connected to the motor and

Table 7.4: Simulation parameters

Parameter	Value
Output capacitor value	1000 μF
Maximum flywheel speed	8000 RPM
Minimum flywheel speed	1000 RPM
Load resistance value	0.1 Ω, (Non-inductive)
Simulation sample time	5 μs.
Load voltage	750 V DC
Rated voltage of the dc machine	400 V DC
Moment of inertia of flywheel	0.681 kgm^2

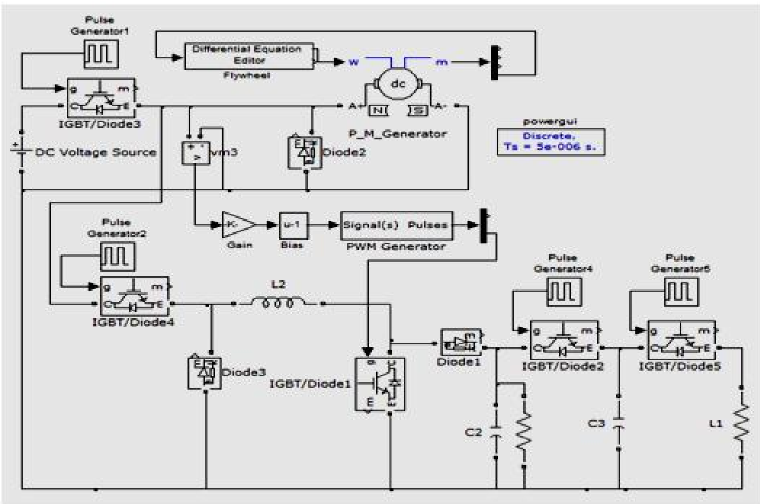

Figure 7.8: Block schematic of the simulink model of CCPS using flywheel

stores the energy. When the motor is disconnected from the mains and connected to the boost converter, the flywheel continues to run due to the inertia driving the machine which starts acting as generator. Since the output of the machine is connected to the boost converter, it charges the boost capacitor. The switching logic of connecting/disconnecting to mains is implemented using the Pulse Generator1 (PG1) and Pulse Generotor2 (PG2). The logic of charging/discharging of output capacitor is implemented by the Pulse Generator4 (PG4) and Pulse Generator5 (PG5). It may be noted from the simulation results that the when the output pulse capacitor is being charged as the energy is drawn the flywheel and the flywheel decelerates; the dc bus voltage drops. The output voltage of the boost converter is maintained constant by varying its control pulse width against the reduction of input voltage. From the simulation it is very clear that the boost converter is able to boost the dc bus voltage to supply the charging voltage to the output capacitor and so constant pulse power to the load during whole of the flywheel deceleration period.

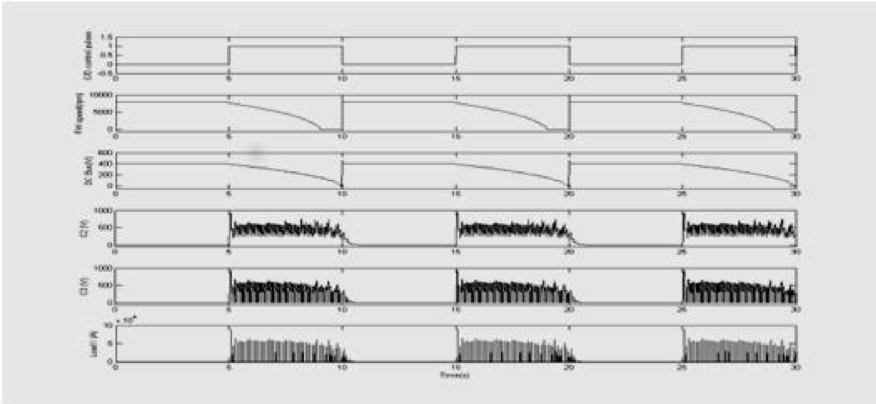

(a) Simulation time 0.0s to 30s.

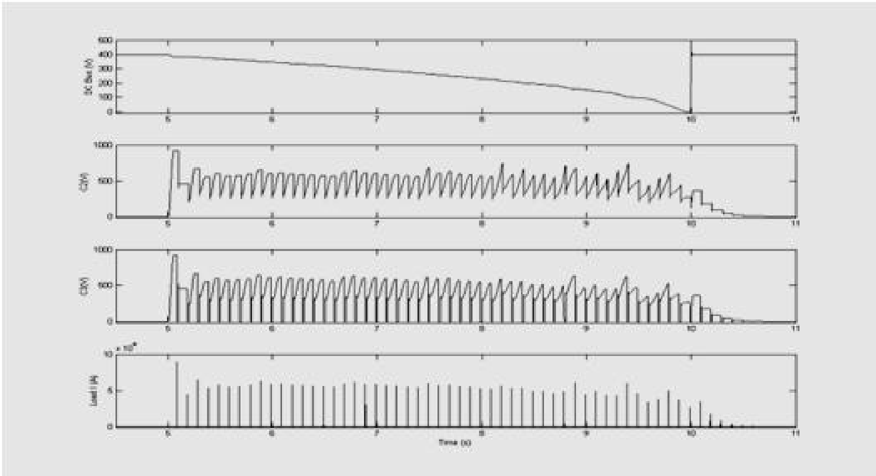

(b) Simulation time 5.0s to 11s.

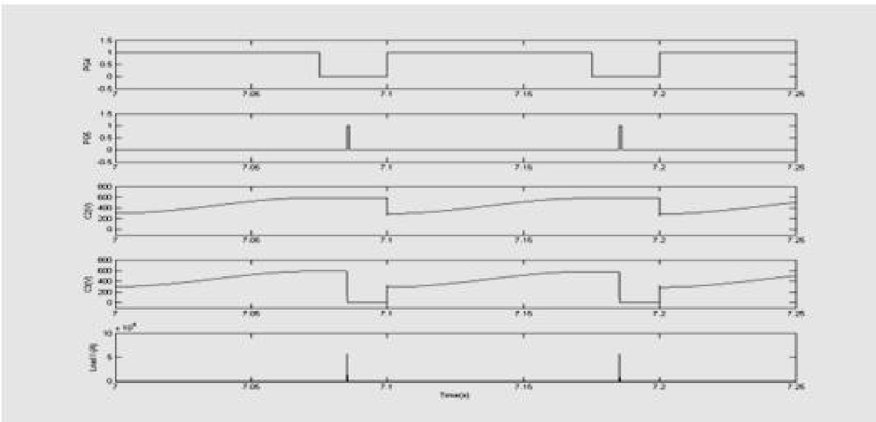

(c) Simulation time 7.0s to 7.25s.

Figure 7.9: Control pulses, voltage, and current waveforms from various simulation time

7.9 Testing, Evaluation and Validation of the proposed system

A prototype system was designed and built using the parameters given in the table 7.2 and tested to validate the design. The block diagram of the system built validating the proposed CCPS is shown in the Fig. 7.10 System was tested to evaluate the performance. In charging mode, the BDC is used as a motor drive and accelerates the flywheel to store the energy. In discharging mode, the BDC is used as a rectifier to feed the boost converter which charges the output capacitor with required voltage.

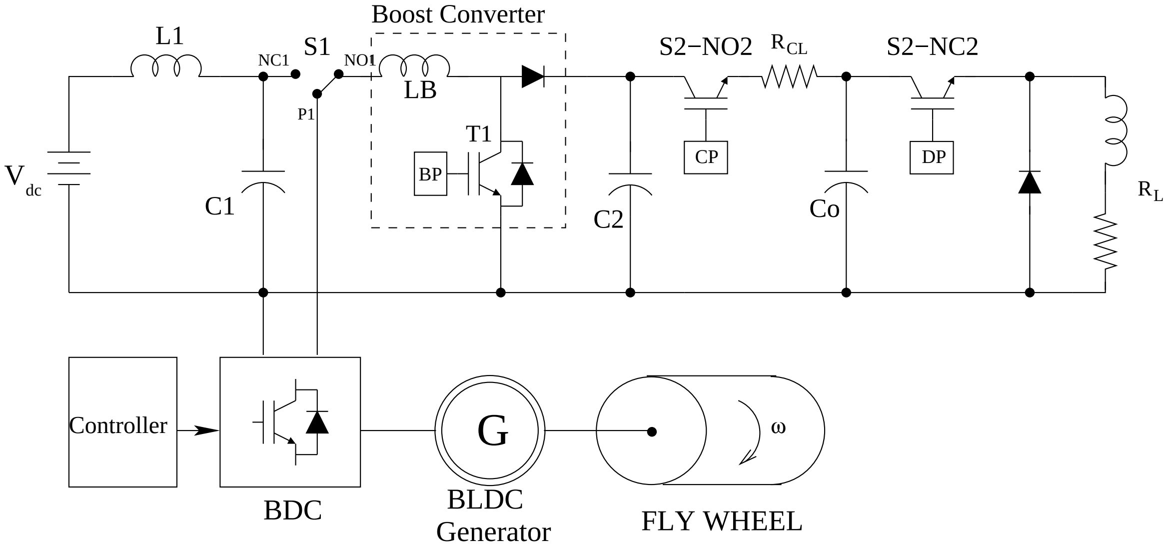

Figure 7.10: Block diagram of the Flywheel based CCPS

7.9.1 Testing with Resistive Load

The voltage and current waveforms obtained from prototype system are viewed in a storage oscilloscope are recorded. These waveforms are reproduced in the Fig. 7.11(a) and Fig. 7.11(b). It may be noted in the waveforms that the output capacitor was charged within 1.0 millisecond and is able supply to the load resistor the required current of 1400 Amps .

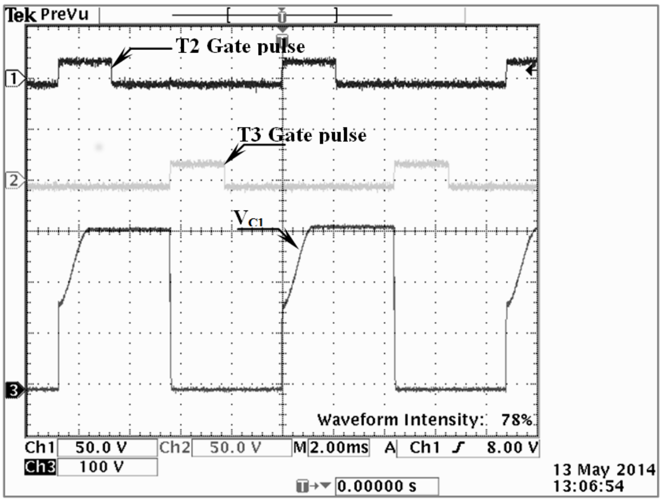

(a) Gate pulse and capcitor voltage

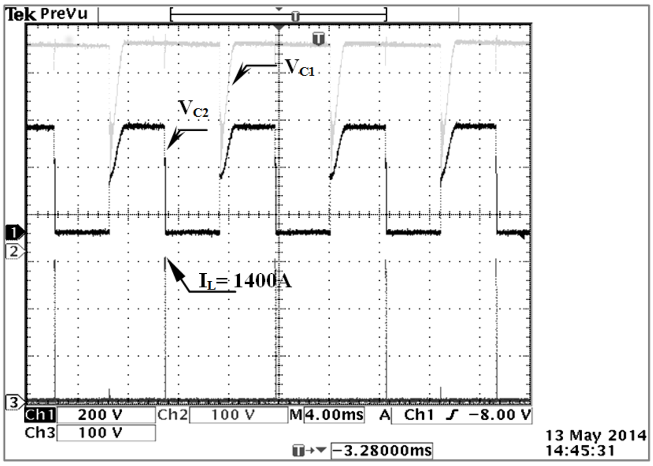

(b) capacitor charging, discharging and discharge current

Figure 7.11: Control pulses, voltage and current waveforms at resistive load recorded in DSO

7.9.2 Testing with Inductive Load

Testing of above systems was carried out using an inductive coil as the load. This coil was used for creating inward force on a thin hollow cylinder made up of aluminium. An energy of 2000 Joules was used (V_c =400V, C_o =27,000 μF). Capacitor voltage and load current waveforms are recorded and reproduced in Fig. 7.12(a) and (b). It is clear from the waveforms that the system was able to charge the output capacitor (value: 27000 μF) to a voltage of 360 V within 2.0 seconds and is able supply to the load resistor the required current of 2300 Amps.

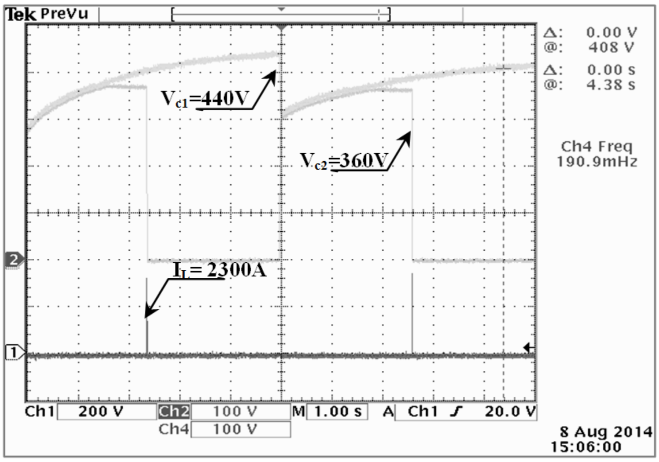

(a) Gate pulse and capcitor voltage

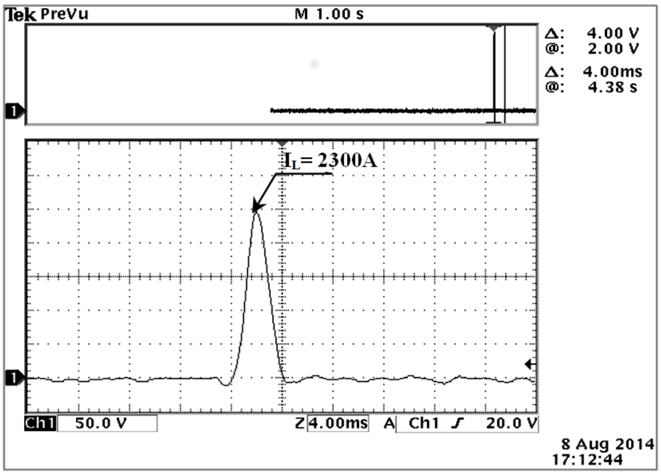

(b) Peak current wave forms at Vdc = 100V

Figure 7.12: Control pulses, voltage and current waveforms at inductive load recorded in DSO

7.10 Summary

The proposed system is analyzed, design equations are presented and the system is simulated using SIMULINK software. The system is designed using the derived design equations, simulated, built, and tested using simulated loads. System worked perfectly as per the design. It may be noted that several FES systems can be connected in parallel to the dc bus conveniently to get higher amount of energy. Round trip efficiency of the overall system can be improved by going for low loss hybrid bearing or non-contact type of bearing for the moving parts. Testing was carried out with a load voltage of 400 V DC, and pulse current of 2300 A with a dummy inductive coil . SIMULINK simulation results, the analytically predicted lines are in good agreement with the experimental results.

Chapter 8

Conclusions and future work

Consciousness on the environmental pollution, increasing energy demand and consequences of climate change has inspired the researcheers to explore the new designs of efficient energy storage systems to conserve the existing energy resources. This has reslulted in shifting the focus on the research work on the area of efficiency improvement of storage devices. The present work focuses on the analysis of the issues related to the design and operation of an efficient Flywheel Energy Storage system and thus save the energy.

8.1 The present work

To begin with the literature survey was done. The literature survey gives the overview of the research work carried out globally. Design challenges involved in various sub systems used in the FESS are highlighted. Design of an FESS for a given specifications was carried out. Based on this design one prototype FESS was built and tested to find out the performance parameters. It is shown that how efficiency and harvestable energy from an FESS can be improved by proper selection and design of various related subsystems used in an FESS. Dependency of harvestable energy from a flywheel on the boost converter gain, source resistance, current dependent losses of the generator has been shown and modelling of various losses in the system was carried out. Loss reduction techniques and novel topology for enhancing the harvested energy are devised to achieve improved efficiency and increased harvested energy from a given flywheel. Building an FESS involves the selection of proper electrical machine and appropriate power converter topology used in the system. Selection criteria of the machine and design procedure of power converter are discussed.

Desired features of an ideal FESS are high reliability, low cost and small size apart from simplicity of structure, ease of control and high energy efficiency. The machine is required to deliver the rated power only for a short time during acceleration and braking. Majority of the time it will be idling only (intermittent duty). Therefore, a low loss, short time rated two-quadrant Permanent Magnet machine is the best choice for this application. From the analysis it is found that the serious limitation of this system is the dependency of boost converter voltage gain (in turn energy extracted from a flywheel for a given top speed) on the losses in the machine at higher armature currents. Apportioning and analysis of various losses in an FESS and mitigation techniques are covered in this work. From the analysis of experimental test results it is found out that the drag loss in the flywheel and eddy current losses in the machine are dominant at higher speeds. In the experimental setup built these losses are measured as 72% and 18% respectively at a speed of 15000 RPM. Providing a vacuum enclosure for rotating parts and usage of two-pole machine will improve the efficiency of the system. Input current increases at lower flywheel speed leading to higher switching loss in the boost converter. This is reduced by adopting a newly developed topology which uses novel ZVT/ZCT switching technique. It has been shown through experimental results that by adopting this technique there is a saving of power to the extent of 1.5% to 2.6% resulting in an increase of the backup time from 60 seconds to 62.5 seconds.

From the equivalent circuit and the FEM analysis of the machine it is found that the armature current dependent eddy current losses in the core of the machine appear as a resistance in series with generator. Decreasing this resistance leads to the increase of harvestable energy from the flywheel. This can be achieved by selecting a PM-BLDC machine with longer air gap, higher tooth width and thinner stator stampings. Usage of Nickel Iron as stator core material will also reduce the current dependent eddy current loss and help in increasing the harvested energy from the flywheel. Circuit analysis and the experimental results show that for a given BLDC machine a two- stage boost converter will draw lesser peak current from the generator as compared to that of single-stage boost converter for delivering the same output power. From the simulation results it is found out that the input current drawn is 400 A if SSBC is used and it is 70 A if TSBC is used for the same output power. It is also found out from experimental results that maximum voltage gain achieved are 1.34 in case of SSBC and 5.46 in case of TSBC at a output power of 4.0 kW load. Hence two-stage boost converter is a better choice as compared to single stage boost converter for FES applications.
Going through the analysis and experimental results it was strongly felt the need to explore new methods for the enhancement of the harvested energy from a flywheel. New scheme called DWBC which uses a novel unique combination of dual armature winding permanent magnet brushless dc machine and a buck converter has been devised and shown that the harvestd energy can be enhanced. From the experimental results obtained from the prototype scheme it has been shown that the harvestable energy is increased by about 20% percentage as compared to existing schemes. Harvested energy can befurther improved by increasing $K-factor$. But increasing the $K-factor$ also increases the voltage stress on the buck converter (chopper device). Another two novel schemes called Multi Winding Single Chopper and Multi Winding Multi Chopper are developed to enhance the harvested energy without increase of voltage stress on converter chopper device.

8.2 Scope for the future work

Future work can be focussed on the general theme of FESS on a few different areas like enhancement of the harvested energy, compactness and modularity of the system. Deployment of this system for the application like, transportation, grid power leveling calls for coordination among multi-discipline groups and the system. Usage of low maintenance cost vacuum system and contactless bearings (magnetic bearings) are the key factors for the improvement of overall efficiency of the system.

8.3 Applications of FESS

The FESS which is developed can be used as an UPS where short support time is required. This will be useful for the installations where the power is backed up with diesel generators. This bi-directional converter along with the BLDC machine can be directly used in hybrid vehicles and material handling equipments to improve their performance in terms of energy efficiency and environmental pollution. With some modifications in the control circuit and software, the FESS explained in this thesis can be used for charging the large capacitor banks which is used for pulse power sources.

Appendix A

Computation of various parameter and design approch

Computation of average value of dc voltage, dc current during the power backup period are carried out here. This is required for selecting the power converter devices and optimizing the size of BLDC generator.
Variation of generator voltage and generator current as a function of time (during the energy extraction at constant power from the flywheel) are shown in Fig. A.1

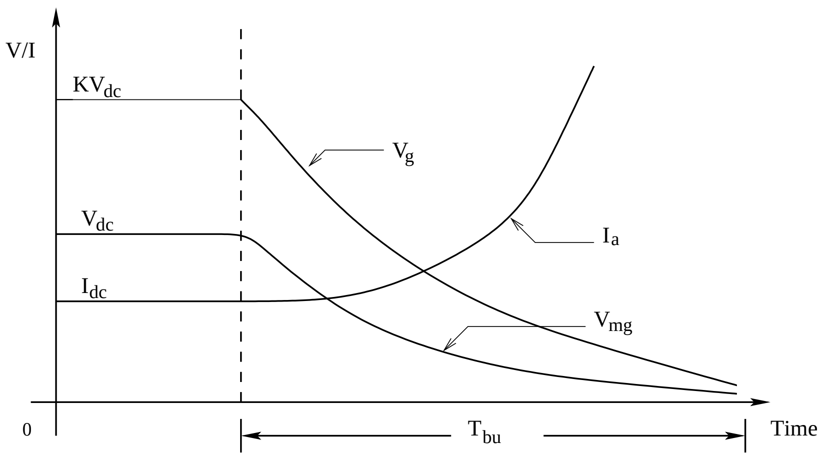

Figure A.1: Variation of generator voltage and current as a function of time

A.1 Computation of average of induced voltage, load current and generated power

Assume $K - factor = 2$

Average Voltage

$$V_{dc(ave)} = \frac{1}{T_{bu}} \int_0^{T_{bu}} 3V_{dc}\ e^{\frac{-t}{T_{bu}}} dt \tag{A.1}$$

$$V_{dc(ave)} = 1.90V_{dc} \tag{A.2}$$

Average armature current (De-rating of the machine)

$$I_{dc(ave)} = \int_0^{T_{bu}} \frac{I_{dc}}{3}\ e^{\frac{+t}{T_{bu}}} dt \left[\frac{1}{T_{bu}}\right] \tag{A.3}$$

$$I_{dc(ave)} = 0.57 I_{dc} \tag{A.4}$$

Average dc Power (Size of the machine)

$$P = v(t) \times i(t) \tag{A.5}$$

$$v(t) = 3V_{dc}\ e^{\frac{-t}{T_{bu}}} \tag{A.6}$$

$$i(t) = \left(\frac{I_{dc}}{3}\right)\ e^{\frac{+t}{T_{bu}}} \tag{A.7}$$

$$P_o = V_{dc} \times I_{dc} \tag{A.8}$$

Armature coil current (Arm Conductor cross section) RMS value of current the current is given by

$$I_{aRMS} = \frac{\sqrt{\frac{2}{3}} P_{av}}{\eta V_{dc}} \tag{A.9}$$

A.2 Power loss in the machine and chopper device

Switching loss

Switching loss in the device can be computed using the following equation

$$P_{sw} = \left(\frac{V_{dc} I_{dc}}{6}\right)\left(\frac{t_s}{T}\right) \tag{A.10}$$

Assuming CCM (and the dc bus current to be constant) of the chopper circuit, with the device current equal to that of inductor current we get

Start of energy harvesting

$$P_{sw1} = \left(\frac{(K+1) \times V_{dc} I_{dc}}{6}\right)\left(\frac{t_s}{T}\right) \tag{A.11}$$

End of energy harvesting

$$P_{sw2} = \left(\frac{(V_{dc} I_{dc}}{6}\right)\left(\frac{t_s}{T}\right) \tag{A.12}$$

Conduction loss

Device

$$P_{c1} = V_{CE} \times I_{Cave} \tag{A.13}$$

$$= 2.0 \times 0.573 I_{dc} \tag{A.14}$$

$$= 1.146 I_{dc} \tag{A.15}$$

Armature conductor

$$P_{c2} = (I_{aRMS}^2) \times R_a \tag{A.16}$$

A.3 Selection of BLDC machine and semiconductor device

BLDC machine

It may please be noted there are two sets of armature windngs in the BLDC machine proposed. One is main winding and the other one is auxiliary winding. The an auxiliary windng has K times number of turns as compared to number of turns of main winding. This results in the total number of turns of the armature winding getting increased to $(K+1)$ and the vaue of leakage inductance increasing to $(K+1)^2$ times the original value in the generating mode. This helps in limiting the machine and power converter current in generating mode of operation. In an ideal energy harvesting system, the machine should have low inductance in motoring mode and high inductance in generating mode of operation.

Selection of BLDC machine and devices

Dimensions

Idealised design equations relating the machine output power to the mechanical dimensions is given by

$$P_o = \frac{\pi^2 B J D_m^2 L N_r \eta}{60} \tag{A.17}$$

Substituting the design parameters in the above equation we get $D_m^2 L = 338e^{-6} m^3$; If L and D are in same magnitude , then we have $L = 70mm, D_m = 70mm$. Nearest dimensions of the standard available frame is $L = 75mm, D_m = 86mm$.

$$V_{mg} = V_{dc}; V_g = K V_{dc} \tag{A.18}$$

A suitable magnet of dimensions $12mm \times 18mm$ is selected for the permanent magnets.

Value of K

Substituting the $\omega_{min} = 0.33\ \omega_{max}$ in (6.12), we get $K = 2$.

Cross section of armature conductors

M winding
(Continuous rating)

$$\alpha_{mg} = \frac{I_{aRMS}}{CurrentDensity} \tag{A.19}$$

G winding
(Short time rating: can be thin conductors)

$$\alpha_{g} = \frac{I_{aRMS}}{2 \times CurrentDensity} \tag{A.20}$$

No of turns

M winding

$$T_{mg} = \frac{60KV_{dc}}{2BL\frac{\pi D_m}{4}(4N_r)} \tag{A.21}$$

G winding

$$T_{g} = \frac{60KV_{dc}}{2BL\frac{\pi D_m}{4}(4N_r)} \tag{A.22}$$

Semiconductor devices

Selection of Semiconductor devices [82, 83]

Voltage and current rating of chopper device

$$V_{CE} = K \times V_{dc} \tag{A.23}$$

$$I_C = I_{dc} \tag{A.24}$$

Voltage and current rating of BDC

$$V_{CE} = V_{dc} \tag{A.25}$$

$$I_C = I_{dc} \tag{A.26}$$

Rectifier

$$V_{AK} = K \times V_{dc} \tag{A.27}$$

$$I_A = I_{dc} \tag{A.28}$$

Coupling diodes

$$V_{AK} = V_{dc} \tag{A.29}$$

$$I_A = I_{dc} \tag{A.30}$$

Appendix B

Speed Variation of flywheel as a function of time

Power balance equation in generating mode can be written as given below:

Generated power = Loss Power + Output power

$$J\omega\frac{d\omega}{dt} = P_o + C_1\omega + C_2\omega^2 + P_{Loss(E)} \tag{B.1}$$

$$\frac{J\omega}{P_o + C_1\omega + C_2\omega^2}d\omega = dt \tag{B.2}$$

$P_o + C_1\omega + C_2\omega^2$ can be written as $(\omega - K_1)(\omega - K_2)$ where

$$K_2, K_1 = \frac{-C_1 \pm \sqrt{C_1^2 - 4C_2P_0 + P_{Loss(E)}}}{2C_2} \tag{B.3}$$

Equation B.2 becomes

$$\frac{J\omega}{(\omega - K_1)(\omega - K_2)}d\omega = dt \tag{B.4}$$

Partial fraction:

$$\frac{\omega}{(\omega - K_1)(\omega - K_2)} = \frac{A}{(\omega - K_1)} + \frac{B}{(\omega - K_2)} \tag{B.5}$$

$$A = \left[\frac{\omega}{\omega - K_2}\right]_{\omega=K_1} = \left[\frac{K_1}{K_1 - K_2}\right] \tag{B.6}$$

$$B = \left[\frac{\omega}{\omega - K_1}\right]_{\omega=K_2} = \left[\frac{K_2}{K_2 - K_1}\right] \tag{B.7}$$

Equation B.4 can be rewritten as

$$J\left[\frac{A}{\omega - K_1} + \frac{B}{\omega - K_2}\right]dw = dt \tag{B.8}$$

$$J\int\frac{A}{\omega - K_1}dw + J\int\frac{B}{\omega - K_1}dw = \int dt \tag{B.9}$$

i.e.

$$[A\ln(\omega - K_1) + B\ln(\omega - K_2)] = \frac{t}{J} + \frac{K_3}{J} \tag{B.10}$$

Assuming A = - B equation B.10 becomes

$$\ln\left[\frac{\omega - K_1}{\omega - K_2}\right] = \frac{t}{AJ} + \frac{K_3}{AJ} \tag{B.11}$$

$$\left[\frac{\omega - K_1}{\omega - K_2}\right] = e^{\left[\frac{t}{AJ} + \frac{K_3}{AJ}\right]} \tag{B.12}$$

$$\left[\frac{\omega - K_2}{\omega - K_1}\right] = e^{-\left[\frac{t}{AJ} + \frac{K_3}{AJ}\right]} \tag{B.13}$$

With $K_2 = -K_1$

$$\left[\frac{\omega + K_1}{\omega - K_1}\right] = e^{-(T)} \tag{B.14}$$

We know that

$$\frac{a}{b} = \frac{a+b}{a-b} \tag{B.15}$$

Then equation (B.14) becomes

$$\frac{2\omega}{\omega - K_1 - \omega - K_1} = \frac{1 + e^{-T}}{1 - e^{-T}} \tag{B.16}$$

Boundary conditions at :
t = ∞
$\omega = K_1$

Appendix C

Photograph of the prototype system built

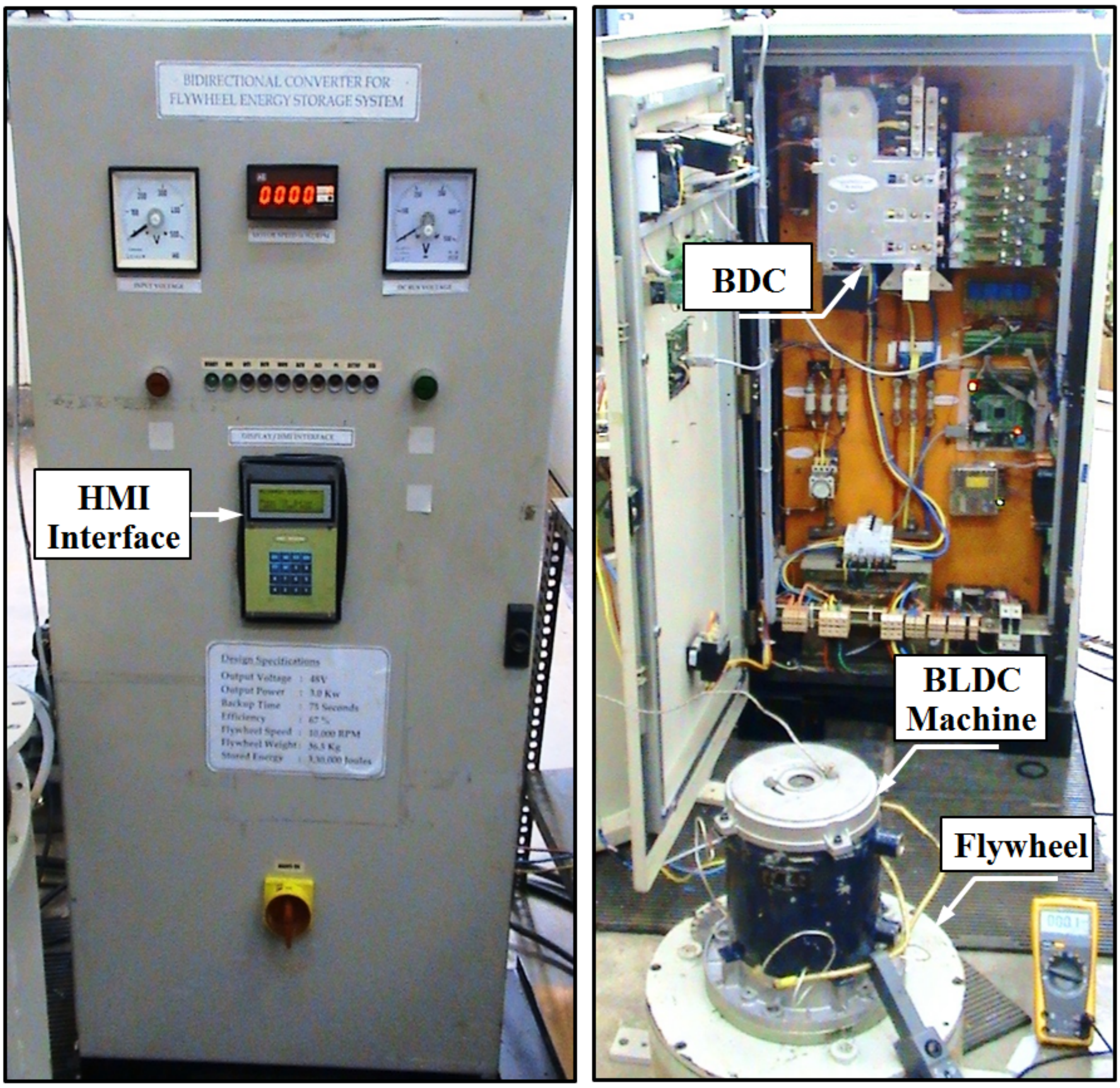

Figure C.1: Experimental test setup of proto type FES system

.

Figure C.2: Arrangement of power and control components in the panel

Figure C.3: Flywheel and BLDC machine assembly

Figure C.4: Experiment readings and waveforms

.

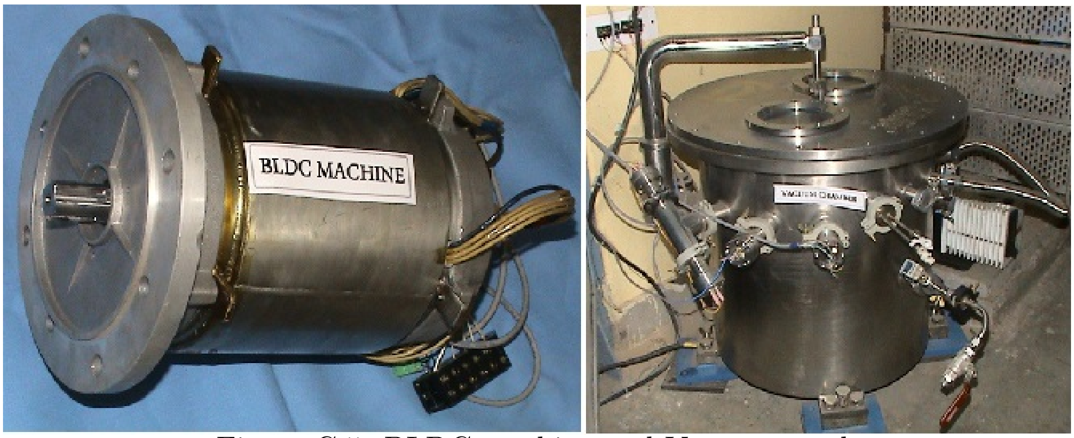

Figure C.5: BLDC machine and Vacumm enclosure

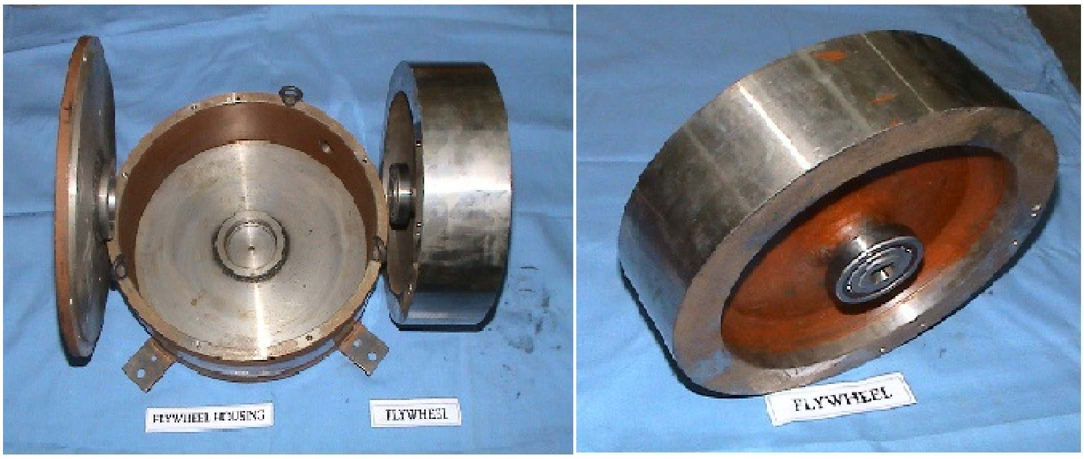

Figure C.6: Flywheel Disc and its housing arrangement

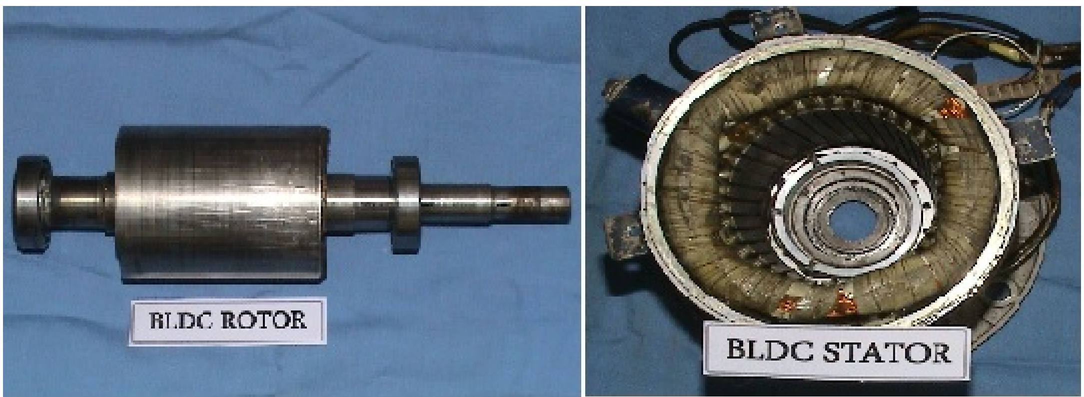

Figure C.7: Rotor and Status assemblies

Appendix D

Specifications of Semiconductors

Digital Signal Processor(Motorola DSP56F805)

DSP Core

- 16-bit DSP engine with dual Harvard architecture
- 40 MIPS at 80 MHz core frequency
- Efficient C compiler and local variable supportBackup time: 30 seconds
- JTAG/OnCE debug programming interface

Memory

- 32K, 16 bit words of Program Flash
- 512, 16 bit words of Program RAM
- 4K, 16 bit words of Data Flash
- 2K, 16 bit words of Data RAM
- 64K, 16 bits of Data memory
- 64K, 16 bits of Program memory

Peripheral Circuit

- 12 bit ADC
- Two Quadrature Decoders
- Two General purpose Quad Timers
- CAN 2.0 Module
- 14 Dedicated General Purpose I/O
- Two Serial Communication Interface
- Serial Peripheral interface

Insulated Gate Bipolar Transistor(IGBT)

Mak	: Semikron
Model	: SKM200GB125D
V_{CES}	: 1200 V
I_C	: 200 A
V_{GES}	: $\pm$ 20 V
V_{CESat}	: 3.3 V
$t_{d(on)}$	: 75 ns
t_r	: 36 ns
$t_{d(off)}$	: 420 ns
t_f	: 25 ns

Silicon Controlled Rectifier(SCR)

Make	: NTE
Model	: 5380
V_{RRM}	: 800 V
$I_{T(AV)}$	: 130 A
$I_{T(RMS)}$	: 690 A
I_t^2	: 120 KA^2
$t_{q(ff)}$	: 10-20 μ s

Hall Effect Posistion Sensor

Make	: Honeywell
Model	: SS413A
Type	: Bi-polar
Supply V	: 3.8 - 30 V
Supply I	: 10 mA
Output V	: 40 V
Output I	: 20 mA
t_r	: 0.05 μs
t_f	: 0.15 μs

Appendix E

Cost benefit analysis of adopting an FESS

Applications of FESS include automobiles, locomotives, energy storage system etc. It is required to estimate the cost benefit derived by adopting the FESS in a given application. As an example, cost benefits analysis is done here for following two sample applications:

- Regenerative braking in a transport application
- Batteryless Uninterruptible Power Supplies

E.1 Regenerative braking in a transport application

If this system is used for harvesting kinetic energy as a part of regenerative braking then whatever quantity of energy is harvested is the net saving. The total cost can be divided into two parts as given below:

E 1.1 Installation cost

The applications like locomotives and electric vehicles, where BLDC machine is a part of the existing rotating system this system can be used for regenerative braking. Following additional modules are required to implement the regenerative braking in a vehicle of rating is 200.0 kW (Assuming 500 V dc, 400 A):

1. BLDC machine (500 V, 200 A) - 1no.
2. Bidirectional converter (500 V, 200 A) – 2nos.
3. Storage device (6200 kJ, High speed Flywheel) along with controller – 1no.

A typical, 200kW locomotive drive would consist of one BLDC machine and a drive of 200.0 kW along with an electronic controller. Extra cost of the above listed additional modules is approximately US$ 30,3000 (Rs. 20,00,000/-)

E 1.2 Revenue cost

Three phases of a typical vehicle drive cycle are depicted in Fig. E.1. They are the acceleration phase, constant speed phase and deceleration phase (braking).

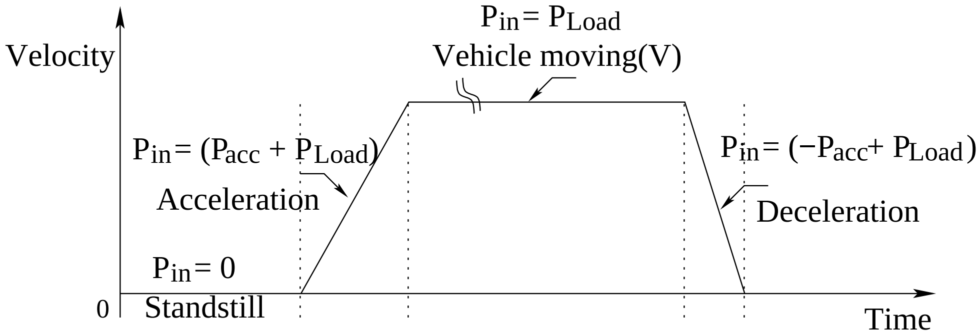

Figure E.1: Various phases of typical drive cycle

E 1.3 Assumptions made for simplifying the analysis:

1. Ideal case (100% of the stored energy is recovered during braking).
2. Specifications of a Volvo bus model: 9400XL coach are used for computation of energy saving. Cost of this vehicle is US$ 1,80,000 (Rs.1,20,00,000).
3. Vehicle moves with a maximum speed of 100 km per hour.
4. Cost of diesel is US$ 0.75 per litre (Rs.50/- per litre).
5. The vehicle (with 200 kW motor) covers 200 km in a day with 100 stops/starts with 30 seconds of acceleration (acceleration phase) and 60 seconds of braking time (deceleration phase).
6. Values taken from the data sheets: Calorific value of diesel = 36.9x106 Joules per litre of diesel; Thermal efficiency of the IC Engine = 0.3.

With the proposed energy harvesting system an energy saving of 6200 kJ is achieved, which is equivalent to 56 litres of diesel. Additional cost involved to implement the new system proposed by us is approximately US$ 30,300 which is around 16% of the cost of the vehicle and it can be recovered in 2.0 years of time whereas the overall life span of the storage system is 10 – 15years. Additional cost involved to incorporate the proposed system into an existing vehicle is expected to be around 10-15% of the cost of the vehicle which can be recovered in about 2 years of time.

E.2 Uninterruptible Power Supplies

E 2.1 Assumptions:

1. Main competitor for FESS is lead acid battery. Hence cost comparison is done with lead acid battery based UPS.

2. Life span of FESS is around 15 years and that of lead acid battery is 5 years.

3. Specifications of typical system:

Output voltage	: 500 Vdc
Output power	: 10 kW
Backup time	: 45 s
Efficiency	: 0.75%
Battery de-rating factor	: 0.05

E 2.2 Cost estimation of systems:

If V_{ave} is the average voltage of each cell (1.9 V) and N (150) is the number of cells required $I_{dc} = \frac{P_o}{V_{ave}N} = 20A$.

Ampere hour capacity of the battery is Ah $= \left(\frac{20X45}{60X60}\right) = 5Ah$.

Table E.1: Cost comparision between Battery based and FES System

Sub system	Battery based system cost in Lakhs	Flywheel based system cost in Lakhs
Power converter	1.0	1.0
Storage system	0.6	2.4
Total initial cost (5 years)	1.6	3.4
Cost for 15 years	3.4	3.4

Initial cost of FES system is higher compared to battery based system. It can be seen from the table that the cost of the flywheel based system is equal to that of battery based system for a period of 15 years.

Bibliography

[1] R. Cardenas, R. Pena, M. Perez and J. Clare, "Power smoothing using a flywheel driven by a switched reluctance machine", *IEEE Trans. Ind. Electron.*, vol. 53, no. 4, pp. 1086–1093, August 2006.

[2] G. O. Suvire and P. E. Mercado:"Combined control of distribution static synchronous compensator/flywheel energy storage system for wind energy applications", *IET Gener. Transm. Distib.*, vol. 6, no. 6, pp. 483–492, June 2012.

[3] S. M. Lukic, J. Cao, R. C. Bansal, F. Rodriguez and A. Emadi,"Energy Storage System for Automotive Applications," *IEEE Trans. on Ind. Electron.*, vol. 55, no. 6, pp. 2258-2267, June 2008.

[4] G. O. Cimuca, C. Saudemont, B. Robyns and M. M. Radulescu,"Control and Performance Evaluation of a Flywheel Energy-Storage System Associated to a Variable-Speed Wind Generator," *IEEE Trans. Ind. Electron.*, vol.53, no.4, pp. 1074-1085, August 2006.

[5] D. W. Swett and J. G. Blanche IV, "FLYWHEEL CHARGING MODULE FOR ENERGY STORAGE USED IN ELECTROMAGNETIC AIRCRAFT LAUNCH SYSTEM," *IEEE Trans. Magnetic.*, vol.41, Iss.1, pp.525-528, January 2005.

[6] Z. Jiancheng, H. Lipei, C. Zhiye and W. Su, "Research on Flywheel Energy Storage System for Power Quality," in Proc IEEE Int. Power System Technology Conf.,vol. 1, pp. 496-499, October 2002.

[7] J. D. Park, C. Kalev and H. F. Hofmann, "Control of high-speed solid-rotor synchronous reluctance motor/generator for flywheel-based uninterruptable power supplies," *IEEE Trans. on Ind. Electron.*, vol. 55, no. 8, pp. 3038-3046, August 2008.

[8] J. G. Bitterly, "FLYWHEEL TECHNOLOGY PAST, PRESENT, AND 21ST CENTURY PROJECTIONS", *32^{nd} Intersociety Energy Conversion Engineering Conference, IECEC-97*, 27 July- 1 August 1997.

[9] S. Samineni, "Modeling and Analysis of a Flywheel Energy Storage System for Voltage Sag Correction". M.Sc (Engg) thesis, College of Graduate Studies University of Idaho, December 2003.

[10] A. Stodola, Steam and C. Jas "Turbines", McGraw-Hill Book Company, Inc., 1927

[11] "Flywheels" By Chris Woodford, Last Updated on September 19, 2014, URL Link http://www.explainthatstuff.com/flywheels.html.

[12] M. K. Yoong, Y. H. Gan, G. D. Gan, C. K. Leong, Z. Y. Phuan, B. K. Cheah and K. W. Chew, "Studies of Regenerative Braking in Electric Vehicle", Proc. of the 2010 *IEEE Conference on Sustainable Utilization and Development in Engineering and Technology.*, Faculty of Engineering, Kuala Lumpur, Malaysia, pp. 40-45, 20-21th November 2010.

[13] A. W. Ballard and S. Yarbrough,"SAFETY-RELATED MAINTENANCE OF EXPLOSION PROOF ENCLOSURES FOR CLASS I, HAZARDOUS LOCATIONS "Copyright Material IEEE Paper No. PCIC-90-9

[14] R. E. Horner, N. J. Proud, "The key factors in the design and construction of advanced Flywheel Energy Storage Systems and their applications to improve telecommunication power back up," *IEEE.* pp.668-674, April 1996.

[15] L. Bakay, M. Dubois, P. Viarouge and J. Ruel, " LOSSES IN HYBRID AND ACTIVE MAGNETIC BEARINGS APPLIED TO LONG TERM FLYWHEEL ENERGY STORAGE," *5th IET International Conference on Power Electronics, Machines and Drives (PEMD 2010)*, 19-21th April 2010.

[16] I. Takahashi, K. Ammei and Y. Itoh, "High Performance and Long Life Uninterruptable Power Source Using a Flywheel Energy Storage Unit," *Conference Record of IEEE Industry Applications Society.*, pp. 1049-1055, vol.2, October 1990.

[17] T. Coombs, A. M. Campbel, R. Storey and R. Weller, " Superconducting Magnetic Bearings for Energy Storage Flywheels," *IEEE Trans. on Applied Superconductivity*, vol. 9, no. 2, pp. 968-971, June 1999.

[18] W. L. Niemeyer, P. Studer, J. A. Kirk, D. K. Anand and R. B. Zmood, "A HIGH EFFICIENCY MOTOR/GENRATOR FOR MAGNETICALLY SUSPENDED FLYWHEEL ENERGY STORAGE SYSTEM " *24th Intersociety Energy Conversion Engineering Conference, IECEC-89* 6-11th August 1989.

[19] S. R. Gurumurthy, "Bi-directional converter for FES Applications", M Sc(Engg) Thesis, Indian Institute Science, Bangalore, 2006.

[20] P. P. Acarnley, B. C. Mecrow, J. S. Burdess, J. N. Fawcett, J.G. Kelly and P.G. Dickinson,"Design principles for a flywheel energy store for road vehicles", *IEEE Trans. Ind. Appl.*, vol. 32, no. 6, pp. 672–678, Nov/Dec 1996.

[21] K. T. Chau, C. C. Chan and C. Liu,"Overview of permanent-magnet brushless drives for electric and hybrid electric vehicles", *IEEE Trans. on Ind. Electron.*, vol. 55, no. 6, pp. 2246–2257, June 2008.

[22] H. Fan, K. Chau, C. Liu and C. Chan,"Quantitative comparison of permanent magnet linear machines for ropeless elevator ", *IEEE International Magnetics Conference (INTERMAG)*, 11-15th May 2015.

[23] L. Wang, J. Y. Yu and Y. T. Chen, "Dynamic stability improvement of an integrated offshore wind and marine-current farm using a flywheel energy-storage system", *IET Renew. Power Gener.*, vol. 5, no. 5, pp. 387–396, 2011.

[24] J. Goncalves de Oliveira, H. Schettino, V. Gama and R. Carvalho, "Study on a doubly-fed flywheel machine-based driveline with an AC/DC/AC converter", *IET Electr. Syst. Transp.*, vo. 2, no. 2, pp. 51–57, June 2012.

[25] H. W. Lee and M. Ehsani, "Practical Control for Improving Power Density and Efficiency of the BLDC Generator," *IEEE Trans. Power Electron.*, vol. 20, no. 1, pp. 192-199, January 2005.

[26] A. Sathyan, N. Milivojevic, Y. J. Lee, M. Krishnamurthy and A. Emadi, "An FPGA-Based Novel Digital PWM Control Scheme for BLDC Motor Drives," *IEEE Trans. Ind. Electron.*, vol. 56, no.8, pp. 3040–3049, August 2009.

[27] N. Milivojevic, M. Krishnamurthy, A. Sathyan,Y. J. Lee and A. Emadi, "Stability Analysis of FPGA-Based Control of Brushless DC Motors and Generators Using Digital PWM Technique," *IEEE Trans. Ind. Electron.*, vol. 59, no.1, pp. 33–351, January 2012.

[28] G. H. Jang and C. I. Lee, "Dual Winding Method of a BLDC Motor for Large Starting Torque and High Speed," *IEEE Trans. Magnetics.*, vol. 41, no. 10, pp. 3922–3924, October 2005.

[29] Z. Zhang, Y. Yan, S. Yang and Z. Bo, "Development of a New Permanent-Magnet BLDC Generator Using 12-Phase Half-Wave Rectifier," *IEEE Trans. Ind. Electron.*, vol. 56, no.6, pp. 2023–2029, June 2009.

[30] Z. Chen and X. Liu, "A 2MW 6-phase BLDC Generator Developed from a PM Synchronous Generator for Wind Energy Application," 2014 *IEEE International Conference on Industrial Technology(ICIT).*, Busan, Korea, pp. 110 - 114, February 26 – March 1, 2014.

[31] US Patent No.: US 7,710,081 B2, D. M. Saban, R. H. Ahmad and Z. Pan, " Electromechanical Energy Conversion Systems," Date of Patent: May 4, 2010.

[32] S. R. Gurumurthy, V. Ramanarayanan and M. R. Srikanthan,"Design and evaluation of a DSP controlled BLDC drive for flywheel energy storage system". National Power Electronics Conf., India, pp. 146–151, 22–24 December 2005.

[33] W. R. Erickson and D. Maksimovie, "Fundamentals of Power Electronics", Second Edition, Published by Springer (India) Pvt Ltd., Rashtriya Printer, Delhi, India, fifth Indian reprint 2011.

[34] S. R. Gurumurthy, V. Agarwal and A. Sharma, "Optimal energy harvesting from a high-speed brushless DC generator-based flywheel energy storage system," *IET Electr. Power Appl.*, vol. 7, Iss. 9, pp. 693–700, November 2013.

[35] C. T. Pan, T. Y. Chang and E. Fang, "A Novel Single Stage Step Up/Down AC/DC Converter for Small BLDC Wind Power Generators," *Proc. IEEE, PEDS 2011.*, Singapore, pp. 861–866, 5-8 December 2011.

[36] R. Hebner, J. Beno and A. Walls, "Flywheel batteries come around again," *IEEE Sprctro.*, vol. 39, no. 4, pp. 46-51, April 2002.

[37] S. R. Gurumurthy, V. Agarwal and A. Sharma, "Apportioning and Mitigation of losses in a Flywheel Energy Storage system," in Conference Proc. *IEEE PEDG 2013*, July 2013.

[38] H. Mao, F. C. Lee, X. Zhou and D. Boroyevich, "Improved zero-current transition converters for high power applications," *IEEE Trans. Ind. Applications*, vol. 33, no. 5, pp. 1220–1232, Sept./Oct. 1997.

[39] L. Solero, D. Borpyevich, Y. P. Li and F. C. Lee "Design of resonant circuit for zero current transition techniques in 100kW PEBB applications," *IEEE Trans. Ind. Appl.*, vol. 39, no. 6, pp. 1783–1794, Nov./Dec. 2003.

[40] Y. Li and F. C. Lee, "A comparative study of a family of zero-current transition schemes for three-phase inverter applications," in *Proc. IEEE, APEC.*, pp. 1158–1164, 2001.

[41] H. Bodur and A. F. Bakan,"An Improved ZCT-PWM DC-DC Converter for High-Power and Frequency Applications," *IEEE Trans. Ind. Electron.*, vol.51, no.1, pp. 89- 95, February 2004.

[42] W. McMurray, "Resonant Snubber with Auxiliary Switches," *IEEE Trans. Ind. Appl*, vol. 29, No. 2, pp. 355–362, March/April 1993.

[43] H. F. Xiao, X. P. Liu and K. Lan, "Zero-Voltage-Transition Full-Bridge Topologies for Transformerless Photovoltaic Grid-Connected Inverter," *IEEE Trans. Ind. Electron.*, vol. 61, no. 10, pp. 5393-5401, October 2014.

[44] S. Dusmez, A. Khaligh and A. Hasanzadeh, "A Zero-Voltage-Transition Bidirectional DC/DC Converters," *IEEE Trans. Ind. Electron.*, vol. 62, no. 5, pp. 3152–3162, May 2015.

[45] M. R. Mohammadi and H. Farzanehfard, "New Family of Zero- Voltage Transition PWM Bidirectional Converters With Coupled Inductors," *IEEE Trans. Ind. Electron.*, vol. 59, no. 2, pp. 912–919, February 2012.

[46] G. Chen, Y. S. Lee, S. Y. R. Hui, D. Xu and Y. Wang, "Actively Clamped Bidirectional Flyback Converter', *IEEE Trans. Ind. Electron.*, vol. 47, no. 4, pp. 770-779, August 2000.

[47] S. S. Lee, S. W. Choi and G. W. Moon, "High-Efficiency Active-Clamp Forward Converter With Transient Current Build-Up (TCB) ZVS Technique," *IEEE Trans. Ind. Electron.*, vol. 54, no. 1, pp. 310–318, February 2007.

[48] W. Li and X. He, "Review of Non-isolated High Step-Up DC/DC Converters in Photovoltaic Grid-Connected Applications," *IEEE Trans. Ind. Electron.*, vol. 58, no. 4, pp. 1239–1250, April 2011.

[49] H. Li, F. Z. Peng and J. S. Lawler, "A Natural ZVS High-Power Bidirectional DC-DC Converter with Minimum Number of Devices," *IEEE Trans. Ind. Appl.*, vol. 39, Issue. 2, pp. 525-535, March 2003.

[50] A. Mousavi, M. Pahlevaninezhad, P. Das and P. Jain,"ZCS PWM Bidirectional DC-DC Converter with One Auxillary switch," Energy Conversion Congress and Exposition(ECCE), IEEE, pp. 1175-1180, September 2011.

[51] K. Jin and X. Ruan, "Hybrid Full-Bridge Three-Level LLC Resonant Converter- A Novel DC–DC Converter Suitable for Fuel-Cell Power System," *IEEE Trans. Ind. Electron.*, vol. 53, no. 5, pp. 1492–1503, October 2006.

[52] F. Zhang and Y. Yan, "Novel Forward–Flyback Hybrid Bidirectional DC–DC Converter', *IEEE Trans. Ind. Electron.*, vol. 56, no. 5, pp. 1578–1584, May 2009.

[53] J. L. Russi, V. F. Montagner, M. L. S. Martins and H. L. Hey, "A Simple Approach to Detect ZVT and Determine Its Time of Occurrence for PWM Converters," *IEEE Trans. Ind. Electron.*, vol. 60, no. 7, pp. 2576–2585, July 2013.

[54] F. Caricchi, F. Crescimbini and A. D. Napoli, "20 kW Water-Cooled Prototype of a Buck-Boost Bidirectional DC-DC Converter Topology for Electrical Vehicle Motor Drives," *Conf. proc. APEC 1995.*, vol. 2, pp. 887-892, March 1995.

[55] G. Ma, W. Qu, G. Yu, Y. Liu, N. Liang and W. Li, "A Zero-Voltage-Switching Bidirectional DC–DC Converter With State Analysis and Soft-Switching-Oriented Design Consideration," *IEEE Trans. Ind. Electron.*, vol. 56, no. 6, pp. 2174-2184, June 2009.

[56] D. J. Tschirhart and P. K. Jain, "A CLL Resonant Asymmetrical Pulse width-Modulated Converter With Improved Efficiency," *IEEE Trans. Ind. Electron.* , vol. 55, no. 1, pp. 114–122, January 2008.

[57] R. J. Wai, C. Y. Lin and Y. R. Chang, "High Step-Up Bidirectional Isolated Converter With Two Input Power Sources," *IEEE Trans. Ind. Electron.*, vol. 56, no. 7, pp. 2629–2643, July 2009.

[58] A. K. Rathore and U. R. Prasanna, "Analysis, Design and Experimental Results Novel Snubberless Bi-directional Naturally Clamped ZCS/ZVS Current-Fed Half-Bridge DC/DC Converter for Fuel Cell Vehicles," *IEEE Trans. Ind. Electron.*, vol. 60, no. 10, pp. 4482-4491, October 2013.

[59] W. Chen, P. Rong and Z. Lu, "Snubberless Bidirectional DC-DC Converter with New CLLC Resonant Tank Featuring Minimized Switching Loss," *IEEE Trans. Ind. Electron.*, vol. 57, no. 9, pp. 3075-3086, September 2010.

[60] K. Hirao, M. Okamoto, E. Hiraki and T. Tanaka, "An Isolated Bidirectional Soft switching DC-DC Converter for Energy Storage System and its Voltage Stress Suppression Approach," *Power Electronics and Drive Systems(PEDS), IEEE*, pp. 555-560, December 2011.

[61] T. Kokilavani, G. Selvakumar and C. C. A. Rajan, "A ZVS Bidirectional DC-DC Converter Phase Shifted SPWM Control for Hybrid Electric and Fuel Cell Automotive Application," Advances in Sceince Engineering and Management (ICAESM), pp. 700-703, March 2012.

[62] H. R. Karshenas, H. Danechpajooh, A. Bakhshai and P. Jain, "Basic Families of Medium-Power Soft-Switched Isolated Bidirectional DC-DC Converter," *Power Electronics Drives Systems and Technologies Conference*, pp. 92-97, February 2011.

[63] R. Ghosh and G. Narayanan, "Generalized Feed forward Control of Single-Phase PWM Rectifiers Using Disturbance Observers," *IEEE Trans. on Ind. Electron.*, vol. 54, no. 2, pp. 984-993, April 2007.

[64] Y. K. Lo, J. Y. Lin and S. Y. Ou, "Switching-Frequency Control for Regulated Discontinuous-Conduction-Mode Boost Rectifiers," *IEEE Trans. on Ind. Electron.*, vol. 54, no.2, pp. 760-768, April 2007.

[65] R. G. Lawrence, K. L. Craven and G. D. Nicols, "Flywheel UPS," IEEE Trans. Ind Appl. Mag., vol. 9, no. 3, pp. 44-50, May/June 2003.

[66] M. M. Flynn, P. Mcmullen and O. Solis, "Saving energy using flywheels," *IEEE Trans. on Ind. Electron.*, vol. 14, no. 6, pp. 69-76, Nov/Dec 2008.

[67] X. D. Sun, K. H. Koh, B. G. Yu and M. Matsui, "Fuzzy-logic-based V/f control of an induction motor for a DC power-levelling system using flywheel energy storage equipment", *IEEE Trans. Ind. Electron.*, Vol. 56, no. 8, pp. 3061–3068, 2009.

[68] O. Briat, J. M. Vinassa, W. Lajnef, S. Azzopardi and E. Woirgard,"Principle, design and experimental validation of a flywheel-battery hybrid source for heavy-duty electric vehicles", *IET Electr. Power Appl.*, 2007, vol. 1, no. 5, pp. 665–674, 2007.

[69] S. Vazquez, S. M. Lukic, E. Galvan and L. G. Franquelo,"Energy storage system for transport and grid applications", *IEEE Trans. Ind. Electron.*, vol. 57, no. 12, pp. 3881–3895, 2010.

[70] V. Brommer, O. Liebfried and S. Scharnholz, "A High-Power Capacitor Charger Using IGCTs in a Boost Converter Topology," *IEEE Trans. Plasma Science.*, Vol. 41, No. 10, pp. 2600-2601, October 2013.

[71] I. R. McNab, "Large-Scale Pulsed Power Opportunities and Challenges," *IEEE Trans. Plasma Science.*, Vol. 42, Iss. 5, pp. 1118-1127, 2014.

[72] A. C. Lippincott and R. M. Nelms, "A Capacitor-Charging Power Supply Using a Series-Resonant Topology, Constant On-time/ Variable Frequency Control, and Zero-Current Switching," *IEEE Trans. Ind. Electron.*, Vol. 38, no. 6, pp. 438- 447, December 1991.

[73] M. M. McQuage, V. P. McDowell, F. E. Peterkin and I. A. Pasour, "High Power Density Capacitor Charging Power Supply Development for Repetitive Pulsed Power", *IEEE International Power Modulator Symposium (27th) and High-Voltage Workshop*, May 14-18, pp. 368-371, May 2006

[74] Iqbal Husain, "Electric and Hybrid Vehicles. Design Fundemnetal", CRC Press, 2003.

[75] A. Langsdor, "Principles of Direct Current Machines", pp.113-133, SIXTH EDITION-1959, International Student Edition, McGRAW HILL BOOK COMPANY INC.

[76] Y. Suzukhi, Koyanki and Kobayashi, "Novel applications of the flywheel energy storage system", Energy, vol. 30, pp. 2128-2143, 2005.

[77] Bakay et al, "Losses in an optimized 8 pole Radial AMB for long term Flywheel Energy Storage", 12^{th} ICEMS, Tokya, Japan, 16-18^{th} November, 2009.

[78] M. M. Ionel, M. Popescu, T. J. E. Miller, M. I. McGilp et. al " Computation of Core Losses in Electrical machines Using Improved Models for Laminated Steel," *IEEE Trans. Ind. Appl.*, Vol. 43, no. 6, pp. 1554-1564, December 2007.

[79] M. M. Ionel, M. Popescu, T. J. E. Miller, M. I. McGilp et al, "On the Variation With Flux and Frequency of the Core Loss Coefficients in Electrical Machines," *IEEE Trans. Ind. Appl.*, Vol. 42, no. 3, pp. 658-666, June 2006.

[80] H. W. Lee, T. Kim, M. Ehsani,"Maximum power throughput in the multiphase BLDC generator". Proc. 30th Annual Conf. IEEE Industrial Electronics Society, pp. 2491–2496, 2–6^{th} November 2004.

[81] C. D. Kulkarni, "Design, analysis, simulation and control of special type permanent magnet brushless DC machine", M.Tech Thesis, Homi Bhabha National Institute, Mumbai, 2012.

[82] D. C. Hanselman, "Brushless Permanent-magnet Motor Design," Orono, Maine, 1959, McGraw-Hill, Inc.

[83] S. P. Smith and M. G. Say, "Electrical Engineering Design manual," Second Edition, 1950, Chapman and Hall Ltd.